

**A STUDY OF THE ROLE OF LOW ENERGY IONS IN  
CAUSING DAMAGE TO III-V SEMICONDUCTORS IN  
PRACTICAL ION ETCHING SYSTEMS**

Research Carried out at the  
Department of Electronics and Electrical Engineering,  
University of Glasgow.

Submitted to the University of Glasgow for the Degree of Doctor of Philosophy

©Ligang Deng, February 2000

ProQuest Number: 11007807

All rights reserved

INFORMATION TO ALL USERS

The quality of this reproduction is dependent upon the quality of the copy submitted.

In the unlikely event that the author did not send a complete manuscript and there are missing pages, these will be noted. Also, if material had to be removed, a note will indicate the deletion.



ProQuest 11007807

Published by ProQuest LLC (2018). Copyright of the Dissertation is held by the Author.

All rights reserved.

This work is protected against unauthorized copying under Title 17, United States Code  
Microform Edition © ProQuest LLC.

ProQuest LLC.  
789 East Eisenhower Parkway  
P.O. Box 1346  
Ann Arbor, MI 48106 – 1346

GLASGOW  
UNIVERSITY  
LIBRARY

11904 (copy 1)

To Siyuan

## Abstract

While dry etching is widely used in the fabrication of advanced III-V semiconductor electronic and optoelectronic devices, the energetic ions employed can inflict damage that impairs the performance of the semiconductor. The avoidance of such material damage is important to ensure the optimum performance of both electronic and optoelectronic devices. The particular aim of the thesis is to study the damage caused by practical etching processes, and so to identify the ion species and mechanisms that cause the damage.

The investigation first focused on optical characterisation of the dry etching damage, followed by an effort to integrate it with electrical characterisation. The optical study consisted of photoluminescence (PL) measurements on specially designed quantum well materials. In these material quantum wells of different widths, hence emitting different PL wavelength, have been placed at different depths. Selective etching technique has been applied in order to accumulate damage in the structure without material removal. Thus the measured photoluminescence data, when normalised, provided depth distributions of the damage. An ion implanter is then used to study the effects of different single ion species found in the practical selective etching processes, using the same conditions as in the etching processes. Comparison between the PL results obtained from both etched and ion-implanted samples was made.

It has been confirmed that channeling is the main mechanism for the extended depth of the damage in III-V materials studied. Of the ion species studied, molecular ions do not channel, but their fragments may. It is found that  $\text{Si}^+$  usually deposit on the sample surface. While  $\text{SiCl}_x$  etches the semiconductors concerned and causes only low damage,  $\text{Cl}^+$  causes much damage. On the other hand,  $\text{Cl}_2^+$  is less damaging. The results therefore point to molecular ions as the desirable species in a low damage process. The experimental results are in excellent agreement with M. Rahman's microscopic theory.

The existence of defect diffusion has been confirmed in the presence of strong above-bandgap photon illumination during the etching, but it remains ambiguous in normal etching environments.

The investigation moved further to integrating both optical and electrical experiments. Modulation doped quantum well materials have been designed to give PL information and allow measurements of electron transport in the channel. Initial experiments to clarify the interconnection between the optical and electrical damage have been carried out. It was found that electrical quality of the sample deteriorates more significantly than its optical quality. A theoretical explanation of this phenomenon based on trapping of carriers by ion induced trap centres has been presented.

# Contents

<b>1. Introduction</b>	<b>1</b>
1.1 General Introduction	1
1.2 Thesis Outline	3
1.3 Reference	5
<b>2. Dry etch damage and quantum well materials</b>	<b>7</b>
2.1 An Introduction to Dry Etch	7
2.1.1 <i>Reactive ion etching</i>	11
2.1.2 <i>Plasma surface interactions in RIE</i>	13
2.1.3 <i>RIE in SiCl<sub>4</sub></i>	15
2.1.4 <i>Selective RIE etching</i>	16
2.2 Dry Etching Damage	18
2.3 The multiple quantum well probe technique	22
2.3.1 <i>A brief theory of quantum well</i>	22
2.3.2 <i>Photoluminescence measurement</i>	28
2.4 Processes for Sample Preparation	30
2.5 References	32
<b>3. Theoretical modelling</b>	<b>35</b>
3.1 Introduction	35
3.2 SCHLEICH MODEL and CHANDID MODEL	37
3.3 Rahman's model	42
3.4 Summary	50
3.5 Reference	55
APPENDIX A: PLANE-SURFACE DAMAGE	57
<b>4. Low damage reactive ion etching of GaAs/AlGaAs and InGaAs/InAlAs.</b>	<b>59</b>
4.1 Introduction	59
4.2 RIE selective etching for GaAs/AlGaAs material	60
4.2.1 <i>GaAs/Al<sub>0.3</sub>Ga<sub>0.7</sub>As QW structure for dry etch damage</i>	60
4.2.2 <i>RIE etching for GaAs/Al<sub>0.3</sub>Ga<sub>0.7</sub>As multiple QWs</i>	60
4.2.3 <i>Results of Selective etching for GaAs /Al<sub>0.3</sub>Ga<sub>0.7</sub>As MQW materials</i>	62
4.3 Selective etching for In <sub>0.53</sub> Ga <sub>0.47</sub> As/In <sub>0.52</sub> Al <sub>0.48</sub> As MQW materials	65

4.3.1 <i>In<sub>0.53</sub>Ga<sub>0.47</sub>As/In<sub>0.52</sub>Al<sub>0.48</sub>As QW structure for dry etch damage</i>	65
4.3.2 <i>RIE etching for InGaAs/InAlAs multiple QWs</i>	66
4.3.3 <i>Results of Selective etching for In<sub>0.53</sub>Ga<sub>0.47</sub>As/In<sub>0.52</sub>Al<sub>0.48</sub>As MQW materials</i>	67
4.3.4 <i>Effect of ambient oxygen on Al</i>	71
4.4 Summary	72
4.5 References	73
<b>5. Contribution of atomic and molecular ions to dry-etch damage</b>	<b>74</b>
5.1 Introduction	74
5.2 Separate ions bombardment in mass resolved ion implanter	75
5.3 Results of separate ion bombardment for GaAs/AlGaAs multiple quantum well.	77
5.4 Propagation of ion damage in GaAs and InGaAs materials	82
5.5 Summary	85
5.6 Reference	87
<b>6. Enhanced damage in low damage RIE processes caused by light</b>	<b>88</b>
6.1 Introduction	88
6.2 Illumination experiments with both GaAs and InGaAs based multiple quantum well materials	89
6.3 Illumination induced additional damage in both GaAs/AlGaAs and InGaAs/InAlAs MQW materials	91
6.3.1 <i>Results of damage assessment in illuminated GaAs/AlGaAs MQW samples</i>	91
6.3.2 <i>Results of damage assessment in illuminated InGaAs/InAlAs MQW samples</i>	94
6.4 The mechanism of illumination contribution to additional damage	96
6.5 Summary	99
6.6 Reference	100
<b>7. Simultaneous optical and electrical characterisation of dry-etch damage</b>	<b>101</b>
7.1 Introduction	101
7.2 Design of modulation doped structure for both electrical and optical	

experimental measurement.	102
7.2.1 <i>Design consideration</i>	102
7.2.2 <i>Structure</i>	104
7.3 Electrical and optical experiments for investigating characteristics of the material change during dry etching	107
7.3.1 <i>Sample preparation</i>	107
7.3.2 <i>The problems in the sample preparing processes</i>	114
7.3.3 <i>Hall effect</i>	115
7.3.4 <i>RIE etching for modulation doped 2DEG material of GaAs/AlGaAs</i>	117
7.3.5 <i>Results of selective etching for modulation doped GaAs/AlGaAs</i>	118
7.3.6 Discussion and Summary of Results	119
7.4 Summary	123
7.5 Reference	125
<b>8 Conclusions and further work</b>	<b>128</b>
8.1 Conclusions	128
8.2 Future work	130
<b>Publications</b>	<b>132</b>

## ACKNOWLEDGEMENT

During the three unforgettable years many people have in various ways contributed to the research leading to this Ph.D. thesis. It is my wish to express my most sincere gratitude to all those people, among whom the following are particularly important.

I owe my biggest thanks to my supervisor James Watt Professor Chris D. W. Wilkinson. Prof. Wilkinson has provided all-round guidance and support to me in these years. Without his constant encouragement and invaluable advice in every possible detail, this whole work would have not been possible.

Dr M. Rahman, who has spent enormous amount of time and effort in examining the experimental data, has provided very useful suggestions and insight into many aspects of the problems.

Prof. Colin Stanley has been very helpful in both discussions on material design and the actual growth of the excellent quality materials, without which the experiments could not be carried out. I'd like to thank other people in the MBE group, including Dr A. Boyd for growing many of the materials used in the experiments, Dr G. Pennelli for providing important advice in making good ohmic contacts, Dr J Pearson for useful discussions, and Mr. J. Cochrane for helps in Hall measurements.

I should thank Prof. Evelyn L. Hu of Department of Electrical and Computer Engineering, University of California, Santa Barbara, for kindly providing me the chance of visiting QUEST centre and carrying out useful experiments there. Dr C Chen of the same department gave valuable discussions and allowed me access to his experimental data and computer program.

Prof. L. J. van der Pauw of Salford University kindly provided access to the mass resolved ion implanter used for separate ion bombardment.

Dr A Ribayrol gave a lot of help in PL measurements and a lot of useful advice. Thanks also to Dr M. Ke, Dr B. Qiu and Dr Y Qian for their help and useful discussions. Mr. A Ross offered great help in PL laboratory, and Mr. R Darkin, Mr. D. Clifton, Mr. W. Ward, and Mr. C Roberts for technical support in the dry etch laboratory. I should also thank Ms Kay Wray for continuous help, particularly at difficult times.

Special thanks must go to Prof. Whitehead, head of the Senate Office, and George Galloway MP for their enormous support during difficult times.

I wish to express my personal gratitude to my supervisor Chris and his wife Judy for their great help and support in all aspects.

My best friends Pei Min, Yin Huabi, Liu Xuefeng, He Wenlong give me a lot of supports and encouragements, I wish give my big thanks to them.

I also wish to express my appreciation to the CVCP for offering my ORS award and Prof. Steve Beaumont, head of department, for financial support during the three years of research at Glasgow University.

Finally, I give my special thanks to my husband Siyuan for his whole-hearted support and a lot of useful advice. Also not to be forgotten is our daughter Haiyue who has always been happy and wonderful. I also would like to thank my parents and my parents-in-law for their forever help and understanding.

# Chapter 1

## Introduction

### ***1.1 General Introduction***

III-V compound semiconductors play very important roles in modern semiconductor technology. Being direct bandgap semiconductors, many of them have the desirable property of being able to emit and detect light over a range of useful wavelengths from ultraviolet (UV) to mid-infrared (IR), which makes them indispensable for the optoelectronic and optical communication industries. The most important optoelectronic devices include semiconductor lasers of various wavelengths and structures, optical modulators, optical amplifiers and gates, nonlinear optical components, semiconductor light detectors, and integrated photonic circuits containing a multiple of these components connected by optical waveguides. At the same time, many III-V semiconductors have high carrier mobility and high saturation carrier drift speed, enabling fast semiconductor devices to be made. These devices include metal-semiconductor field effect transistors (MESFETs) and high electron mobility transistors (HEMTs), which operate in frequencies up to tens of gigahertz.

Development of these III-V devices relies on accurate pattern transfer and profile control at dimensions down to nanometer scale. These requirements are usually impossible to achieve with wet chemical etching. Dry etching involving plasma or ion beams is better suited to the fabrication of high performance III-V semiconductor devices. In comparison to wet etching, control over etch depth is easier, high anisotropy can be achieved and uniformity is better. Patterns as small as a few tens of nanometers have been successfully transferred by dry etching<sup>1</sup>.

But in dry-etch processes, the action of energetic ion bombardment can cause damage in the material being etched<sup>2</sup>. As a result the electrical and optical characteristics of the material change after dry etching. The presence of damage manifests itself in many ways. Optically it could result in reduced radiation recombination efficiency. This will reduce the photoluminescence intensity of the material. It also leads to poorer semiconductor lasers. Electrically dry-etch damage could result in reduced carrier mobility in the material. This will reduce the material's conductivity, leading to lower transconductance, lower speed and increased noise figure in transistors. Therefore, in order to produce high quality

devices, it becomes important to understand the possible attendant damage to the material introduced by dry-etch process itself.

Dry etch damage has been investigated by many different techniques and much quantitative understanding has been gained<sup>2-6</sup>. The depth to which damage may be introduced is observed to increase with bombardment energy but decrease with ion mass<sup>7-9</sup>. Deep sub-surface damage induced in semiconductors exposed to low-energy process plasmas and beams is believed to arise primarily from the channelling of a small fraction of incident ions scattered into low-index directions<sup>10,11</sup>. In the experiments where Ar<sup>+</sup> ion etching of GaAs was done with the sample oriented in different direction, Germann *et al* found that damage penetration was maximum when the beam was aligned with the <110> direction. Stoffel<sup>11</sup> has confirmed that the <110> axis in diamond /zinc -blende permits channelling readily due to the associated large aperture size. Stoffel *et al*<sup>12</sup> have performed molecular dynamics simulations of channelling under dry etch conditions which is called the SCHLEICH (Scattering of Heavy, Low Energy Ion into CHannels) model<sup>11,12</sup>. Chen, Green, and Hu have incorporated defect diffusion into these simulations to form the CHANDID (Channelling And Diffusion in Ion Damage) model<sup>13</sup>. Their model can calculate the profile of incident ions deposited in a crystalline semiconductor. Photoluminescence (PL) measurements were carried out on samples exposed to Ar plasma<sup>13,14</sup>. These samples were designed with quantum wells (QWs) of different widths at different depths so their PL peak intensities indicated the depth distribution of etch-induced damage. The experimental data were well explained by the simulations of Stoffel and Chen *et al*.

While these previous investigations using Ar<sup>+</sup> helped to understand the nature and mechanism of damage introduction in low energy ion interactions, practical materials processing often demanding the use of multi-component glow discharges<sup>15,16, 17</sup>. Non-reactive argon gas is rarely used alone. In the contrary, reactive ion species play dominant roles in practical processes. While some investigation into these processes already took place, a more systematic and fuller understanding of damage production in such cases is of urgent interest. In this project, it is intended to conduct such an investigation.

It is sensible to focus on a few most useful material systems, such as GaAs/GaAlAs and InGaAs/InAlAs. A good understanding of damage induced material property changes will have to cover both optical and electrical properties in these direct

bandgap semiconductors. By observing both optical and electrical changes caused by the same processes and in the same materials, it is hoped that some insight can be gained towards the damage mechanism and how these two aspects can be related.

For optical studies, the successful approach of multi-quantum well probe technique mentioned earlier will be adopted<sup>6</sup>. Specially designed GaAs/AlGaAs and InGaAs/InAlAs multiple quantum well probe materials will be dry etched in real reactive ion etching environments. The technique of selective etching<sup>16,18</sup> will be used as a way to damage material for long times without changing the etch depth. In this way the dry-etch damage can accumulate in QWs because no material is removed. The sensitivity of the QW probe method can be greatly enhanced by this technique, and it can be applied to investigate so-called low damage etching processes. The extent of the damage will be evaluated by measuring PL intensity from the quantum wells. On the other hand, a microscopic theory of dechannelling<sup>18-21</sup>, which has been developed by M.Rahman, will be employed to estimate the damage inflicted by various ionic species under these dry-etch conditions. The experimental data is interpreted using this model in order to identify the main cause of damage.

Modulation doped QW structures will be designed to combine optical and electrical measurements on the same material. The extent of damage will be evaluated electrically by both resistance and Hall measurements, which enables electrical parameters such as material resistivity, carrier concentration and carrier mobility to be obtained, and optically by measuring PL intensity from the quantum wells. Comparisons will be made between optical and electrical data, which should reveal the relative sensitivity of electrical and optical properties to the extend of damage, and the possible link, if any, between them.

## **1.2 Thesis Outline**

In Chapter 2 a general description of the processes, materials and experimental methods used in this work is given. An account of dry etching principles and processes for different III-V semiconductor materials is provided. The design considerations for the multiple quantum well (MQW) probe are discussed and the layer structure of the materials used throughout are presented, and the experimental methods used to measure photoluminescence are described. The experimental procedures used in preparation of samples are described.

In chapter 3, theoretical models developed by different ways are presented. The analytic model developed by M.Rahman, incorporating both channelling and diffusion mechanisms, is described in more detail. Comparisons between theoretical calculation and experimental data are presented.

In chapter 4, dry-etching damage in GaAs/GaAlAs and InGaAs/InAlAs under very low ion energy conditions has been studied in real etching environments. Damage profiles are measured using PL measurements on QW probe materials. By comparing photoluminescence spectra for damaged and undamaged areas, normalised damage distributions at various reactive ion etching (RIE) selective etching conditions are obtained. The microscopic theory described in chapter 3 is used to model the distribution of the damage in such dry-etching processes. The different effects of atomic ions and molecular ions on the samples are discussed.

In chapter 5, an attempt to further identify the main damaging ion species is described. A low energy ion implanter is used to study ion induced damage in III-V semiconductors due to separate  $\text{Cl}^+$ ,  $\text{Si}^+$ ,  $(\text{Cl}_2)^+$ ,  $(\text{SiCl})^+$ , and  $(\text{SiCl}_2)^+$  ion bombardment. In this way their individual effect in producing damage are assessed.

In chapter 6, enhanced damage in GaAs/GaAlAs and InGaAs/InAlAs quantum well structures due to additional light illumination is studied in low-power RIE environments. Comparisons are made between the two material systems in terms of damage enhancement. Possible mechanisms (enhanced defect diffusion in particular) of this illumination enhancement of dry etching damage are discussed.

In chapter 7, the effort to link optical and electrical studies is presented. A modulation doped QW structure is designed to combine optical and electrical measurements on the same material. The extent of damage is evaluated electrically by both resistance and Hall measurements to obtain electrical parameters such as material resistivity, carrier concentration and carrier mobility, and optically by measuring PL intensity from the quantum wells. A theoretical analysis is presented to interpret the observed optical and electrical data and, as a first attempt, to form a unified understanding of the underlying mechanism for both optical and electrical changes.

### **1.3 References**

- [1]. S. M. Sze, “ Semiconductor devices Physics and Technology” John wiley& sons, 1985.
- [2]. S. K. Murad, M. Rahman, N. Johnson, S. Thoms, S. P. Beaumont, and C. D. W. Wilkinson, *J.Vac.Sci.Technol.* **B 14**, 3658-3662 (1996).
- [3]. M. A. Foad, S. Thoms, and C. D. W. Wilkinson, *J. Vac. Sci. Technol.* **B 11**(1), 1993, P. 20
- [4]. M.Watt, C.Sotomayor-Torres, R.Cheung, C.D.W.Wilkinson, H.E.G.Arnot, and S.P.Beaumont, *J.Mod. Opt.* **35**, 1988, P365.
- [5]. P. D. Wang, M. A. Foad, C. M. Sotomayor - Torres, S. Thoms, M. Watt, R. Cheung, C. D. W. Wilkinson, and S. P. Beaumont, *J.Appl. Phys.* **71**(8), 1992, P.15.
- [6]. H. F. Wong, D. L. Green ,T. Y. Liu, D. G. Lishan, M. Bellis, E. L. Hu, P. M. Petroff, P. O. Holtz, and J. L. Merz, *J.Vac.Sci.Technol.* **B 6**, 1906-1909 (1988).
- [7]. K.L Seaward, and N. J. Moll, *J.Vac.Sci.Technol.* **B 10**, 46, (1992).
- [8]. K.L Seaward, N. J. Moll, and W.F. Stickle, *J Electron mater.* **19**, 385 (1990).
- [9]. T. L. Cheeks, M. L. Roukes, A. Scherer, and H. G. Craighead, *Appl. Phys. Lett.* **53**, 1964 (1998).
- [10] R.Germann, A. Forchel, M.Bresch, and H.P. Meier, *J.Vac.Sci.Technol.* **B 7**, 1475 (1989).
- [11] N. G. Stoffel, *J. Vac. Sci.Technol.* **B 10**, 651-658 (1992).
- [12]. N.G. Stoffel, S. A. Schwartz, M. A. A. Pudensi, K. Kash, L. T. Florez, J. P. Harbison, and B. J. Wilkens, *Appl. Phys. Lett.* **60**, 1603 (1992).
- [13]. Ching-Hui Chen, Debora L. Green, and E. L. Hu, *J.Vac.Sci.Technol.* **B 13**, 2355-2359 (1995).
- [14]. D.L. Green, E. L. Hu, and N. G. Stoffel, *J. Vac. Sci. Technol.* **B 12**, 3311 (1994).
- [15]. S. K. Murad, S. P. Beaumont, M. Holland and C. D .W. Wilkinson, *J. Vac. Sci. Technol.* **B 13**, 2344 -2349 (1995).
- [16]. S. K. Murad, C. D. W. Wilkinson, and S. P. Beaumont, *MNE* **23**, 357-360 (1994).
- [17]. S. K. Murad, C. D. W. Wilkinson, and S. P. Beaumont, *MNE* **27**, 439-444 (1995).
- [18]. M. Rahman, N. P. Johnson, M. A. Foad, M. C. Holland and C. D. W. Wilkinson, *Appl. Phys. Lett.* **61**, 2335-2337, (1992).

[19] M. Rahman, J. Appl. Phys **82** 2215 (1997).

[20] M. Rahman, PRB **52**, 3383 (1995).

[21] M. Rahman, (unpublished).

## **Chapter2**

### **Dry etch damage and quantum well materials**

This chapter contains a general description of the processes, materials and experimental methods used in this work. Firstly, an account of dry etching principles and processes for different III-V semiconductor materials is given. Secondly, the design considerations for the multiple quantum well (MQW) probe are discussed and the layer structure of the materials used throughout are presented, and the experimental methods used to measure photoluminescence are described. Finally, the experimental procedures used in preparation of samples are described.

#### ***2.1 An Introduction to Dry Etch***

In general, when transferring patterns into solid substrates, the substrate material can be removed in two ways: wet or dry etching. Even though wet etching<sup>1</sup>, i.e., immersion of the substrates into a suitable chemical solution, can be highly selective and give a high etch rate, the action of the etchant is normally isotropic. In isotropic etching, the removal of materials etching occurs in the lateral as well as in the vertical direction. So isotropic etching leads to the profile shown in Figure 2-1(a). This leads to an undercutting of the mask, which is undesirable, particularly if the required etch depth is comparable to the width of the mask. In dry-etching<sup>1</sup>, the sample is bombarded by a flux of ions. Surface removal here proceeds via physical sputtering, or the chemical reaction of the ions with the surface, or a mixture of both. The etching occurs predominantly in the direction of ion incidence and therefore can be anisotropic [Figure 2-1(b)]. By using dry-etching techniques it is possible to etch the material to make structures that have little undercutting, and so to maintain accurate transfer of the pattern of the mask. Reproducibility is increased due to better dimensional control compared to the existing wet-etching processes. There are many desired profiles that can only be obtained by dry etching. In addition, the etching of material by reaction with chemically active radicals in a glow discharge is a dry process, producing less waste than wet etching. This makes dry-etching preferable to wet-etching for defining very narrow features.

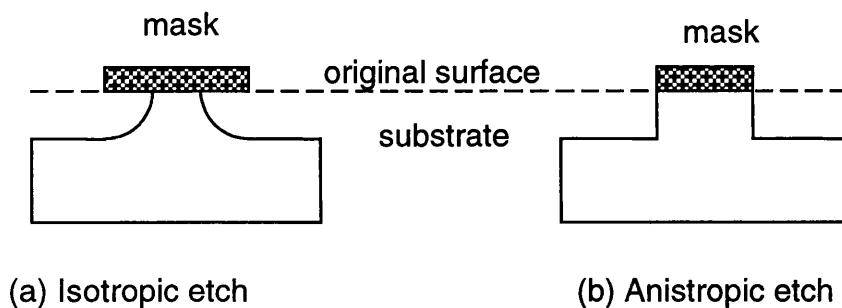


**Figure 2-1.** Wet-etches are generally isotropic, producing rounded profiles, whereas dry-etches can be made anisotropy, with much more vertical etch profile

Dry-etching is classified into various techniques, depending on the etching state of the gas (e.g. neutral or ionised), gas type, excitation method (e.g. radio, or microwave frequency) and geometrical configuration of the etching system (e.g. barrel, parallel plates or down stream). A summary of the characteristics of six common types of dry etching machine is shown in Table 2-1. The machines are divided up by the names often used in the literature, but the notation is not always consistent.

The action of the energetic ions on the substrate can be described as physical if the material is removed purely through momentum transfer – the atoms are knocked out by the impinging flux of ions. Purely physical etching is not widely used as the etch rate tends to be slow, and the profiles of an etched feature are not vertical. However it is employed in ion beam machines employing noble gas ions. In such machines (often known as ion millers) the ions are initially created using a hot wire to ionise the gas and then extracted by an ion gun. The resulting beam drifts towards the target.

In reactive etching, the ion is chosen so that it (or an associated radical) undergoes a chemical reaction with the substrate preferably one that gives a chemical product that is volatile at the process pressure so that it can be pumped away. This can be done in an ion beam etching machine by introducing a reactive gas in front of the substrate so that it is ionised by collision with the beam of noble gas ions.

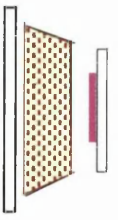
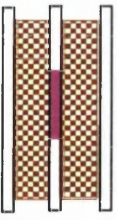
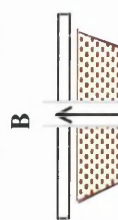
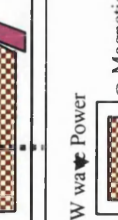
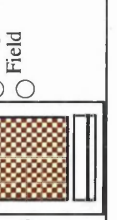
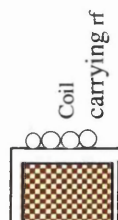
Usual Name	Ions generated by:	Ions extracted by:	Gas selected to be:	Diagram and distinguishing features
Reactive ion etching (RIE)	rf discharge	same rf field	reactive	 $<50\text{mT}$ pressure, dc bias $\sim 20\text{-}50\text{V}$ , phys+chem
Plasma Etching (PE)	rf discharge	same rf field	reactive	 pressure $\sim 0.1\text{-}2.0\text{T}$ dc bias $< 20\text{V}$ chemical
Magnetron Sputtering	rf discharge	same rf field	not reactive	
Magnetron reactive	rf discharge	same rf field	reactive	
Ion Beam Etching (IBE)	hot wire (dc)	dc fields	not reactive	
Chemically Assisted Ion Beam Etching (CAIBE)	hot wire (dc)	dc fields	reactive	
Radical beam and ion beam etching (RBIBE)	hot wire	dc field + microwave	reactive	
Electron Cyclotron Resonance- Reactive Ion Etching (ECR-RIE)	microwave field with magnetic field	separate rf field	reactive	 $\mu\text{W}$ wa Power Magnetic Field ECR increases ion density phys+chem
Inductively Coupled Plasma Etching (ICP Etching)	rf field induced by a driven loop	separate rf or rf field	reactive	 Coil carrying rf ICP increases ion density phys+chem

Table 2-1. A summary of the characteristics of six common types of dry etching machine

More usually the discharge is formed by the action of an alternating electric field. The field accelerates any electrons, which collide with the atoms or molecules of the gas producing ions and more electrons. This process continues until a discharge is build up. Recombination of the ions into atoms or molecules by the capture or emission of an electron may be accompanied by the emission of light. The light – emitting plasma has over-all electrical neutrality. At low pressures, say less than 50mT, a dark space that is essentially free of ions appears between the electrodes and the plasma. A dc voltage is developed across this dark space, its magnitude depending on the pressure and frequency. This rectification occurs as the electrons being of very low mass can follow the variation of a high frequency field, while the ions being much heavier may not be able to.

A reactive ion etching (RIE) machine typically is driven at 13.6 MHz and at pressure less than 50mT. The two electrodes normally have different diameters, and the smaller one that carries the sample to be etched, is driven by the rf field, the larger one being grounded. A voltage – the (self)-bias voltage is developed across the dark space above the driven electrode and the ions are accelerated across this dark space and so land from a vertical direction upon the sample. Only a small proportion of the gas molecules are ionised in a RIE machine, and this proportion can be increasing the rf power. Increasing the rf power also increase the bias voltage.

In a magnetron sputtering machine an axial magnetic field is applied to a machine that otherwise is similar to a RIE machine. The magnetic field causes the electrons to spiral and so increase the time they are available to ionise the gas. Thus a more heavily ionised plasma may be obtained, and this tends to increase the etching rate at a given power level.

It can be desirable to separate the generation of the plasma from the extraction of the plasma, as this allows the density of the plasma (associated with etch rate) to be adjusted independently of the bias voltage (associated with the damage inflicted on the sample).

In an Electron cyclotron resonance (ECR) reactive ion etching machine (ECR/RIE), the plasma is generated by a microwave field, normally at a frequency of 2.56 GHz and extracted by a rf field at 13.6 MHz. A magnetic field (the cyclotron field  $B = m/e\omega_c$ ) around 0.08T is applied axially. The effect of this field allows efficient transfer of energy to the electrons and so allow efficient ionisation of the gas. Such

machines create relatively high density plasma; however the use of a low bias voltage is not a necessary guarantee of low damage etching.

The inductively coupled plasma (ICP) etching machine is an alternatively way of separating the generation of the plasma from the bias voltage. The plasma is formed by inductively coupling of rf power from a rf coil wrapped around the chamber; the ions are extracted by another rf or low frequency supply applied to a RIE type electrode.

The plasma etching machine usually has symmetric electrodes with the sample immersed in the plasma. The self-bias voltage is low. If the etch is anisotropic this arises from the formation of a polymeric film (from the decomposition products of the etching gas) during the process. It is widely used, with many variations in silicon processing.

In these processes, material is removed either by subjecting the surface to reactive ions and radicals generated in a plasma, which form volatile compounds with the substrate material, or by ejecting material particles off the substrate surface with an energetic beam of ions/reactive ions. The etching profile of substrate depends strongly on choosing which kind of etching system. In a purely physical etching system such as IBE, the sputtering plays a major role for taking surface material away. But since it is solely physical, most material poses a similar etching rate and consequently etch selectivity is poor. The substrate material can be damaged by highly energetic ion bombardment. In a purely chemically system such as Plasma Etching (PE), chemical etching is dominant for removing material away. It is selective etching, but also isotropic etching. However reactive ion etching can provide a chemically assisted energetic ion etching but careful controlling is very important for obtaining a given etching profile. Reactive ion etching is predominantly used in this work, and will be given more detailed discussion in the next section.

### **2.1.1 Reactive ion etching**

Reactive-ion etching (RIE)<sup>2</sup> is a very popular method for transferring patterns into III-V semiconductors. Because the substrate is held on the rf-driven electrode instead of the grounded electrode as in a plasma etcher, the grounded electrode can have a significantly larger area than the driven electrode. This larger grounded area

combined with lower operating pressure (5-100 mTorr) leads to plasma-sheath potentials in the range 20-500V.

A simplified schematic diagram of a RIE system is shown in Figure 2-2. The etching chamber consists of two parallel electrodes. The top electrode is grounded, and the bottom electrode (the cathode) is driven by a r.f. signal at 13.56MHz, connected through a capacitor and an impedance matching circuit. With the system under vacuum, the etching gas is introduced into the chamber. Free electrons in the chamber gain energy from the rf electron field. The energetic electrons collide with the gas molecules and so ions are formed. The combination of electrons and ions is known as a plasma. Due to the high mobility of electrons, compared to the ions, the electrode surface in contact with the plasma develops a negative potential relative to the plasma volume. This repulsive field causes the electron population in the region close to the electrode to be depleted, so that few ions are formed in this region and a glow is not observed there. This region is therefore known as the plasma dark space<sup>3</sup>, or plasma sheath. The potential drops across the r.f. driven electrode dark space is particularly high because of the rf driven bottom electrode has a smaller area than the top electrode. This potential drop is known as the d.c. self-bias voltage. The d.c. self-bias is found to increase with increasing ratio of the ground electrode surface area to the r.f. driven surface area. In most RIE apparatus, the driven electrode is much smaller than the ground electrode in order to obtain a high self bias voltage, e.g., the RIE80 machine used in Glasgow has grounded electrode of 300mm in diameter and a driven electrode of 170 mm diameter. The d.c. self-bias voltage is determined mainly by the amplitude of the r.f. signal. Increasing the r.f. power in RIE increases the dc self-bias.

The electric field due to the negative d.c. self-bias causes a downward flow of positive ions from the plasma across the dark space. The pressure used in the reactive ion etch is very low (5- 100mTorr), therefore the mean free path of the ions is long so that they are not randomised in direction while traversing the plasma sheath. If the substrate is placed on the driven electrode, the ions will strike the substrate from a vertical direction. Etching will occur in this direction if the ions react chemically with the semiconductor to form volatile compounds which are then pumped away. Etching will also occur due to physical sputtering caused by energetic

ion bombardment. Therefore RIE utilises both chemical and physical etching mechanisms.

We see that using electrodes of different area, placing the sample on an electrode and using relatively low pressure all lead to an ion beam which is energetic and directed vertical at the sample, all help towards achieving anisotropic etching in a RIE machine.

While the energetic ions bombarding the substrate may cause damage<sup>4</sup> to material. Therefore, in order to gain a fuller understanding of the induced damage, a knowledge of the fundamental processes involved during etching concerning the role of reactive radicals and ion bombardment is beneficial and will be discussed in the next section.

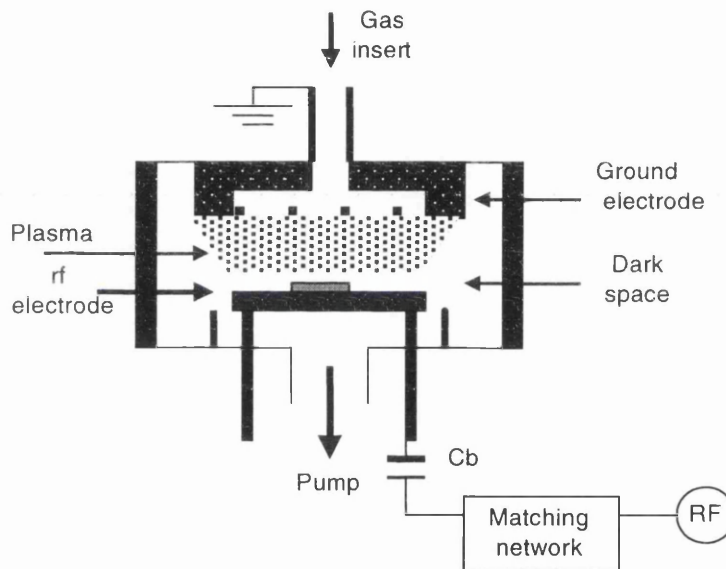


**Figure 2-2** The schematics diagram of parallel plates r.f RIE system.

### 2.1.2 Plasma surface interactions in RIE

It is convenient to consider the interaction of reactive plasmas with a surface as having two components: physical and chemical. A physical interaction refers to the surface bombardment by energetic ions accelerated across the dark space; the ions sputter away the surface but remain chemically unchanged. Here the loss of kinetic energy of ions in the surface region dominates the interaction. In reactive etching, a chemical interaction takes place in which ions react with chemical species and results in the formation or dissociation of chemical species on the surface.

The plasma-assisted etching process proceeds in five steps as illustrated in Figure 2-3. (1) The process begins with the generation of the etchant species (the reactant) in the plasma. (2) The reactant is then transported by diffusion through to the surface of substrate. (3) The reactant is adsorbed on the surface. (4) This is followed by chemical reaction (along with physical effects such as ion bombardment) to form volatile compounds. (5) These compounds are desorbed from the surface, and pumped out by the vacuum system<sup>5</sup>.

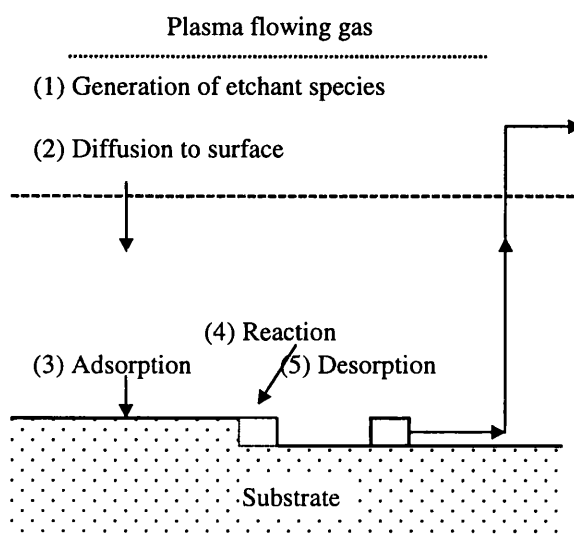


**Figure 2-3.** Basic steps in a dry etching processing.

Before any reaction can take place on the substrate surface, the reactive radicals have to be adsorbed at surface sites. After the reaction has taken place, the reaction product has to be desorbed from the surface. Often in an etching process, the rate limiting step (which determines the etch rate of a particular material) is governed by one of these mechanisms. In reactive ion etching, the gases are chosen so that they will absorb and react with the substrate, the rates of adsorption and reaction will normally be high, so an important parameter is often the desorption rate. This is related to the vapour pressure of the etching products, the higher the vapour pressure, the faster the desorption rate. However, the presence of ion bombardment in RIE can also play an important role in the etching process. While ions can etch the substrate by physical sputtering processes, there are also other ways in which the ions can participate in enhancing an etching reaction:

(1) On an adsorption/reaction level. By creating surface damage ion bombardment serves to create or enhance reactive sites on the substrate surface. This implies that in certain cases no reaction will take place without ion bombardment and has been used by Balooch *et al*<sup>6</sup> to explain why GaAs can only be etched in the presence of argon ions in an CAIBE study using molecular Cl<sub>2</sub>. The effect of enhancement of adsorption was observed by Coburn *et al*<sup>7</sup> by independently controlling the impingement of Ar<sup>+</sup> and XeF<sub>2</sub> on silicon. Moreover, a mechanism involving the creation of surface damage has been proposed for the production of anisotropy<sup>8</sup>, as long as the ions are directional, as in the case of RIE.

(2) On a desorption level. By chemically enhanced physical sputtering, ion bombardment can stimulate or increase the rate of desorption and help remove reaction products held on the substrate surface<sup>9</sup>.

### 2.1.3 RIE in SiCl<sub>4</sub>

Stern *et al*<sup>10, 11</sup> were the first workers to report using SiCl<sub>4</sub> for the high resolution reactive ion etching of GaAs and InP. 20 nm wide patterns, defined by electron beam lithography, were transferred into GaAs using NiCr as the dry etch mask. At pressures around 20mT and at a lower power, crystallographic etching in the (100) orientation of GaAs has also been observed<sup>12, 13</sup>. Rowe<sup>14</sup>, using optical emission spectroscopy, found that SiCl<sub>4</sub> gas is broken down to SiCl<sup>+</sup>, SiCl<sub>2</sub><sup>+</sup>, and Cl<sup>+</sup> in RIE plasma. More recently, at the University of Glasgow, S. Murad found more ionic species such as Cl<sub>2</sub><sup>+</sup>, *etc.*<sup>15</sup> Analysis by Murad showed that the applied r.f. power plays a decisive role in the way SiCl<sub>4</sub> breaks down to its constituent radicals and atoms. Two power regimes were identified: in the low power regime SiCl<sub>4</sub> molecules break down gradually by multi-step electron impact dissociation and excitation processes, whereas in the high power regime SiCl<sub>4</sub> molecules break down more rapidly through single electron impact dissociative excitation and ionisation processes. The main ions in the plasma in the low power regime are Cl<sub>2</sub><sup>+</sup> with little Cl<sup>+</sup>, whereas in the high power regime Cl<sup>+</sup> predominates. Therefore both Cl<sub>2</sub><sup>+</sup> and Cl<sup>+</sup> are believed to be responsible for the etching of GaAs. It is highly possible that the type of etch mechanism and products produced in the SiCl<sub>4</sub> processes are similar to the species produced from studies of the ion assisted etching GaAs using molecular Cl<sub>2</sub> and argon ions<sup>9, 19</sup>. In Balooch's experiment, etching of GaAs in

molecular chlorine was observed only in the presence of argon ion bombardment. Using a  $\text{Cl}_2$  flux of  $1 \times 10^{17}$  molecular / $\text{cm}^2$  sec to impinge on the GaAs surface, they observed  $\text{AsCl}_3^+$ ,  $\text{AsCl}_2^+$ ,  $\text{AsCl}^+$ ,  $\text{GaCl}_3^+$ ,  $\text{GaCl}_2^+$ , and  $\text{GaCl}^+$  ions, and suggested that they had arisen from  $\text{AsCl}_3$ , and  $\text{GaCl}_3$ . It was also evident, according to their data, that ion bombardment did not cause sputtering of Ga or As but instead, enhanced the production and /or desorption rate of  $\text{GaCl}_3$ . On the other hand, McNivin *et al*<sup>16</sup> employed a maximum  $\text{Cl}_2$  flux of  $5 \times 10^{14}$  molecules / $\text{cm}^2$  sec and found  $\text{AsCl}_3$ ,  $\text{GaCl}_2$  and possibly  $\text{GaCl}$  as major species leaving the GaAs surface. In addition, from their experimental data, they proposed a very different reaction model which involves the enhancement of the reaction of adsorbed  $\text{Cl}_2$  with arsenic on the GaAs surface which produces  $\text{AsCl}_3$ .

#### **2.1.4 Selective RIE etching**

Dry etching can produce different etching rate for different materials, therefore providing selectivity between different materials, which can simplify device fabrication processes. Selective RIE of GaAs over AlGaAs in  $\text{CCl}_2\text{F}_2$ -based plasmas<sup>17-20</sup>,  $\text{SiCl}_4/\text{SiF}_4$  and  $\text{SiCl}_4/\text{SF}_6$ <sup>21, 22</sup> has been reported. In these processes, etching stops when a non-volatile layer of  $\text{AlF}_3$  is formed. However, the formation of such a layer requires the use of relatively high pressures and low dc bias which results in isotropic profiles and lateral etching which is difficult to control. The selectivity obtained are smaller than 350:1 in the  $\text{SiCl}_4/\text{SiF}_4$  mixture etching. A selective and anisotropic RIE process for etching GaAs/AlGaAs in pure  $\text{SiCl}_4$  has been developed by S. Murad in Glasgow University which can stop on an extremely thin AlGaAs layer (1.13nm; 4 monolayers).<sup>23</sup> While maintaining very good anisotropy, selectivity up to 10000:1 has been achieved. It is believed that etching is stopped by a non-volatile layer of  $\text{Al}_2\text{O}_3$  or  $\text{AlN}$  formed by residual oxygen, air or moisture in the chamber.

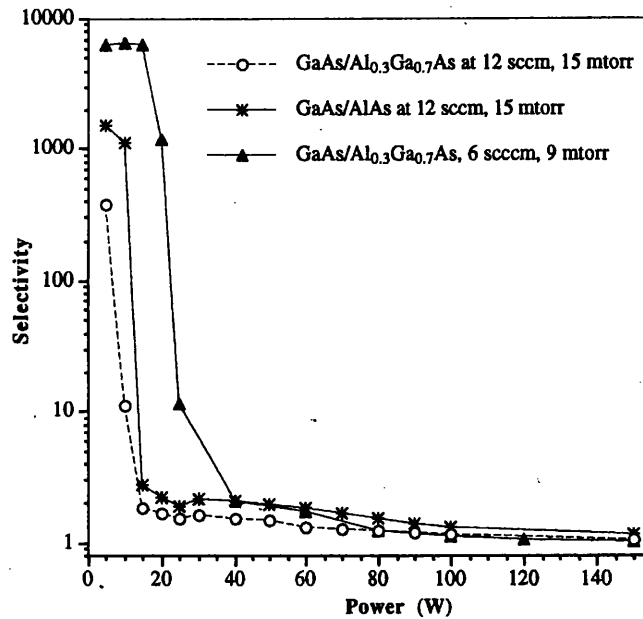


**Figure 2-4:** The etch rate ratios (the selectivity) of GaAs/Al<sub>0.3</sub>Ga<sub>0.7</sub>As and GaAs/AlAs in SiCl<sub>4</sub> plasma as a function of r.f. power for two values of flow rate and pressure; 12sccm at 15mTorr and 6sccm at 9mTorr

In Murad's experiments, selective etching of GaAs/AlGaAs using SiCl<sub>4</sub> was performed in an Oxford plasma technology RIE80. The etching chamber was usually pumped down to base pressure of 0.1mTorr. The selectivity was measured at various rf power, pressure and gas flow rate.

His experimental data, which is reproduced in Figure 2-4, indicated that r.f. power has a dominant effect on GaAs/AlGaAs selectivity. It is very clear to see from the figure that the selectivity are very high at low power and the etching is non-selective at higher powers. The range of power in which high selectivity is obtained depends on the pressure and/or the flow rate. A lower flow rate/pressure results in a higher power limit for high selectivity. For example, at pressure of 15mTorr and flow rate of 12sccm, the selectivity is high in the power range up to 10W. But at pressure of 9mTorr and flow rate of 6sccm the selectivity remains high in a wider range of power up to 20W. This behaviour has been attributed to the density of the etchant compared to that of residual O<sub>2</sub> or air in the chamber and by the ion energies. At low flow rate and low pressure, the density of etching species is so low that a very small O<sub>2</sub> or air residual can stop the surface reaction by oxidation<sup>15</sup>. This sustains until such a point (at power  $\geq 25$  W) where the ion energies are high enough to sputter off the thin aluminium oxide which continuously forms layer on the surface, leading to AlGaAs etching.

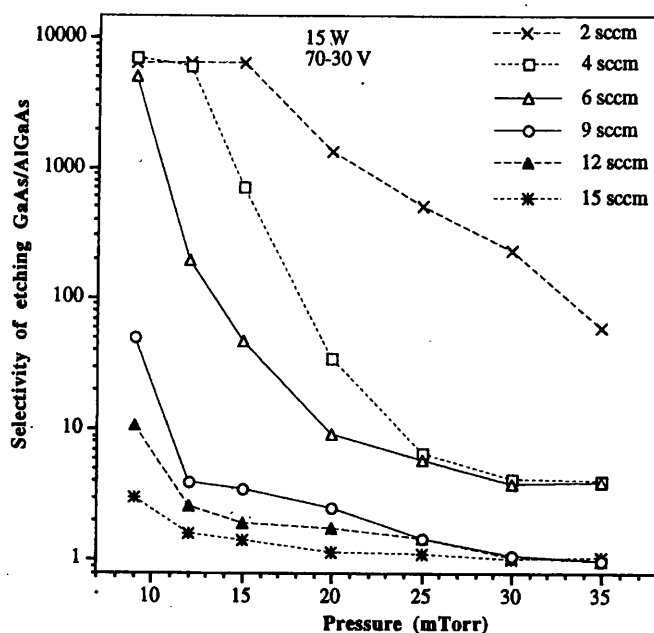


**Figure 2-5:** Selectivity of etching GaAs/AlGaAs in  $\text{SiCl}_4$  plasma as function of pressure for flow rate value of (2, 4, 6, 9, 12 and 15 sccm), all at constant rf power of 15W and dc self bias range of 35-70 V.

In another experiment by Murad, reproduced in Figure 2-5, selectivity of the etching of GaAs/AlGaAs was measured as function of the pressure and the flow rate at a constant rf power of 15W. From this data, the conditions for selective etching of GaAs with very high selectivity and anisotropy have been identified as a flow rate of 4-6 sccm, a pressure of 9 mTorr, a power of 15W and a bias voltage range of 30- 70V obtained.

## 2.2 Dry Etching Damage

In reactive ion etch processes, the energetic ions bombard the material and can cause damage to the material being etched<sup>4</sup>. As a result the electrical and optical characteristics of the material change after dry etching. The presence of damage manifests itself in many ways. Optically it results in reduced radiation recombination efficiency. This will reduce the photoluminescence intensity of the material. It also leads to poorer semiconductor lasers. Electrically it results in reduced carrier mobility and carrier density in the material. This will reduce the material's conductivity, leading to lower transconductance, lower speed and increased noise figure in transistors. Therefore, in order to produce high quality devices, it becomes

important to understand the possible attendant damage to the material introduced by dry-etch process itself.

When ions strike upon a surface, they both remove the surface material and cause damage beneath the surface. The sidewalls, if vertical, are not at first sight bombarded by the incident ions. They will, however, be bombarded by ions re-emitted from or ricocheting from the substrate as shown in Figure 2-6, and by ions attacked by the image charge they induce in the semiconductor.

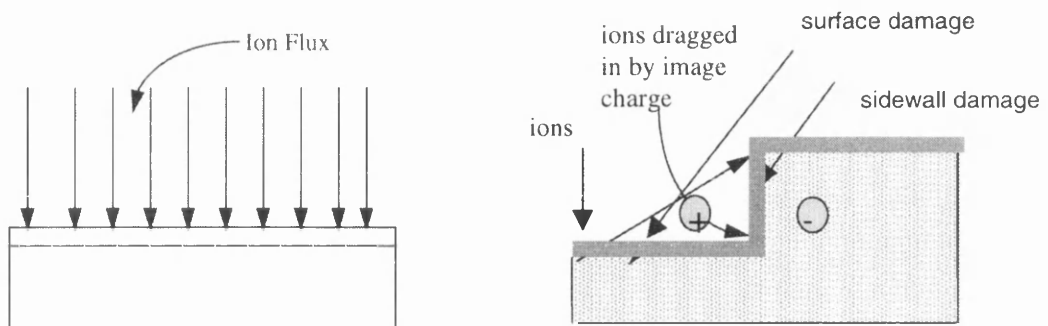


**Figure 2-6.** The distinction between surface and sidewall damage.

Figure 2-6 illustrates some of the possible interactions that can take place within an ion process. The energy and size of the impinging ion determine the impact it will have on the lattice. When the incident ion comes in contact with the material, the transfer of the energy and momentum of the ion causes several things to happen. It can either react chemically with the material, be reflected off the surface, or penetrate the material. If the ion enters the material, the structure of the crystalline lattice can be disturbed by the creation of vacancies, interstitial, or dislocations. Energy can also be released in the form of photons, phonons (heat), or electrons during the many collisions that occur in the material. All of the initial processes that occur with the incident ions can then, in turn, create any of the interactions illustrated in Figure 2-7. Since it is difficult to differentiate between the numerous interactions, the reference to ion-induced damage in the material can include any of these interactions.

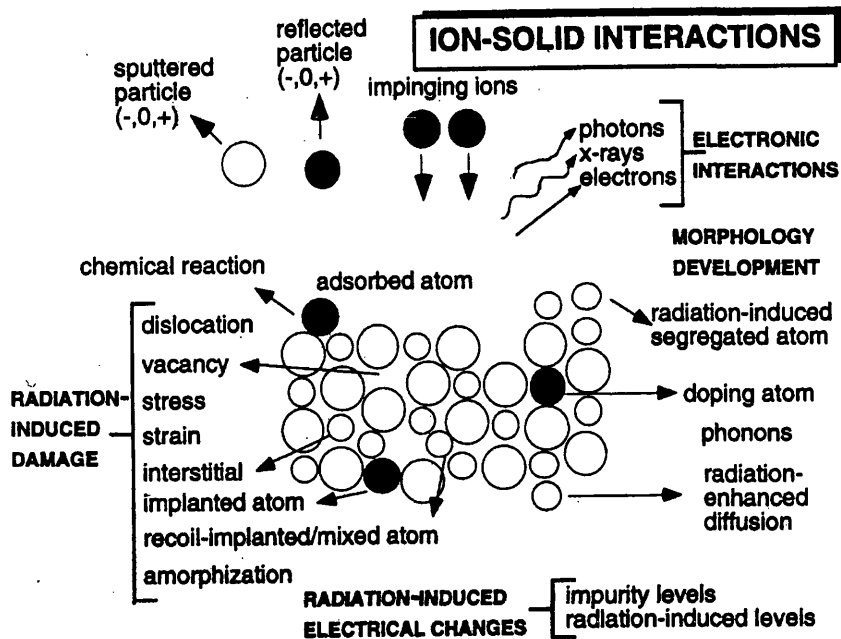


**Figure 2-7.** Schematic of ion-solid interactions that takes place during an ion process. (after review paper by Malherbe on sputtering of semiconductor surface)<sup>24</sup>.

Over recent years, there has been a lot of research in the area of dry-etch damage. A variety of sophisticated characterisation techniques are now available for the study of etch-induced damage.

To measure the damage by electrical means, Schottky metal-semiconductor junction has been made on the etched surface of III-V semiconductor and their characteristics has been compared with those of a Schottky diode on an unetched surface<sup>25</sup>. The surface depletion depth, free carrier concentration, and barrier height can be measured. Deep level transient spectroscopy is a sensitive technique for defect characterisation in semiconductors. Johnson<sup>26</sup> has used it to find the nature of the traps introduced by dry-etching. Foad<sup>27</sup> has used surface conductance measurement employing the transmission line model(TLM) technique to measure the conductance of the surface layer after dry-etching.

There are also several optical techniques that can be used to detect dry-etch damage. Raman scattering is a very useful probe for the investigation of damage on the surface region caused by the dry etching. It has been used to investigate RIE damage on undoped GaAs materials by Watt, *et al*<sup>28</sup>. They reported that after high power etching by SiCl<sub>4</sub>, the forbidden transverse optical (TO) line has been observed indicating changes in the polarisability of the crystal surface. Wang, *et al*<sup>29</sup> reported

Raman investigations of the coupled LO phonon-plasmon scattering on heavily doped  $n^+$ -GaAs after dry etching. They used two Si-doped epitaxial GaAs layers 140nm thick grown by MBE on semi-insulating (100) GaAs substrate (one was doped to  $3 \times 10^{18} \text{cm}^{-3}$  and another one  $2 \times 10^{18} \text{cm}^{-3}$ ), and etched under different conditions by using different etching systems RIE 80, IBE and ECR-RIE. It is found that in RIE etching, as etching proceeds, the depletion depth saturates while for purely physical etching (IBE) the depletion depth increases continuously. The X-ray photoelectron spectroscopy(XPS) has high surface sensitivity and the ability to elementarily analyse the elemental composition of the surface region qualitatively as the core binding energies are characteristic of an element. In addition, characterisation of the bonding state and chemical environment of the atom concerned can be achieved through the interpretation of the measured shift in binding energy. It has been used to investigate the modifications in the chemistry of (100) GaAs surface following reactive ion etching using  $\text{CH}_4/\text{H}_2$  and  $\text{SiCl}_4$  by Cheung<sup>30</sup>. The group of Hu<sup>31</sup> designed a series of quantum well of different thickness and at different depths below the surface of the semiconductor, so that the wavelength of light in photoluminescence (PL) indicates the depth from which it comes. Therefore this method identifies the penetration range of the damage by observing the change of PL intensity at different wavelengths.

Much quantitative understanding has been gained in dry etching damage<sup>4, 31, 32</sup>. The depth to which damage may be introduced is observed to increase with bombardment energy but decrease with ion mass<sup>33-35</sup>. Deep sub-surface damage induced in semiconductors exposed to low-energy process plasmas and beams is believed to arise primarily from the channelling of a tiny fraction of incident ions scatter into low-index directions<sup>36, 37</sup>. In the experiments where  $\text{Ar}^+$  ion etching of GaAs was done with the sample oriented in different direction, Germann *et al* found that the damage of penetration was a maximum when the beam was aligned with the  $\langle 110 \rangle$  direction. Stoffel<sup>37</sup> has confirmed that the  $\langle 110 \rangle$  axis in diamond/zinc-blende permits channelling readily due to the associated large aperture size by using molecular dynamics.

However with modern materials processing often demands the use of multi-component glow discharges<sup>38, 39</sup>. The presence of both atomic and molecular ions in the discharge is the main complication. It is of urgent interest to understand in

greater detail damage production in such cases. Therefore, further understanding of the changes in optical and electrical properties of semiconductors induced by dry-etch damage, particularly the relations and comparison between them is the major.

### 2.3 The multiple quantum well probe technique

The multiple quantum well (MQW) probe technique is a highly sensitive technique for the characterisation of low energy ion induced damage in III-V semiconductors. This technique was first reported by Hu's group<sup>31</sup>. The MQW probe technique is a non-invasive method that provides the requisite high sensitivity for depth resolution of damage<sup>31, 40</sup> with no additional processing of the ion exposed surface required. Basically the technique utilises the high sensitivity of a quantum well to the concentration of non-radiative defects, or traps, created within its vicinity. As the wavelength of radiation emitted after excitation varies with the thickness of the well, by placing wells of different thickness at different depths, the variation of PL (and so damage) with depth can be studied.

The MQW probe technique is extensively used in our experiments, so quantum wells were been specially designed for this purpose as described in next section.

#### 2.3.1 A brief theory of quantum well

A quantum well is a layer of one semiconducting material, sandwiched between two other semiconducting materials (the cladding). The material of the well is chosen to have a lower energy gap than the cladding layer. A sandwich with GaAs as the filling between two layers of  $\text{Al}_x\text{Ga}_{1-x}\text{As}$  gives a potential well for both electrons in the conduction band and holes in the valence band<sup>41</sup>, as shown in Figure 2-8

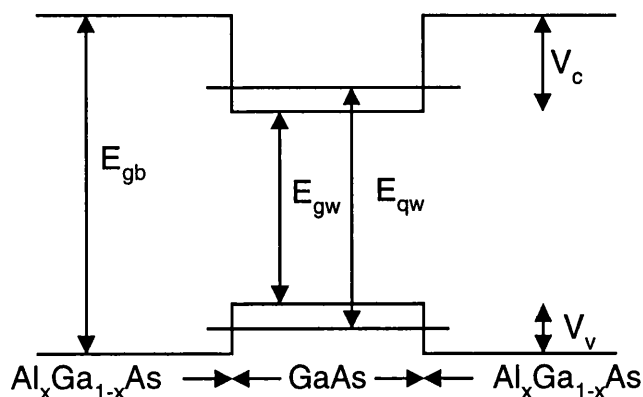


Figure 2-8: Energy band diagram of GaAs- $\text{Al}_x\text{Ga}_{1-x}\text{As}$  QW.

The energy bandgap of  $\text{Al}_x\text{Ga}_{1-x}\text{As}$  is related to the aluminium concentration  $x$  and the bandgap  $E_{gb}$ <sup>42</sup> (here we consider materials at liquid helium temperature)

$$E_{gb} = 1.424 + 1.247x \quad \text{Eq.2-1}$$

In a quantum well (QW) formed by GaAs- $\text{Al}_x\text{Ga}_{1-x}\text{As}$ , GaAs acts as a well that traps both electrons in the conduction band and holes in the valence band, so electrons and holes can exist in bound states in this QW. The difference in the band gap is taken up by a shift in the conduction band offset ( $V_c$ ) and the rest by the shift in the valence band ( $V_v$ ). Experimentally it has proved difficult to determine the offset ratio  $Q=V_c/V_v$ . In this work, the value of  $Q$  is taken as  $0.65$ <sup>43,44</sup>.

$$V_c = Q * 1.247x$$

$$V_v = (1 - Q) * 1.247x \quad \text{Eq.2-2}$$

We consider electron and hole (both heavy hole and light hole) states in the GaAs and  $\text{Al}_x\text{Ga}_{1-x}\text{As}$  system as shown in Figure.2-9. The quantum states in a QW can be calculated by Schrodinger's equation.

$$-\frac{\hbar^2}{2m} \frac{d^2}{dz^2} \psi(z) + V_0 \psi(z) = \epsilon \psi(z)$$

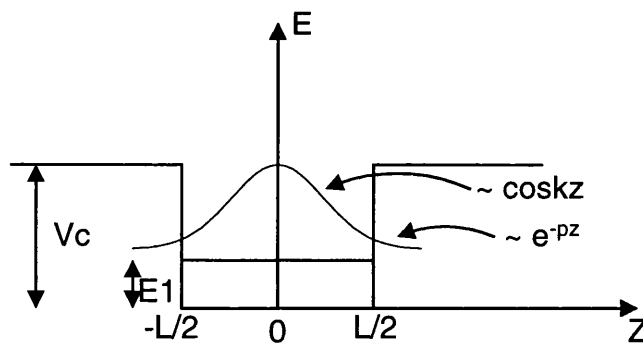


Figure 2-9: First bound energy level and wavefunction in a finite QW.

The electron wave eigenfunction for the lowest bound state is<sup>45</sup>

$$\psi(z) = A \cos kz \quad |z| < L/2 \quad \text{Eq.2-3}$$

$$\psi(z) = B e^{-pz} \quad z > L/2 \quad \text{Eq.2-4}$$

$$\psi(z) = Be^{pz} \quad z < -L/2 \quad \text{Eq.2-5}$$

where

$$\varepsilon = V_c - \frac{\hbar^2 k^2}{2m_{ew}} \quad \text{in the well; } \varepsilon = \frac{\hbar^2 p^2}{2m_{eb}} \quad V_c < \varepsilon < 0 \quad \text{in the barrier} \quad \text{Eq.2-6}$$

$m_{eb}$  and  $m_{ew}$  are the relevant effective masses. From Eq.2-3 and Eq.2-4 the continuity conditions on  $\psi$  and  $d\psi/dz$  at  $Z=L/2$  yield

$$A \cos(kL/2) = Be^{-pL/2}$$

$$A(k/m_{ew}) \sin(kL/2) = (pB/m_{eb})e^{-kL/2}$$

Therefore

$$k \tan(kL/2) = \frac{m_{ew}}{m_{eb}} p \quad \text{Eq.2-7}$$

From Eq2-6, we have

$$p = \sqrt{\frac{2m_{eb}}{\hbar^2} (V_c - \frac{\hbar^2 k^2}{2m_{ew}})} \quad \text{Eq.2-7'}$$

Therefore

$$\tan(\theta) = \sqrt{\frac{m_{ew}}{m_{eb}} \left( \frac{\theta_0^2}{\theta^2} - 1 \right)} \quad \text{Eq.2-8}$$

where

$$\theta_0^2 = \frac{m_{ew} V_c L^2}{2\hbar^2}$$

$$\theta = \frac{kL}{2}$$

Eq.2-8 can be solved numerically. Taking  $m_{ew}=0.067m_0$  as the electron effective mass in GaAs,  $m_{eb}=0.087m_0$  is the electron effective mass in  $Al_xGa_{1-x}As$ <sup>46</sup>, where  $m_0=9.1 \times 10^{-31}$  kg is electron mass. A and B are arbitrary constants.

The normalised wavefunction is:

$$\psi(z) = \frac{1}{\sqrt{\frac{1}{k} + \frac{L}{2}}} \cos kz \quad |z| < L/2 \quad \text{Eq.2-3'}$$

$$\psi(z) = \frac{\cos kL/2}{\sqrt{\frac{1}{k} + \frac{L}{2}}} e^{-p(z-L/2)} \quad z > L/2 \quad \text{Eq.2-4'}$$

$$\psi(z) = \frac{\cos kL/2}{\sqrt{\frac{1}{k} + \frac{L}{2}}} e^{p(z-L/2)} \quad z < L/2 \quad \text{Eq.2-5'}$$

For electron energy level in a quantum well

$$E_e = \frac{\hbar^2 k^2}{2m_{ew}} \quad \text{Eq.2-9}$$

For holes, the situation is much more complicated due to the existence of heavy and light holes. Here we only consider the heavy hole bands and present the results. The energy levels of the heavy holes in a QW are <sup>44</sup>:

$$E_{hh} = \frac{\hbar^2 k^2}{2m_0} (\gamma_1 + \gamma_2)$$

$$\gamma_1 = 6.85(1-x) + 3.45x \quad \text{Eq.2-10}$$

$$\gamma_2 = 2.1(1-x) + 0.68x$$

When an electron and a holes recombine to create a photon, its wavelength  $\lambda$  relation can be expressed as <sup>47</sup>:

$$\frac{hc}{\lambda} = E_e - E_{hh} + E_{gw} \quad \text{Eq.2-11}$$

Therefore, we can design a quantum well to our requirement according to above theory.

### ***Photoluminescence from quantum wells***

A free electron and a free hole are created whenever a photon of energy greater than the bandgap is absorbed in a semiconductor. Photoluminescence occurs when these excited electron-hole pairs recombine to emit photons. Therefore, the wavelength of the PL signal is determined by the energy difference between electron and hole states. As described above, the electron and hole state energy difference in a QW is essentially determined by the bandgap of the well material and their first quantum state energies. However, an electron and a hole may be bound together by their coulomb attraction to create a bound electron-hole pair which is known as an exciton, just as an electron is bound to a proton to form a neutral hydrogen atom. As in the case of the hydrogen atom, this attraction leads to bound levels characterised by the binding energies of the exciton. Excitons are unstable. They will either recombine when the electron drops into the hole in the valence band, accompanied

by the emission of a photon, or disintegrate due to thermal excitation to become free electrons and holes again. At low temperatures, thermal excitation is minimal, so excitons dominate the emission process in the QWs. The resulting PL spectrum will be a narrow peak. Its central peak will then have slightly smaller photon energy than free carrier state energy difference by an amount of the exciton binding energy (effective Rydberg). The width of the peak is reduced compared to high temperature spectrum because the thermal lifetime decay of the exciton is minimised. The width will then be determined mainly by inhomogenities in well width during growth.

### ***Design considerations***

Usually, the full width at half maximum (FWHM) of PL peaks of well made QWs is less than 30meV. The photon energy separation between adjacent PL peaks should be larger than this value. On the other hand, to estimate the depth of the damage it is desirable to incorporate as many as possible different QWs. The barriers between these QWs should be thick enough in order to prevent electron wavefunction coupling between QWs. The criteria used was that probability of electrons and holes in the middle of the barriers should be less than 0.0001%.

### ***Structures***

Bearing in mind the above consideration, the photon energies for different QW thickness and associated barrier thickness for the GaAs-Al<sub>x</sub>Ga<sub>1-x</sub>As system that satisfied the uncoupling condition were calculated. The Aluminium concentration  $x$  was chosen to be 0.35. The results are listed in the Table.2-2, where  $L$  is the quantum well width,  $Z$  is the distance from the well boundary needed to satisfy the de-coupling condition,  $\Delta E$  is the energy difference between lowest electron and hole states.  $\lambda$  is the corresponding light wavelength. To satisfy energy separation condition and QW thickness of 2.0nm, 2.5nm, 3.1nm, 4.0nm, 5.0nm, 7.0nm were chosen to be at different depths. The resulting QW structure is shown in Figure 2-10.

L(nm)	Z(nm)	$\lambda$ (nm)	$\Delta E$ (ev)	Increment of $\Delta E$ (mev)
2.0*	12.7	731.53	1.6974	41
2.5*	11.1	749.64	1.6564	33.7
3.0	10.1	765.21	1.6227	27.5
3.5*	9.38	778.40	1.5952	22.5
4.0	8.85	789.52	1.5727	18.5
4.5*	8.44	798.92	1.5542	15.3
5.0	8.01	806.90	1.5389	12.9
5.5	7.82	813.69	1.5260	10.8
6.0*	7.59	819.52	1.5152	17.2
7.0	7.20	828.89	1.4980	12.7
8.0	6.90	836.02	1.4853	9.8
9.0*	6.64	841.50	1.4755	7.5
10.0	6.42	845.90	1.4680	

**Table 2-2.** Calculation results for GaAs-Al<sub>x</sub>Ga<sub>1-x</sub>As quantum well material structure.

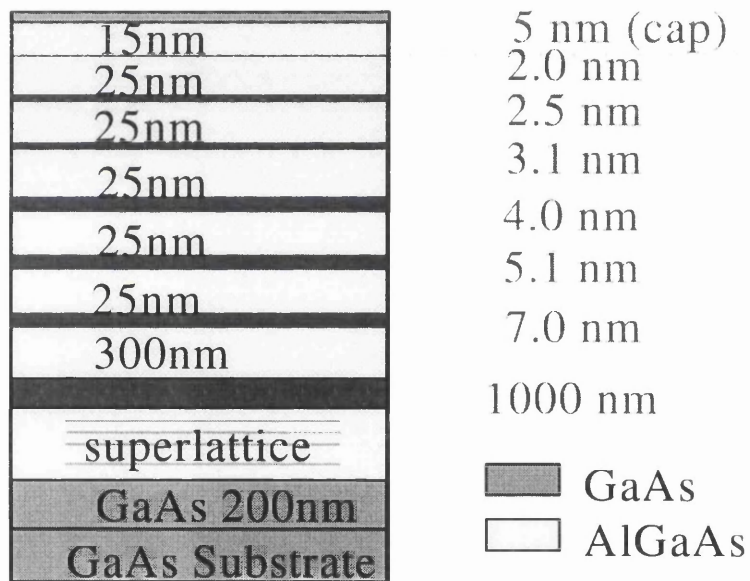


**Figure 2-10:** Layer structure of Al<sub>0.35</sub>Ga<sub>0.65</sub>As-GaAs quantum well material.

Applying above theory and considerations to InGaAs-InAlAs QW, we can also obtain a similar structure as shown in Figure 2-11. Here, lattice matched material In<sub>0.53</sub>Ga<sub>0.47</sub>As-In<sub>0.52</sub>Al<sub>0.48</sub>As was chosen to give an unstrained multiple quantum well structure. The results are listed in the Table2-3.

L(monolayer)	Z(nm)	$\lambda$ (nm)	$\Delta E$ (mev)	increment of $\Delta E$ (mev)
7	9.453	1171	1061	38
8	8.808	1204	1023	39
10	7.905	1262	984	37
12	7.306	1312	947	41
15	6.694	1372	906	30
18	6.269	1418	876	28
22	5.857	1465	848	36
31	5.247	1531	812	

**Table 2-3.** Calculation results for  $\text{In}_{0.53}\text{Ga}_{0.47}\text{As}-\text{In}_{0.52}\text{Al}_{0.48}\text{As}$  quantum well material structure.

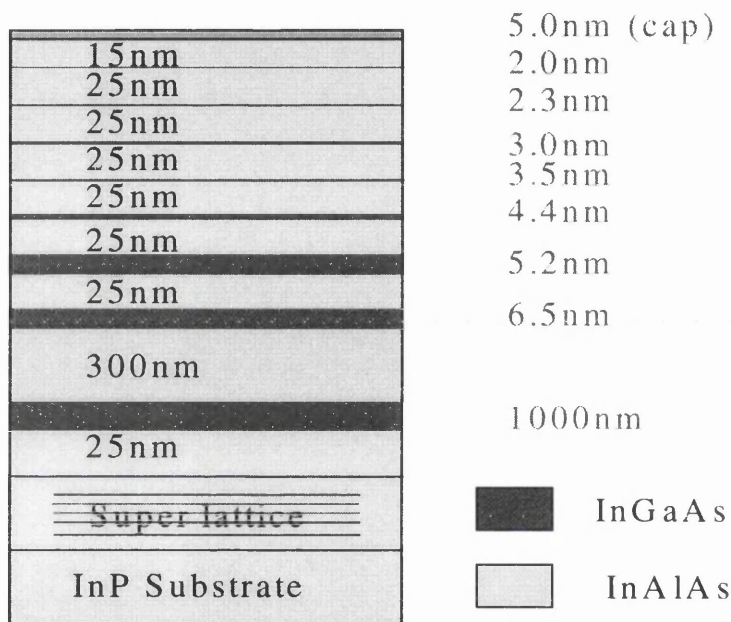


**Figure 2-11:** Layer structure of  $\text{In}_{0.53}\text{Ga}_{0.47}\text{As}-\text{In}_{0.52}\text{Al}_{0.48}\text{As}$  quantum well material.

Both multiple quantum well structures were grown on (100) semi-insulating substrates by molecular beam epitaxy in the Department. They have been used throughout the whole PhD work.

### 2.3.2 Photoluminescence measurement

PL measurement is a very sensitive tool for investigating QW characteristics. It does not require any particular sample preparation, and is a non-destructive process for analysing properties of QWs. The experiments of photoluminescence usually are carried out at low temperature ( $\leq 77\text{K}$ ).

Figure 2-12 shows the experimental set-up of the PL system used to assess ion bombardment damage. The 514.5nm line of an argon laser is focused by a microscope objective lens, giving a spot size of  $70\mu\text{m}$  diameter onto the sample

surface to excite the luminescence from QWs. The pump power density was about  $1.7 \times 10^3 \text{ W / cm}^2$ . For low temperature ( $\sim 5\text{K}$ ) PL measurement, the sample is cooled by continuously feeding liquid helium into the vacuum system where the sample is placed. Temperature is controlled by adjusting the pumping rate and the helium flow. Another lens is used to focus the PL on the input slit of the monochromator. The output luminescence from the monochromator is detected by either a liquid nitrogen cooled Ge-detector (for the InGaAs/InAlAs sample) or an photomultiplier tube (PMT) (for the GaAs/AlGaAs). The spectral data are recorded using a computer. PL intensities were recorded for both protected and ion exposed areas. In both areas the PL intensities from the deepest quantum wells have been chosen as the reference for the normalisation of the PL intensity. The normalised PL intensity indicates the relative change in the photoluminescence in the ion-bombarded regions with respect to the reference area for every quantum well.

One example of the two PL spectra for the MQW structures is shown in Figure 2-13 for a GaAs/GaAlAs sample that was etched using  $\text{SiCl}_4$ , 12W, 7mins. These spectra clear show the degradation of the first several QWs.

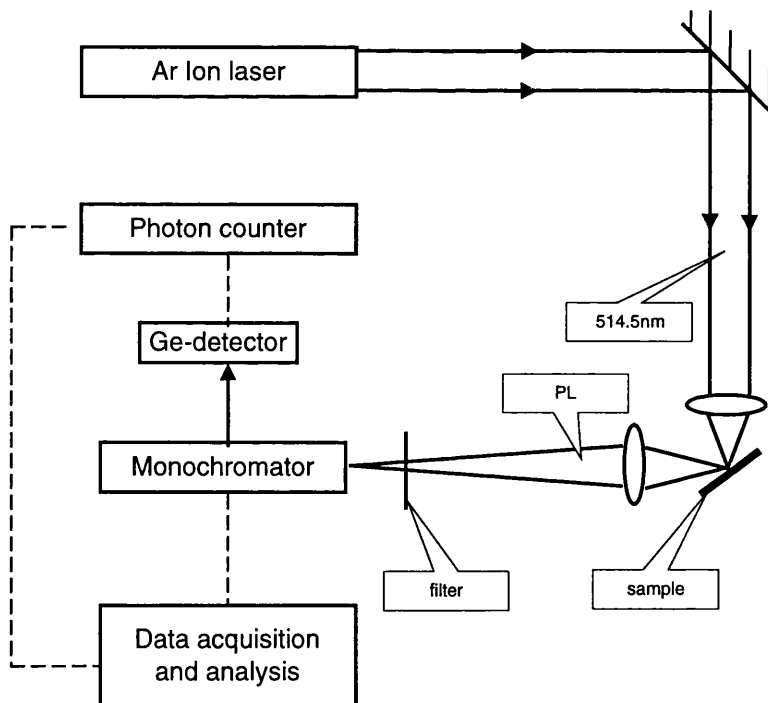


**Figure 2-12:** The experimental set-up for PL measurement.

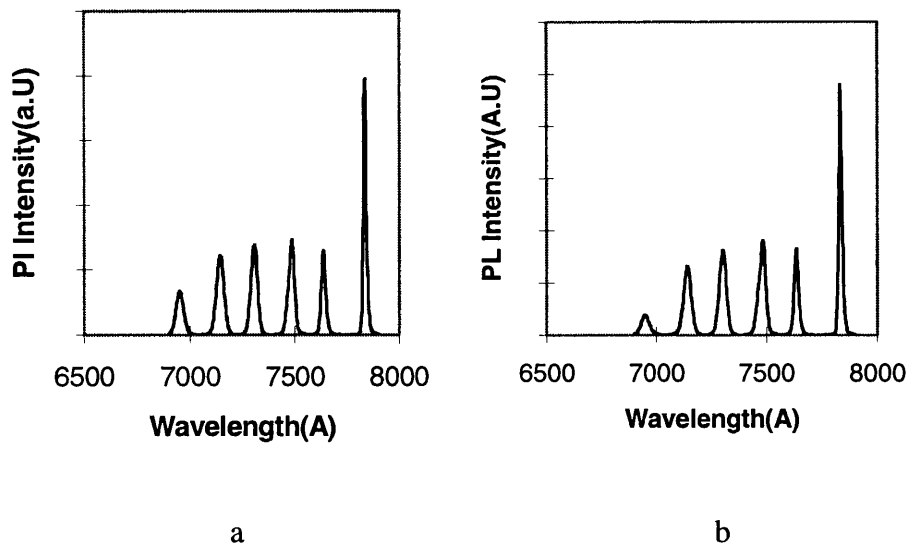


**Figure 2-13.** a) PL spectrum of the undamaged region. b) PL spectrum of damage region with  $\text{SiCl}_4$ , at 12W, 7mins.

## **2.4 Processes for Sample Preparation.**

### ***Sample preparation and cleaning***

The substrate material is cleaved into samples of the desirable size. The size of the sample depends on the dimension of the devices and the number of the devices made on the sample. It is not suitable to place too many devices on the same sample, because this would result in waste of material should the fabrication process go wrong. Yet the number of devices should neither be too few if convincing data is to be obtained from them. The sample should not be smaller than 5x5mm, otherwise the photoresist will pile up on the edges of sample during spinning

The samples are cleaned in subsequent solvent washes in an ultrasonic bath. The most popular recipe is methanol, acetone and iso-propanol (IPA), each for at least 4 minutes, follows by rinsing in abundant RO water. The sample is then blown dry with nitrogen jet.

### ***Photolithography***

Photolithography is used to transfer patterns from the designed mask to the substrate. In this work it is used to produce a mask on the sample so that, after dry-etching, comparisons can be made between the properties of the exposed and the protected areas on the semiconductor sample. It is also used to make electrode patterns for Hall effect measurement.

In the photolithography step, a thin layer of photoresist is first spun on the surface of the sample. Shipley photoresist S1805 and S1818 give a film thickness of 0.5 and 1.8 $\mu\text{m}$ , respectively, when spun at 4000rpm (revolutions per minute) for 30 seconds. The sample is brought into contact with the mask and is exposed to an ultraviolet (UV) light source for 4 seconds (S1805) and 12 seconds (S1818). The photoresist exposed to the UV light is then washed away when the patterns are developed.

### ***Lift-off***

Lift-off is an additive way of patterning thin films. The film to be patterned is deposited on the sample after the photoresist is exposed and developed. The sample is then soaked in a solvent that dissolves the photoresist. The film on the photoresist is therefore removed, leaving only the film where without photoresist.

When the film to be patterned is thick compared to the thickness of the photoresist (as is the case lift-off of ohmic contacts to make Hall measurement patterns), an undercut profile at the photoresist's edge is essential for the lift-off to be successful (Figure 2-14). This can be achieved by treating the photoresist in Chlorobenzene prior to exposure.

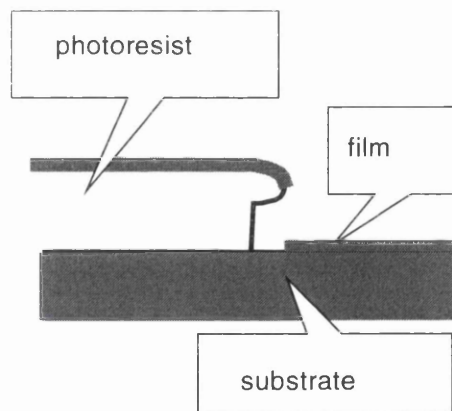


**Figure 2-14.** Undercut photoresist profile for lift-off.

## 2.5 Reference

- [1]. S. M. Sze, "Semiconductor devices Physics and Technology" John Wiley & Sons, 1985. p457.
- [2]. D Bollinger, S Iida, O Matsumoto, Solid State Technology May, 1984, p111.
- [3]. B. N. Chapman, "Glow Discharge Processes" John Wiley & Sons, 1980, p97.
- [4]. S. K. Murad, M. Rahman, N. Johnson, S. Thoms, S. P. Beaumont, and C. D. W. Wilkinson, J.Vac.Sci.Technol. **B 14**, 3658-3662 (1996).
- [5]. S. M. Sze, Jpn. J. Phys., **22**, Suppl. 22-1, 3(1983).
- [6]. M. Balooch, and D. R. Olander, J.Vac.Sci.Technol. **B 4**, 794 (1986).
- [7]. J. W. Coburn, and H. F. Winters, J. Appl, **50**, 3189 (1979).
- [8]. D. L. Flamm, and V. M. Donnelly, Plasma Chem. Plasma Proc, **1**, 317 (1981).
- [9]. J. L. Mauer, J. S. Logan, L. B. Zielinski, and G. S. Schwartz, J.Vac.Sci.Technol. **15**, 1734 (1978).
- [10]. M. B. Stern, and P. F. Liao, "J.Vac.Sci.Technol. **B 1**, p1053 (1983)
- [11]. M. B. Stern, H. G. Craighead, P. F. Liao, and P. M. Mankiewich, Appl. Phys. Lett, **45**, 410 (1984).
- [12]. J. Z. Li, I. Adesida, and E. D. Wolf, Appl. Phys. Lett, **45**, 897 (1984).
- [13]. J. Z. Li, I. Adesida, and E. D. Wolf, J.Vac.Sci.Technol. **B 3**, 406 (1985).
- [14]. M. D. Rowe, 5th Int. Conf. on Ion and Plasma assisted Techniques (IPAT), pp87 (1985).
- [15]. S. Murad, Ph.D thesis, Glasgow University (1995).
- [16]. S. C. McNevin, and G. E. Barker, J. Appl. Phys, **58**, 4670 (1985).
- [17]. A. Seabough, J. Vac. Sci. Technol., **B 6**, 77, (1998).
- [18]. C. M. Knoedler and T. F. Kuech, J, Vac. Sci. Technol., **B 4**, 1223, (1986).
- [19]. K. Hikosaka, T. Minura and K. Joshin, Jpn. J. Appl. Phys., **20**, L847, (1981).
- [20]. K. L. Seawood, N. J. Moll, D. J. Coulman and W. F. Stickle, J. Appl. Phys., **61**, 2358, (1987).
- [21]. S. Salimian and C. B. Cooper, J, Vac. Sci. Technol., **B 6**, 1641, (1988).
- [22]. S. Salimian and C. Yuen, C. Shih, C. Smith and C. B. Cooper, J, Vac. Sci. Technol., **B 9**, 114, (1991).
- [23]. S. K. Murad, C. D. W. Wilkinson, P. D. Wang, W. Parkes, C.M. Sotomayor-Torres, and N. Cameron, J.Vac.Sci.Technol. **B 11**(6), 2237-2243 (1993).

- [24]. J. B. Malherbe, *Crit ReV. Solid State Mater. Sci.* **19**, 55 (1994).
- [25] N. I. Camerson, S. P. Beaumont, C. D. W. Wilkinson, N. P. Johnson, A. H. Kean, and C. R. Stanley, *J.Vac.Sci.Technol.* **B 8(6)**, 1990, P1966-1969.
- [26]. N. P. Johnson, M. A. Foad, S. Murad, M. C. Holland, and C. D. W. Wilkinson, *Mater. Res. Soc. Symp. proc.* **325**, 443, (1994).
- [27]. M. A. Foad, S. Thoms, and C. D. W. Wilkinson, *J. Vac. Sci. Technol.* **B 11(1)**, 1993, p 20-25.
- [28]. M.Watt, C.Sotomayor-Torres, R.Cheung, C.D.W.Wilkinson, H.E.G.Arnot, and S.P.Beaumont, *J. Mod. Opt.* **35**, 1988, p365.
- [29]. P. D. Wang, M. A. Foad, C. M. Sotomayor - Torres, S. Thoms, M. Watt, R. Cheung, C. D. W. Wilkinson, and S. P. Beaumont, *J.Appl. Phys.* **71(8)**, 1992, P.15.
- [30]. R. Cheung, Ph.D thesis, Glasgow university(1992).
- [31]. H. F. Wong, D. L. Green , T. Y. Liu, D. G. Lishan, M. Bellis, E. L. Hu, P. M. Petroff, P. O. Holtz, and J. L. Merz, *J.Vac.Sci.Technol.* **B 6**, 1906-1909 (1988).
- [32]. M. A. Foad, S. Thmos, and C. D. W. Wilkinson, *J.Vac.Sci.Technol.* **B 11**, 20-25 (1993).
- [33]. K. L. Seaward and N. J. Moll, *J.Vac.Sci.Technol.* **B 10**, 46 (1992).
- [34]. K. L. Seaward, N. J. Moll and W. F. Stickle, *J. Electron. Mater.* **19**, 385 (1990).
- [35]. T. L. Cheeks, M, L, Roukes, A. Scherer, and H. G. Craighead, *Appl. Phys. Lett.* **53**, 1964 (1998).
- [36]. R.Germann, A. Forchel, M.Bresch, and H.P. Meier, *J.Vac.Sci.Technol.* **B 7**, 1475 (1989).
- [37] N. G. Stoffel, *J. Vac. Sci.Technol.* **B 10**, 651-658 (1992).
- [38]. S. K. Murad, S. P. Beaumont, M. Holland and C. D .W. Wilkinson, *J. Vac. Sci. Technol.* **B 13**, 2344 -2349 (1995).
- [39]. S. K. Murad, C. D. W. Wilkinson, and S. P. Beaumont, *MNE* **23** , 357-360 (1994).
- [40]. D. L. Green, PHD thesis, University of California at Santa barbara. (1994).
- [41] John H. Davies, “ The physics of low dimensional semiconductors”, Cambridge University Press, 1998. P.93.
- [42]. Scott W. Corzine, Ran-Hong, and Larry A. Coldren, “Quantum well lasers”, Jr. edit, Academic Press, P79, 1993.

- [43]. R. C. Miller, A. C. Gossard, D. A. Kleinman, and O. Munteau, Phys. Rev. **B** **vol.29**, 7085, 1984.
- [44]. R. C. Miller, A. C. Gossard, and D. A. Kleinman, Phys. Rev. **B** **vol.29**, 3740, 1984.
- [45]. C. Weisbuch, and B. Vinter, “ Quantum semiconductor structures”. Academic Press, 1991, P13.
- [45]. Sadao Adachi, “ Properties of Aluminum Gallium Arsenide”, Shorter Run Press Ltd, 1993.
- [46]. Rechar H. Bube, “Electrons in solid”, Academic Press, 1987, Second edition.

## Chapter 3

### Theoretical modelling

#### 3.1 Introduction

Several models have been built up over the years to simulate the general effects of processes in which ions bombard semiconducting materials. These processes can generally be divided into high ion energy and low ion energy processes.

#### *High Ion Energy Processes*

A number of models<sup>1-5</sup>, such as TRansport of Ions in Matter (TRIM), exist for predicting the range of incident ions with high energies in the range typically used in ion implantation. At high ion energies, ions not travelling in or close to a crystallographic direction of high symmetry (100, 111, 110, etc) suffer a random scattering process. As a result, they penetrate an average depth (the range) into the material, but there is a Gaussian distribution (the straggle) of their final position around this average depth. This is illustrated in Figure 3-1.

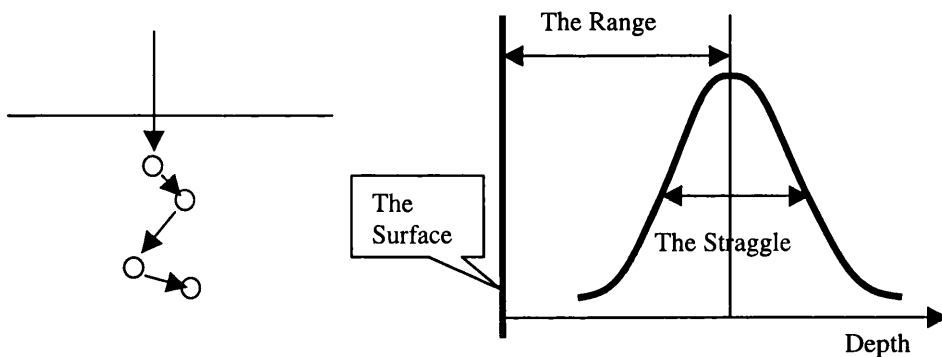


**Figure 3-1** (a) The scattering process of an implanted ion. (b) The Gaussian distribution of implanted ions in the material.

However, ions travelling in or close to a crystallographic direction of high symmetry will 'see' openings in the lattice around the high symmetry direction, and they travel down this direction suffering very few collisions. This effect, in which the ions are 'guided' by the lattice potential along certain crystallographic directions, is known as

channelling. There is a critical angle of acceptance around the crystallographic directions for incident ions to channel. This angle decreases with increasing ion energy. In ion implantation, channelling is usually avoided by implanting a few degrees off crystallographic directions.

### ***Low Ion Energy Processes***

Typical etching processes always take place at lower energies (<500eV). The ions in general also suffer a chain of random collisions but the range is very short. However a small proportion of ions, after the first collision, are correctly aligned so that they channel. The role of channelling becomes important at low ion energies because of its longer range than implantation and the larger acceptance angle for channelling. The channelling ion trajectory avoids direct impact with lattice ions, which serve instead to create a guiding potential, like a gutter, that stabilises the ion motion. The guiding influence of the channel potential is countered by destabilising forces arising from random lattice and electron density fluctuations in the crystal, which act to increase the energy transverse to the channelling direction. If the transverse energy exceeds some critical energy, the ion will dechannel.

Above high energy models breakdown at these lower energies because these effects have not been taken into account. To address this problem, Stoffel<sup>6</sup> *et al* have performed molecular dynamics simulations of channelling under dry-etch conditions with a so-called Scattering of Heavy, Low Energy Ion into CHannels model- SCHLEICH. It takes into account the probability that incident ions channel through different lattice directions and has been very useful in understanding damage producing mechanisms at ultra-low energies. However such a simulation could not completely explain the experimental damage profiles in GaAs, so Chen, Green, and Hu<sup>7</sup> have incorporated defect diffusion into this simulation to form the Channelling And Diffusion in Ion Damage-CHANDID-model.

M.Rahman has developed a microscopic theory of dechannelling<sup>9-12</sup>. This is an analytic model which incorporate both channelling and diffusion mechanisms. It is able to estimate the damage inflicted by various ionic species under dry-etch conditions. It benefits from Stoffel's simulations together with a knowledge of channelling behaviour

at higher energies<sup>13,14</sup> to deal with channelling effect at ultra-low energies analytically. The major parameter affecting damage depth-the mean channelling length-can be calculated by solving a Folkker-Planck equation.

In this chapter, a basic description of the both SCHLEICH and CHANDID is given. Then, detailed analytic expressions of Rahman's model are presented, followed by a comparison of the simulation results for the channelling of low energy RIE ions into layered MQW structure samples.

### **3.2 SCHLEICH MODEL and CHANDID MODEL**

The SCHLEICH model is a Monte Carlo model developed by N.G.Stoffel to describe channelling of < 1keV ions into layered, zincblende materials<sup>6, 15</sup>.

The existing high energy models, which rely on simple classical continuum models or binary-collision Monte Carlo methods, do not predict the depth of the damage observed in RIE of III-V semiconductors<sup>28, 30</sup>. In the high energy, simple classical continuum models, the discrete atomic nature of the channel walls are ignored, so the calculations consider only the average atomic potential along the channel axis. In the high energy, binary-collision Monte Carlo models the ion-lattice interactions are calculated as a sequence of straight-line, isolated scattering events. These two methods are accurate for the higher ion energy regime, where the period of the lattice atomic lateral forces along the channelling axis is much greater than the de Broglie wavelength of the ion. However in the lower ion energy, Germann's experiments in 1989<sup>17</sup> showed the importance of the effects of low energy ion channelling during dry etching. They measured the PL efficiency of GaAs quantum wells as a function of the energy and incidence angle of an Ar ion etching beam. They report a decrease in PL efficiency in quantum wells much deeper than the ion penetration range (as calculated from TRIM) when the Ar ions are incident close up  $15^\circ$  of the <011> crystal channelling directions. There was no similar increase in ion damage along the <001>, <112>, or <111> directions. Stoffel<sup>6</sup> has confirmed the < 110> axis in diamond /zinc-blend lattices permits channelling readily. Theoretically, at low energies the de Broglie wavelength of the incident ions becomes comparable to the lattice period, so the channelling ions are likely to interact strongly with the lattice. In other word, the oscillation of the ions is close to resonance with the

periodic lateral potential, the ion trajectory in the channel will be unstable, and a destabilising resonance condition should define a minimum energy for channelling along a particular axis<sup>6</sup>. Therefore, low energy ion channelling must be described with a model that includes the effect of the interactive potential, and interactions with the nearby lattice atoms must be simultaneously treated. N. G. Stoffel developed SCHLEICH in this manner.

SCHLEICH is a molecular dynamics simulation program written in FORTRAN. The program models the target substrate as a semi-infinite zincblende lattice of independently vibrating atoms, having random thermal energies. Alloy layers (for example GaAlAs) are defined by random placements of the constituent atoms. Figure 3-2 is a reproduction of Soffel's simulation plot<sup>6</sup> for the channelling of 1000eV Ar ions into GaAs. For this simulation the ions are incident normal to the (001) target surface. While the majority of the low energy ions stop in the near surface region, deep channelling of the remaining ions along the <011> crystallographic directions is evident. In fact, simulations show that the <011> channel is the only direction in III-V material that allows the deep channelling of low energy ions. The <011> channel is highly symmetric and is the most "open" direction in zincblende structures.

The simulated ion profiles are plotted<sup>18</sup> in Figure 3-3. This simulation was run for 100000 Ar ions with an energy of 1000eV into AlGaAs, with the ions initially incident along the <001> direction. Figure 3-3 shows that the largest concentration of ions is within 100Å of the surface, yet some ions do channel to a distance of 600Å into the material. D. L. Green has used this model into her experiment<sup>8,19</sup>. She found that the SCHLEICH MODEL describe in vary conditions the channelling dynamics of low energy ions into III-V materials than did TRIM; however the predicted ranges are still less than the observed damage ranges of the MQW probe studies by a factor of two.

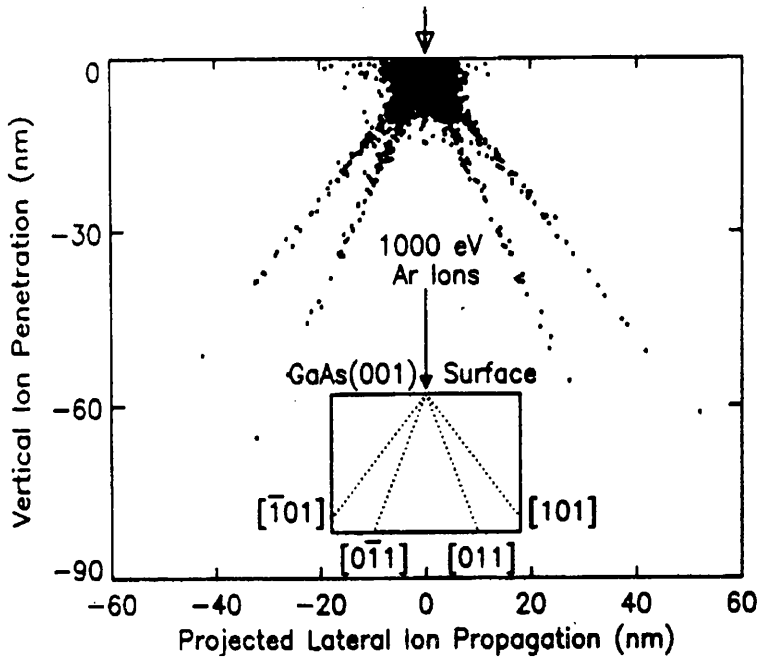


**Figure 3-2.** A reproduction of N. G. Stoffel's simulation plot showing the channelling of 1000eV, Ar ions into the  $\langle 011 \rangle$  directions of GaAs.

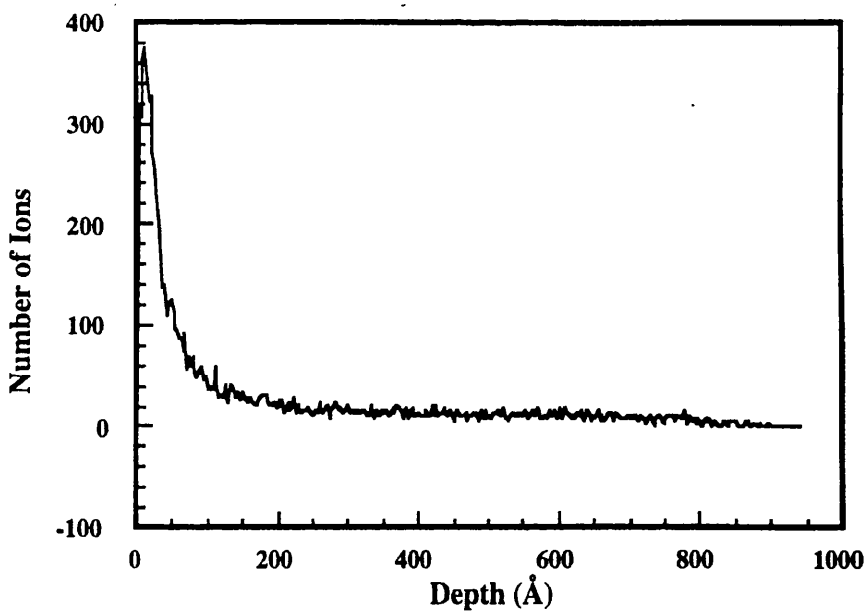


**Figure 3-3.** SCHLEICH simulation data for 100000 Ar ions with an energy of 1000eV channelling along the  $\langle 011 \rangle$  direction of AlGaAs ( $x = 0.35$ ), showing the number of the ions.

On the other hand, the experiments carried out by Green *et al*<sup>8</sup> in 1993, in which samples were bombarded by an Argon beam at 400eV constant dose but with varying exposure times, showed increasing damage with increasing exposure time. In another very interesting experiment, Chen *et al*<sup>20</sup> observed the damage in a series of GaAs/AlGaAs quantum wells at different depths caused by etching in Argon, with and without red light being projected on the sample during etching. They found that the depth of damage was increased if the illumination was present. It was therefore believed that defect diffusion plays a very important role in forming the damage distribution. For this reason, Chen *et al*<sup>21</sup> developed a model called CHANDID (Channelling AND Diffusion in Ion Damage) which includes both channelling and diffusion effects.

In the CHANDID model, the effects of the channelling and diffusion as two independent processes were considered. The diffusion process is superimposed on the channelling profile provided by SCHLEICH. This profile after channelling,  $S(x, t)$ , forms the initial condition,  $N_1(x, t)$ , ( $x$  is the direction into the substrate surface, with  $x = 0$  at the substrate surface) and the following diffusion equation was solved by a finite difference method:

$$\frac{\partial N_j(x, t)}{\partial t} = D_k \frac{\partial^2 N_j(x, t)}{\partial x^2}$$

Where  $k = 1, 2$  and  $D_1 = D_{eff}$ ;  $D_2 = D_{eff, sl}$  stand for diffusion coefficients with and without a superlattice structure near the sample surface. In each step the following calculation is carried out:

$$N_j(x, t) = N_{j-1}(x, t) + S(x, t)$$

where  $j = 1, 2, 3, \dots$ ,  $S(x, t)$  is the channelling profile, provided by SCHLEICH.  $N_j(x, t)$  is the defect distribution at the  $j$ th time interval. The boundary conditions are the following:

$$(1) N_j(x, t) \rightarrow 0 \text{ as } x \rightarrow \infty$$

(2) the diffusion flux of ions,

$$D_k \frac{\partial N_j(x, t)}{\partial x}$$

is continuous at the interfaces between the superlattice and the AlGaAs.

In this model, although in fact the spatial distribution of various defects, such as interstitial and vacancies, will differ from the distribution of the ions themselves, for simplification it is assumed that the distributions are identical. Three other assumptions were also made. The first was that the effective defect diffusion coefficient,  $D_{eff}$ , was equal within both the GaAs and AlGaAs material, although different defects might well have differing diffusion coefficients which vary for GaAs and AlGaAs. The second was that the effect of the superlattice was modelled by using an effective diffusion coefficient  $D_{eff,sl}$  characteristic of the diffusion of the defects within the superlattice region, and  $D_{eff,sl} \ll D_{eff}$ . The third assumption was that the diffusion coefficient was constant and independent of the local density of hole-electron pairs created by the ion flux.

The value of the diffusion coefficients,  $D_{eff}$  and  $D_{eff,sl}$ , were chosen to be the best fit to the experimental data. With an argon ion energy of 500eV, the value of  $D_{eff}$  in GaAs material was  $\sim 3 \times 10^{-15} \text{ cm}^2 / \text{s}$ , and  $D_{eff,sl}$  was around  $\sim 10^{-17} \text{ cm}^2 / \text{s}$ <sup>21</sup>. These values are much higher than the diffusion coefficient for defects in GaAs at room temperature without radiation.

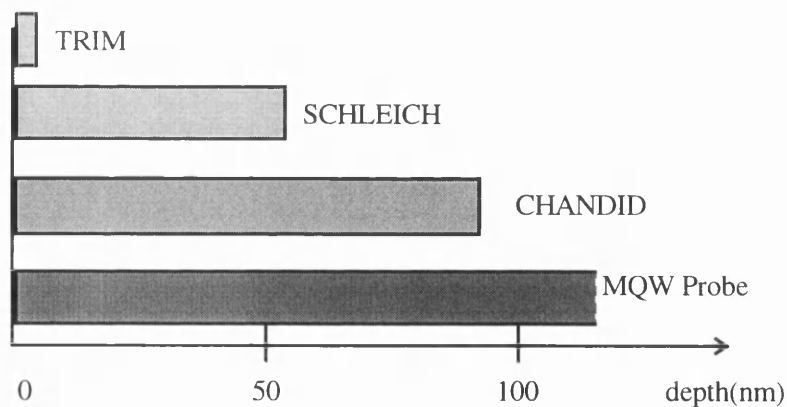


**Figure 3-4.** A summary of the range of ion damage for 500eV argon ion bombardment, experimentally observed from MQW probe and calculated by TRAM, SCHLEICH, CHANDID models<sup>7</sup>. The range is taken as the penetration distance of the last ion with  $10^4$  incident.

Figure 3-4 shows a comparison of the damage distributions simulated using the CHANDID and SCHLEICH models. The sample has been bombarded by 500eV argon ions for 3 minutes. The CHANDID simulation predicts a higher defect concentration deeper in the substrate due to the introduction of diffusion effects.

The range of ion damage for 500eV argon ion bombardment as observed using MQW probe is also shown in Figure 3-4.

### **3.3 Rahman's model**

A microscopic theory of dechannelling<sup>10, 12</sup> has been developed to calculate the mean channelling distance of low energy ions along <110> directions of semiconductor materials and give a distribution of etch induced defects by M. Rahman. The model can incorporate both channelling and diffusion contributions to dry-etch damage distributions at ultra-low energies.

In the following sections the creation of ion-induced damages in III-V substrates will be discussed using Rahman's model. Channelling in the low energy regime (less than a few keV) will be discussed and how it can lead to defect creation deep beneath the material surface. Then an expression for the defect distribution beneath dry etched plane surfaces will be given by solving a diffusion equation.

#### ***Plasma discharge***

In a typical etch chamber such as the RIE 80 system described in previous sections, the plasma discharge is generated by high frequency excitation, usually at 13.56 MHz. The electric field across the sample sheath draws ions from the discharge region to bombard the samples. Assuming the ions accelerate without collision across the sheath, the ion current impinging upon the sample is given by the Child-Langmuir relation<sup>22</sup>

$$J_i = \frac{4\epsilon_0}{9} \left( \frac{2e}{M} \right)^{1/2} U_0^{3/2} \frac{1}{d^2} \quad \text{Eq 3-1}$$

Where M is the ion mass, d is the sheath thickness, e is the electronic charge and U<sub>0</sub> is the dc self-bias.

#### ***Defect creation rate***

As suggested, deep defect penetrations is thought to be due to the channelling of ions, which can occur when an ion is injected into a crystal along a low-index direction.<sup>6, 10</sup>. Ions impinging upon the sample surface have a projected range of a few nm and most will be stopped rapidly by nuclear collisions. The energy dissipated will disorder the surface region to a depth of a few nm, assuming that any oxide layer has already been etched away. A well directed ion flux passing through this disordered layer will experience multiple scattering, causing a spread in its velocity distribution which we assume as a Maxwell velocity distribution,  $f_m(\mathbf{v})$ . Only ions scattered into directions parallel to low-index axes of the crystal continue their motion. Subsequently, these ions dechannel.

At very high energies, bombarding ions initiate collision cascades leading to extended damage formation. At the much low energies used as in dry etching, the dechannelling ions create point defects and localised defect complexes. Point defects include vacancies, interstitials, vacancy-interstitial (Frenkel) pairs, and antisite defects. The typical energy required to form a Frenkel pair in GaAs, for example, is about 10 eV<sup>23,24</sup>. Defect recombination may occur and some defects may become bound to the dechannelled ions. DLTS suggests that several different deep level defects may be introduced<sup>25</sup> although their precise nature remains to be confirmed fully.

These qualitative arguments lead to an analytic approximation for the defect creation rate due to dechannelling. For simplicity we develop the arguments for a single ion species. It is assumed that there is a uniform ion flux  $J_i$  impinging upon the sample surface with distribution  $f_0(\mathbf{v}) = f_m(\mathbf{v} - \mathbf{v}_0)$ , where  $\mathbf{v}_0$  is the net drift velocity acquired by the ion as it accelerates towards the sample. Multiple scattering decreases the magnitude of  $\mathbf{v}_0$  to  $\mathbf{v}_0'$  and broadens  $f_0(\mathbf{v})$  into

$$f(\mathbf{v}) = \left( \frac{1}{2\pi\Delta_v} \right)^{3/2} \exp \left[ -\frac{(\mathbf{v} - \mathbf{v}_0')^2}{2\Delta_v} \right],$$

With  $\Delta_v > k_B T^* / M$  and  $|\mathbf{v}_0'| < |\mathbf{v}_0|$ . This distribution has an angular spread centred about the velocity  $\mathbf{v}_0'$ . It is this angular spread that permits ions to enter channels not directly in line with the original ion path.

The ions may enter into one of a number of channels. Only one set of equivalent low-index directions is considered although channelling along other axes or planes is possible. In the case of diamond or zinc-blend lattices and for the etching of the (100) surface and only set of four  $\langle 110 \rangle$  axes emanating from that surface. These have the largest aperture size for such fcc Bravais lattices and give the dominant contribution to defect creation by ion channelling at low energies<sup>6, 17</sup>.

The ions entering any one of these channels are those lying within a narrow solid angle  $\delta\Omega$ . These constitute the number  $f(\mathbf{v})\delta\Omega$ . Thus, of the original flux  $J_i$  only the fraction  $\alpha J_i$  enters  $\langle 110 \rangle$  channels., with  $\alpha \propto f(\mathbf{v})\delta\Omega$  being the probability of an ion impinging upon the sample surface actually entering a channel. Previous work<sup>6, 9</sup> have shown that  $\alpha \approx 10^{-3}$ . However, the precise value may be slightly higher if  $\mathbf{v}_0$  is aligned with a  $\langle 110 \rangle$  direction.

An ion will dechannel when its transverse energy exceeds some critical energy. Since ions enter the channel with a spread of directions, a significant fraction will dechannel close to the mouth of the channel and comparatively fewer will continue their motion deeper into the crystal. This can be approximated by the normalised probability

$$P(z) = \frac{1}{\lambda} e^{-z/\lambda_c},$$

Where  $z$  is the distance along the channel from the surface and  $\lambda_c$  is the characteristic channelling length. Therefore,  $p(z)\delta z$  is the net probability of an ion being dechanneled when it is a distance between  $z$  and  $z + \delta z$  from the mouth of the channel.

This simple form may not be perfectly accurate but it describes the essential trend of the dechannelling probability and permits the diffusion parts of the defect distribution calculation to be solved explicitly. In principle,  $\lambda_c$  may be found from a detailed examination of the kinetics of the channelling ion; it will scale with the initial velocity of the ion, which depends on the self-bias  $U_0$  and the mass  $M$ , and also with the mass through the friction coefficient governing the slowing of the ion. The expression for  $\lambda_c$  is given as follows without proof. The full analysis is in M. Rahman's paper<sup>10</sup>. Note that there are no adjustable parameters. The  $\lambda_c$  values agree with the simulations of Stoffel to  $\sim 30\%$  for energies  $\leq 1$  keV.  $\lambda_c$  has been gained by using a Fokker-Planck

equation describing the statistical behaviour of a channelled ion subject to nuclear and electronic multiple scattering<sup>10, 12</sup>.

$$\lambda_c = 4.511 \times 10^{-9} \frac{Z_1 Z_2}{D_0 a} \left[ 1.077 \times 10^5 \frac{E_0 a^2 a_{TF} (f+1) D_0 a^3}{Z_1^2 Z_2^2 u_2^2} \right]^{1/f} \quad \text{Eq 3-2}$$

$$D_0 = 3.729 \times 10^{-11} \frac{Z_1^2}{M_1 a}$$

$$f = 2.59 - 0.02 \ln Z_1 Z_2$$

$$a_{TF} = \frac{0.4693}{(Z_1^{1/2} + Z_2^{1/2})^{2/3}}$$

$$u_2 = 17.071 \times \left[ \frac{1}{M \theta_m} \left( \frac{\varphi x}{x} + \frac{1}{4} \right) \right]^{1/2}, \quad x = \frac{\theta_m}{T}$$

$$\varphi(x) = 0.9957 - 0.2448x + 0.0278x^2 - 0.0012x^3$$

where  $Z_1$ ,  $Z_2$  and  $M_1$ ,  $M_2$  are atomic numbers and masses (amu) of incident and target nuclei,  $E_0$  is the incident energy (eV),  $a$  the lattice constant,  $T$  the lattice temperature,  $\theta_m$  the Debye temperature. For GaAs, we approximate  $Z_2$ ,  $M_2$  by values for Ge and  $\theta_m$  by the Debye temperature of GaAs (320K).

Based on above description it is assumed that 1) the bombarding ion flux  $J_i$  is constant and uniform, 2) the probability of ions impinging upon the sample actually entering a channel is given by the surface transmission factor of  $\alpha \approx 10^{-3}$ , 3) the ions channel along the  $\langle 110 \rangle$  directions, which carry almost all the channelled flux in the crystal<sup>6</sup>, and 4) a single dechannelled ions results in a single defect or localised defect cluster. Therefore, the channelled flux  $\alpha J_i$  creates defects with probability  $P(z)$ , the rate of defect creation is given by  $\alpha J_i P(z)$ . We want this as a function of depth  $y$  below the

sample surface. If the channel forms an angle  $\theta$  with respect to the surface, then the rate is

$$g(y) = g_0 e^{-y/\lambda}, \quad \text{Eq 3-3}$$

$$g_0 = \frac{\alpha J_i}{\lambda_c}, \lambda = \lambda_c \sin \theta \quad \text{Eq 3-4}$$

Where  $y$  and  $\lambda_c$  are the depth below the etched surface and characteristic channelling length along  $\langle 110 \rangle$ , respectively and  $\theta$  is the angle of the channel to the surface,  $\theta = 45^\circ$  for  $\langle 110 \rangle$ .  $\lambda$  is the characteristic depth below the surface for creation of defects.

### ***Defect distribution beneath the plane surface***

An expression for the defect distribution beneath a dry etched plane surface may be obtained by solving a diffusion equation. This diffusion equation incorporates effects of defect creation at etched surface and of ion dechannelling, as well as the motion of the etched surface. The Mathematical details are given in the Appendix, where the exact solutions are written. The solutions are complicated. For plane surface etching a simpler expression for the defect distribution, valid for not too short etch times, that includes effects of diffusion is possible. Great simplification is possible for negligible diffusion.

The contribution of diffusion to the evolution of dry etch damage profiles is curious. It has been observed that this diffusion, if it occurs, does so only during the time of the etching. In other words, before and after etching the defect diffusion coefficient is negligible. This has been attributed to radiation enhanced diffusion during ion bombardment<sup>4</sup>. Sample illumination increases this effect<sup>20, 26</sup>. We will not probe into detailed microscopic mechanism for how D can attain significant values during etching, since these are not understood entirely, but will focus on what may follow as a consequence.

Defect migration introduces a number of complications. Interstitial and on-site defects such as vacancies and antisites, may possess different mobilities. Defects may aggregate, two vacancies attracting one another through their strain fields to form a di-vacancy. Also, defects may annihilate one another, an effect called annealing, so a dechannelled ion may initially create several defects but recombination may leave finally just one. For simplicity these complications are ignored and analyse problems for

only one type of defect. This is sufficient to develop a basic understanding of defect distributions.

For plane surface damage, a one-dimensional defect distribution  $n_D(y,t)$  can be obtained by solving a diffusion equation<sup>10</sup>, which is described as a function of depth  $y$  below the surface while the surface is being etched away. There are two mechanisms by which defects are created. One is due to a physical or sputtering mechanism from direct ion bombardment at the surface. Defects are created at a rate  $F$  within a distance of a few nm of the surface. If these defects did not diffuse, they would affect only the surface properties. They are removed continuously by etching (except at etch stop layers). The second is by ion dechannelling, in which case the rate of creation is given by equation 3-

3.  $g(y) = g_0 e^{-y/\lambda}$ , with  $\lambda$  being the characteristic penetration depth of channeled ions below the surface.

Both mechanisms of defect creation may be incorporated in the diffusion equation. Etching is included by defining the surface to move at a constant rate  $v$ . It is assumed that only one type of defect is created and that it diffuses with coefficient  $D$ . Mathematical details are given in Appendix. The solution for the defect density  $n_D(y)$  at depth  $y$  is

$$n_D(y) = \frac{g_0}{\gamma} e^{-y/\lambda} + \frac{1}{v} \left( F - \frac{g_0 D}{\lambda \gamma} \right) e^{-y/D} \quad \text{Eq 3-5}$$

If the etching time  $T$  is greater than  $v^2/4D$  and  $D \geq \lambda v$ , and  $\gamma = (v/\lambda)(1 - D/\lambda v)$ .

In the limit of negligible diffusion,  $D \ll \lambda v$ , the distribution  $n_D$  is governed by the simple equation

$$\frac{\partial}{\partial t} n_D(\bar{y}, \tau) = g_0 e^{-(\bar{y}-v\tau)/\lambda},$$

which is the diffusion equation, Eq.(A1a), with  $D$  set to zero. Here  $\bar{y}$  is the distance from the original surface of the material and  $y = \bar{y} - v t$  is the distance from the etched surface. Integrating the equation gives

$$n_D(y, \tau) = \frac{\lambda g_0}{v} (1 - e^{-v\tau/\lambda}) e^{-y/\lambda}. \quad \text{Eq 3-6}$$

Given the defect creation rate  $g(y)$  we therefore have two relatively simple expressions are found for the defect distribution function, one with significant diffusion (as shown Eq 3-5.) the other with negligible diffusion (as shown Eq 3-6.).

In the multiple quantum well probe technique, the intensity of the PL after ion damage at depths corresponding to the depths of the quantum wells is measured. In the earlier work of the et al, experimental results from PL and the theoretical predictions (from CHINDID etc) were compared by relating the depth at which the prediction gave the last ion of 10000 incident as dechannelling as the depth at which no change in the PL was observed.

In the present work, the explicit formula for the density of defects given by M. Rahman is used directly to predict a functional form for the expected variation of the PL intensity with well depth. This removes the somewhat arbitrary definition of predicted damage depth which Chen *et al* used and makes much better use of the information available as a prediction is made for each well.

The relationship between the destitution function  $\eta(y)$  and the PL intensity data can be found as follows. The row PL intensity  $I(y_i)$  at each well depth is normalised to the intensity without damage  $I_o$ ;

$$\eta(y_i) = \frac{I(y_i)}{I_o}.$$

This normalised PL intensity must fall to zero at some level of defects  $n_a$ .

The above equation therefore relates the PL intensities before and after exposure to the etching plasma. For selective etching the etch rate is zero. Ignoring defect diffusion a simplified equation for  $\eta_e(y)$  is then obtained from Eq 3-3, Eq 3-4, and Eq 3-5.

$$\eta_e(y) = 1 - \frac{g_0 \tau}{n_a} \ell^{-y/\lambda}, n_D < n_a, \quad \text{Eq 3-7}$$

Where  $\tau$  is the bombardment time.

This is an experimentally measurable relation by the method described in experiment section, and will be applied to various species in the etching plasma to assess their effect in causing damage.

Under typical etch conditions  $j_i \sim 4 \times 10^{13}$  ions/cm<sup>2</sup>s as estimated from the Child-Langmuir relation<sup>22</sup> and  $n_a \sim 3 \times 10^{18}$  cm<sup>3</sup> as estimated from experiments on impurity-induced disordering<sup>8, 15</sup>. Stoffel's simulations<sup>8, 15</sup> suggest  $\alpha \sim 10^{-3}$ . While the precise values of these parameters are uncertain and may deviate a few percent from what is given, the value quoted have been used here. The value of  $\lambda$  is found from the model with no adjustable parameters.

The above is valid for atomic ions. Molecular ions do not channel. Their irregular shapes and possible tumbling motion as they pass by lattice nuclei ensure rapid large-angle scattering before channelling can be began. They do not experience the smooth channel potential felt by atomic ions and so cannot penetrate to any significant depth along a low index axis. However, molecular ions may fragment into atomic ions upon impact at the surface. These secondary atomic ions may channel, but at an energy much less than that of the incident molecular ions.

From the measured PL spectra, the peak PL intensities for all the QWs in both exposed and protected regions are first normalised with respect to the peak intensity of the deepest QWs, the normalised intensity of corresponding QWs in the two regions are compared, giving a normalised PL intensity  $\eta$ <sup>27</sup>, where

$$\eta = \frac{(I_{QW} / I_{QW6})^{Exposed}}{(I_{QW} / I_{QW6})^{Unexposed}}.$$

A reduction in the normalised PL intensity  $\eta$  reflects the effect of the ion bombardment in the exposed region.

In Figure 3-5, the normalised PL intensity is plotted against QW depth. The PL was measured from a GaAs/Al<sub>0.35</sub>Ga<sub>0.75</sub>As quantum well sample which was etched by SiCl<sub>4</sub>, at 12W of power, dc self bias 80V, 4.1sccm of flow rate, and 5.8 mTorr of etching pressure. The theoretical curves were calculated from Eq 3-5 for 80eV and 20eV of C<sup>1+</sup> channelling. Here a simplified figure is given to show how the theoretical curve can relate to the experiment data. The theoretical expression given previously can be tested directly against experimental profiles. The detailed analysis of experimental data will be given in the following chapters.

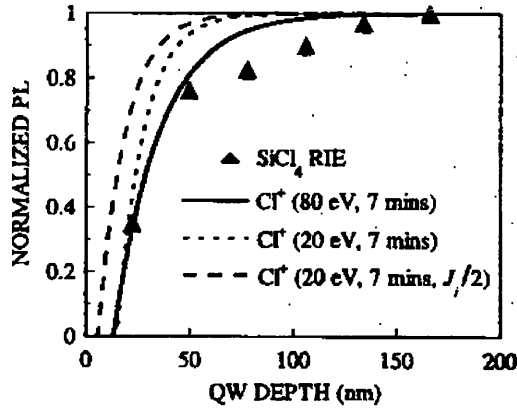


**Figure 3-5** Normalised PL Intensity from the GaAs/AlGaAs MQW material etched in low power SiCl<sub>4</sub>, dc self-bias 80V, etch time 7mins. Theoretical PL calculated for Cl<sup>+</sup> channelling is also given.

### 3.4 Summary

Theoretical models developed in different ways have been presented. Stoffel in his SCHLEICH simulation first introduced the effects of channelling. The results of this simulation approached more nearer to the results of experimental data than previous simulation such as TRIM. Chen added the effect of diffusion into Stoffel's simulations which provided much better agreement with the approximate extent of the experimental data. The analytic model developed by M.Rahman incorporates both channelling and diffusion mechanisms, and fits well to our experimental data where the experiments are carried out in real etching environments. Without differential equations to solve, calculation is straightforward by simply putting parameters into the simulation and results are obtained immediately. Comparison between theoretical calculation and experimental data can direct shown.

When using Rahman's model the effect of diffusion is often ignored. This is because Equation 3-5 shows that diffusion by itself cannot account for deep damage. Setting  $g_0 = 0$ , thereby suppressing the channelling contribution, gives the steady-state distribution  $n_D(y) = (F/v)e^{-yv/D}$ . As an example, at an etch rate of 60nm/min.,  $D = 10^{-13} \text{ cm}^2 / \text{ s}$  would be required for the defects to penetrate to a characteristic depth

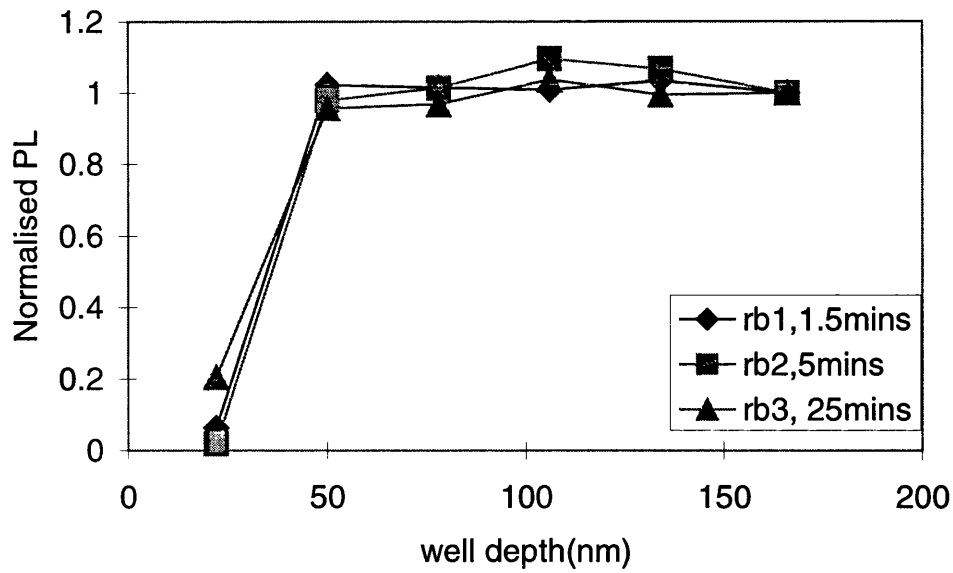
of only  $\sim 10\text{nm}$ . Such a high value of  $D$  is not practical and would require considerable sample heating during etching, which is known not to happen. Samples on temperature-controlled electrodes, for example, still show deep damage<sup>28</sup>. Therefore, even if the principle of distribution of etching damage may haven't yet been entirely understood, it may still be said that diffusion cannot be the primary factor in forming deep damage in the etched materials, particularly with ultra low ion energy ( $< 500\text{eV}$ ).

An experiment intended for studying the diffusion effect by varying the ion exposure time while keeping the exposure dose constant is described below. The samples were etched at University of California at Santa Barbara (UCSB) and PL measurements were carried out at University of Glasgow.

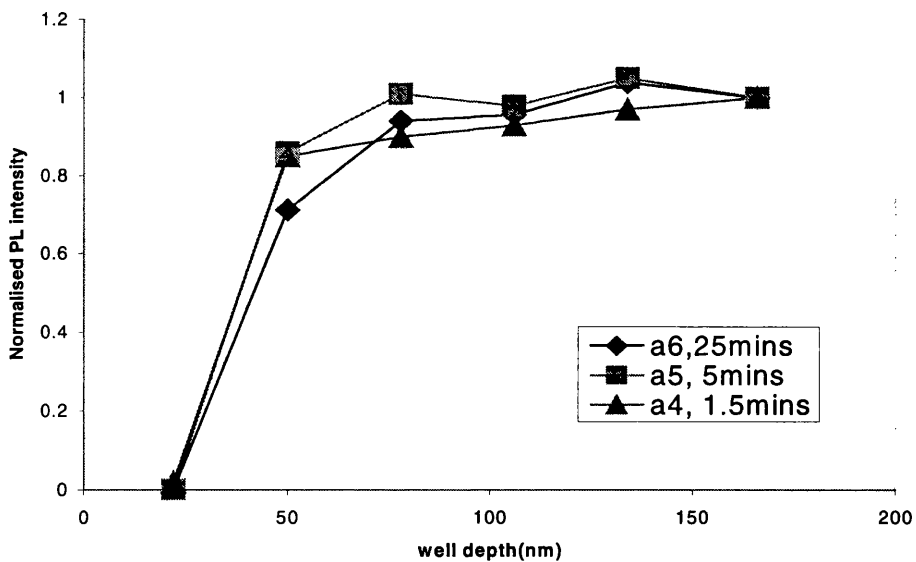
In this experiment, GaAs/AlGaAs quantum well samples (structure shown in chapter 2) were bombarded by constant dose of argon ion beam at  $140\text{eV}$ ,  $300\text{eV}$ , and  $500\text{eV}$  respectively, with varying exposure times. Ar ion beams from the radical-beam ion beam etching (REIBE) system of above energies have been used at normal ion beam incidence. Exposure times of 1.5, 5, and 25 minutes, and correspondingly ion current density at 100, 30,  $6\mu\text{A}/\text{cm}^2$  have been used to maintain a constant total integrated ion dose of  $5 \times 10^{16} \text{cm}^{-2}$ .

Figure 3-6 shows the damage profiles that were observed with each increase in the exposure time (and the associated decrease in the ion current) at Argon ion energy of  $140\text{eV}$ . In Figure 3-6, the longest exposure time gave **less** damage in QW1, but similar extent of damage are produced for exposure times of 1.5, and 5 minutes.

Figure 3-7 shows damage profiles for the Argon ion bombardment of  $300\text{eV}$ . From this figure, it is shown that almost same extent of damage in the QW1 was sustained for different exposure times, but longest exposure did cause more damage in QW2.



**Figure 3-6.** Damage profile for GaAs/AlGaAs MQW following Ar ion beam exposures at 140eV, 1.5, 5, and 25 minutes respectively, to maintain a constant integrated ion dose of  $5 \times 10^{16} \text{cm}^{-2}$ .



**Figure 3-7.** As in Figure 3-6 but Ar energy at 300eV.

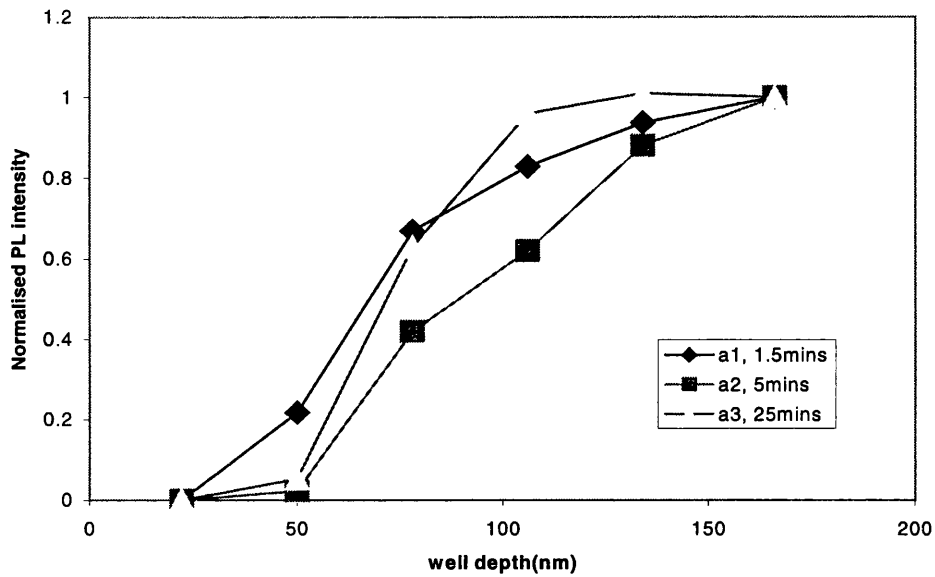


**Figure 3-8.** As in Figure 3-6 but Ar energy at 500eV.

Figure 3-8, in which samples have been bombarded at 500eV with 1.5, 5, 25 minutes, shows that the more damage was given by Ar bombardment of 5 minutes rather than 25 minutes.

Therefore, from these experimental data there is no conclusive evidence on the effect of diffusion, which should increase with exposure time. This is contrary with the earlier results of the same experiment obtained by Chen, which showed more damage in longer exposed samples<sup>7</sup>.

Figure 3-4, taken from Chen *et al*<sup>28</sup>, shows more than 40nm difference in theoretical final ion-induced damage depth with and without consideration of diffusion effect (i.e., between the SCHLEICH and CHANDID results), even though  $D_{eff}$  was chosen around  $3 \times 10^{-15} \text{ cm}^2 / \text{ s}$ , 100 times lower than value of  $D$  in Rahman's simulation. However in the above experiment intended to highlight the effect of diffusion by the using same Argon ion dose and same energy of bombardment at varied exposure times, we have not observed much difference in damage profile. So, the extent of diffusion is still somewhat unclear.

A number of experiments together with theoretical simulations, have confirmed the important role played by fortuitous channelling of ions, deep into the material. It is now accepted that the primary mechanism for deep defect creation in crystalline material is channelling. However there is no exclusive experimental evidence for the role of diffusion and its extent in deep damage, particularly in ultra-low ion energies, and whether other mechanisms also contribute to the final distribution of deep damage. Further investigations are needed here.

### 3.5 References

- [1]. M. Taneya, Y. Sugimoto, and K. Akita, *J. Appl. Phys.* **66**, 1375 (1989).
- [2]. K. L. Seaward and N. J. Moll, *J. Vac. Sci. Technol. B* **10**, 46 (1992).
- [3]. K. L. Seaward, N. J. Moll, and W. F. Stickle, *J. Electron. Mater.* **19**, 385 (1990).
- [4]. J. Weber, *Physica B* **170**, 201 (1991).
- [5]. J. F. Ziegler, J. P. Biersack, and U. Littmark, "The stopping and range of Ions in solid", ed. by J. F. Ziegler, pergamon Press, New York, (1985).
- [6]. N. G. Stoffel, *J. Vac. Sci. Technol. B* **10**, 651-658 (1992).
- [7]. Ching-Hui Chen, Debora L. Green, and E. L. Hu, *J. Vac. Sci. Technol. B* **13**, 2355-2359 (1995).
- [8]. D.L. Green, E. L. Hu, and N. G. Stoffel, *J. Vac. Sci. Technol. B* **12**, 3311 (1994).
- [9]. M. Rahman, N. P. Johnson, M. A. Foad, M. C. Holland and C. D. W. Wilkinson, *Appl. Phys. Lett.* **61**, 2335-2337, (1992).
- [10] M. Rahman, *J. Appl. Phys* **82** 2215 (1997).
- [11] M. Rahman, *PRB* **52**, 3383 (1995).
- [12] M. Rahman, " Microscopic theory of channelling-mediated ion penetration in dry-etched semiconductors". (unpublished).
- [13]. J. Lindhard, *K. Dan. Vidensk. Mat. Fys. Medd.* **34**, 1 (1965).
- [14]. N. Matsunami and L. M. Howe, *Radiat. Eff.* **51**, 111(1980).
- [15]. N.G. Stoffel, S. A. Schwartz, M. A. A. Pudensi, K. Kash, L. T. Florez, J. P. Harbison, and B. J. Wilkens, *Appl. Phys. Lett.* **60**, 1603 (1992).
- [17]. R.Germann, A. Forchel, M.Bresch, and H.P. Meier, *J. Vac. Sci. Technol. B* **7**, 1475 (1989).
- [18]. D. L. Green, PHD thesis, University of California at Santa barbara. (1994).
- [19]. D. L. Green, E. L. Hu, P. M. Petroff, V. Liberman, M. Nooney, and R. Martin, *J. Vac. Sci. Technol. B* **11**(6), 2249 (1993)
- [20]. Ching-Hui Chen, D. L.Green, and Evelyn L. Hu, *Appl. Phys. Lett* **69** (1), 58 (1996)
- [21]. Ching-Hui Chen . PHD thesis, University of California at Santa barbara. (1997).
- [22]. B. N. Chapman, *Glow Discharge Processes* (Wiley- Interscience, New York, 1988).

- [23]. J. C. Bourgoin and H. J. von Bardeleben, *J. Appl. Phys.* **64**, R65(1988).
- [24]. H. Lim, J. von Bardeleben, and J.C. Bourgoin, *Phys. Rev.Lett.***58**, 2315(1987).
- [25]. D. Lootens, P. van Daele, P. Demeester, and P. Clauws, *J. Appl. Phys.* **70**, 221 (1991).
- [26]. Ching-Hui Chen, D. G. Yu, Evelyn L. Hu, and Petroff, *J. Vac. Sci. Technol.* **B14**, 3684(1996).
- [27]. L. G. Deng, M.Rahman, S. K. Murad, A. Boyd, and C.D.W.Wilkinson, *J. Vac. Sci. Technol.* **B 16**, 3334(1998).
- [28]. Evelyn L. Hu, Ching-Hui Chen, and D. L. Green, *J. Vac. Sci. Technol.* **B 14**(6), 3632 (1996).
- [29]. *Handbook of Mathematical Functions*, edited by M. Abramowitz and I. A. Stegun (Dover, New York, 1970).
- [30]. S. K. Murad, M. Rahman, N. Johnson, S. Thoms, S. P. Beaumont, and C. D. W. Wilkinson, *J.Vac.Sci.Technol.* **B 14**, 3658-3662 (1996).

## APPENDIX A: PLANE-SURFACE DAMAGE

Here we calculate the one dimensional defect distribution at an etched plane surface, assuming that the defects created at the surface and by dechanneled ions diffuse with coefficient  $D^{10}$ . The surface is etched away at a constant rate  $v$ , so we must solve a one - dimensional diffusion equation with a moving boundary. A closely related example is that of dopant diffusion during the growth of thermal oxide on silicon. Moving boundary problems in a more complicated form are known in thermal physics as Stefan problems.

The defect density  $n_D(y, t)$  must satisfy the diffusion equation

$$\left(\frac{\partial}{\partial t} - D \frac{\partial^2}{\partial y^2}\right) n_D(y, t) = g(y - vt) \quad , \quad (A1a)$$

where  $y \geq vt, t \geq 0$ . There are no defects at  $t = 0$  and the defect flux at the etched surface is defined as

$$n_D(y, 0) = 0, \quad -D \frac{\partial n_D}{\partial y}(vt, t) = F. \quad (A1b)$$

The flux  $F$  represents the creation of defects directly at the surface being etched and it is assumed that the bombardment is uniform and constant during the period of the etching. Defect creation due to dechannelling is represented by  $g(y) = g_0 e^{-y/\lambda}$ , derived in chapter 3.

It is useful to solve this problems using Laplace transforms, for the domain  $y \geq 0, t \geq 0$ .

This is obtained by shifting to a frame moving with the etched surface using the Galileo transformation  $(y, t) \rightarrow (y + vt, t)$ . In Laplace space, the solution is

$$\tilde{n}_D(y, s) = \tilde{n}_1(s) + \tilde{n}_2(s) + \tilde{n}_3(s) \text{ with}$$

$$\tilde{n}_1 = \frac{g_0 e^{-y/\lambda}}{s(s + \gamma)}, \quad \tilde{n}_2 = \frac{g_0 e^{-\zeta y}}{\lambda s(s + \gamma)\zeta}, \quad \tilde{n}_3 = \frac{F e^{-\zeta y}}{D s \zeta},$$

where  $\gamma = (v/\lambda)(1 - D/\lambda v)$  and  $\zeta = (v + \sqrt{v^2 + 4Ds})/2D$ . Inverting gives

$$n_1(\tau) = \frac{g_0}{\gamma} e^{-y/\lambda} (1 - e^{-\gamma\tau}), \quad (A2a)$$

$$n_2(\tau) = -\frac{D g_0}{\gamma \lambda} \int_0^\tau dt [1 - e^{-\gamma(\tau-t)}] G(y, t), \quad (A2b)$$

$$n_3(\tau) = F \int_0^\tau dt G(y, t), \quad (A2c)$$

$$G(y, t) = \frac{\exp(-\xi_t^2)}{\sqrt{\pi D t}} - \frac{v}{2D} \operatorname{erfc} \xi_t, \quad (A2d)$$

where  $\operatorname{erfc}$  is the complementary error function and  $\xi_t = (y + vt) / 2\sqrt{2Dt}$ . To obtain  $n_2(\tau)$  and  $n_3(\tau)$  it is expedient to use the convolution theorem together with Eq. (29. 3. 88) of Abramowitz and Stegun<sup>29</sup>. Denoting  $\tau$  as the etch time and  $y$  as the depth below the etched surface gives, finally,  $n_D(y, \tau) = n_1(\tau) + n_2(\tau) + n_3(\tau)$ . This is the exact solution to Eqs. (A1).

One very useful approximation results from a small- $s$  expansion of the laplace space function  $\tilde{n}_D(y, s)$ . Taking  $s \rightarrow 0$ , corresponding to the condition  $\tau \gg v^2 / 4D$ , gives  $e^{-\zeta y} \approx e^{-y v / D}$  and  $1 / \zeta \approx v / (s + b)$ , where  $b = v^2 / D$ . Then  $\tilde{n}_2(s)$  and  $\tilde{n}_3(s)$  simplify

$$\text{to } \tilde{n}_2 \approx -\frac{g_0 v e^{-y v / D}}{\lambda s (s + \gamma) (s + b)}, \quad \tilde{n}_3 \approx \frac{F v e^{-y v / D}}{D s (s + b)}.$$

Inverting yields

$$n_D(y, \tau) = \frac{g_0}{\lambda} e^{-y/\lambda} (1 - e^{-\gamma\tau}) - \frac{g_0 v}{\lambda} e^{-y v / D} \left[ \frac{1}{\gamma b} - \frac{e^{-\gamma\tau}}{\gamma(b - \gamma)} - \frac{e^{-b\tau}}{b(\gamma - b)} \right] + \frac{F}{v} e^{-y v / D} (1 - e^{-b\tau}). \quad (A3)$$

From this approximate solution the limits of steady state ( $\tau \rightarrow \infty$ ), zero channelling ( $g_0 = 0$ ), and zero surface defect creation ( $F = 0$ ) are easily obtained. An expression valid for zero defect diffusion ( $D \rightarrow 0$ ) is most readily obtained from the original Eq. (A1) as shown in chapter 3. Noting that  $\gamma$  becomes zero for the special etch rate when  $D = v \lambda$ , it appear that  $n_1(\tau)$  diverges. In fact, by Taylor expanding  $e^{-\gamma t}$  it is easy to show that it actually grows linearly with time.

## Chapter 4

### Low damage reactive ion etching of GaAs/AlGaAs and InGaAs/InAlAs.

#### 4.1. Introduction

Dry etch damage has been investigated by many different techniques. Much quantitative understanding has been gained for relatively simple situations, where a single ion species predominates the etch process<sup>1-4</sup>, as detailed in prior chapters. However with present materials processing often demanding the use of multi-component glow discharges<sup>5,6</sup>, it is of urgent interest to understand in greater detail damage production in such cases. The presence of both atomic and molecular ions in the discharge is the main complication. In this and following chapters, this situation will be investigated. The processes involved are low damage RIE processes for GaAs/AlGaAs and InGaAs/InAlAs materials, respectively. These processes have been developed in the University of Glasgow and been widely used in the fabrication of both electronic and optoelectronic devices.

In order to investigate these processes, specially designed GaAs/Al<sub>0.35</sub>Ga<sub>0.65</sub>As and In<sub>0.53</sub>Ga<sub>0.47</sub>As/In<sub>0.52</sub>Al<sub>0.48</sub>As multiple quantum well layers (described in Chapter 2) have been dry etched in these reactive ion etching environments. The technique of selective etching<sup>5,6</sup> has been used as a way to damage material for long periods without changing the etch depth. In this way the dry-etch damage can accumulate in QWs because no material is removed. This approach has proved necessary and effective for increasing the sensitivity of the QW probe method to these low damage processes. The extent of the damage has been evaluated by measuring PL intensity from the wells. On the other hand, a microscopic theory of dechannelling<sup>7,8</sup> detailed in Chapter 3 has been employed to estimate the damage inflicted by various ionic species under these dry-etch conditions. The experimental data is interpreted using this theoretical model in order to identify the main cause of damage.

**4.2. RIE selective etching for GaAs/AlGaAs material.**

**4.2.1. GaAs/Al<sub>0.3</sub>Ga<sub>0.7</sub>As QW structure for dry etch damage**

The detailed design of GaAs/Al<sub>0.35</sub>Ga<sub>0.65</sub>As multiple quantum well structures have been given in Chapter 2. Figure 4-1 reproduces the material structure, which has been grown on (100) GaAs semi-insulating substrates by molecular beam epitaxy in the department’s MBE group. The design of the materials ensured good depth resolution with low inter-QW coupling. The GaAs cap layer, 5nm thick, was to be removed during dry-etch with the underlying Al-containing layers as etch stop layers.

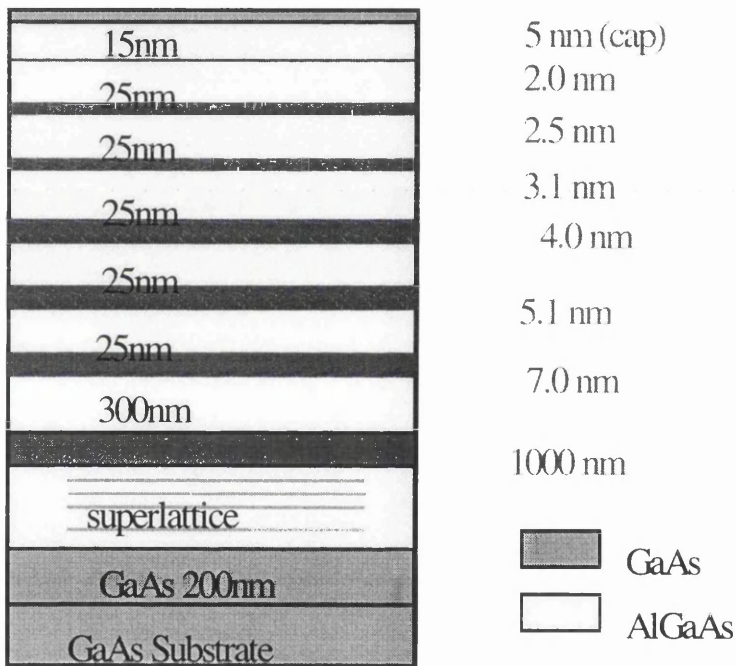


**Figure 4-1.** GaAs/AlGaAs multiple quantum well structure used in the experiment.

**4.2.2. RIE etching for GaAs/Al<sub>0.3</sub>Ga<sub>0.7</sub>As multiple QWs**

*Sample preparations.*

The wafers were cleaved into 2x4 mm<sup>2</sup> samples, and marked. Then the samples were cleaned using a standard cleaning process (acetone, IPA, and RO water each for 5mins in an ultrasound water bath). Photolithography was then carried out on the samples, so

that half the sample surface area was covered with photoresist (S1818), which was 1.8 $\mu$ m thick, to protect this area from etching. The etching depth could then be measured by a Tally Step after photoresist was removed using acetone. The unetched area also served the important purpose as a reference to compare the difference in material properties with and without etching.

### ***RIE process systems***

The reactive ion etching of the AlGaAs/GaAs material was carried out using the Plasma technology RIE 80 machine which was described in section 2.1.1.

The purpose of this work is to study etching damages in real etching environments, in which material removal takes place. On the other hand, the QW structure of the etched samples should not be changed by the etching in order for the PL measurements to be meaningful. In other words, it is necessary to accumulate damage in samples without changing the structure. Selective etching technique can satisfy this purpose.

The selective etching processes use SiCl<sub>4</sub> plasma in the low RF power regime (<15W), which give a selectivity > 10000:1 between GaAs and AlGaAs<sup>5</sup>. In previous work a etch stop layer of about 4 monolayers thick (1.1nm) was used and a highly anisotropic etch was obtained. The selectivity was achieved by the formation of an involatile layer of Al<sub>2</sub>O<sub>3</sub> or AlN on the sample surface from the residual oxygen, air or moisture in the chamber. The details of the selective etching processes for GaAs/AlGaAs have been given in section 2.1.4.

In this study, the etching was carried out using different RF powers and for varying times, while the 4.1sccm of gas flow rate and 5.8mTorr of etching pressure were kept constant. The temperature of the cathode (sample table) was maintained at around 40<sup>0</sup> C.

Table 4-1 gives the etching conditions used in this work.

Sample No	Etching condition
B2	SiCl <sub>4</sub> , 4.1 sccm, 5.8mT, <b>10W, 50V, 5mins</b>
F3	SiCl <sub>4</sub> , 4.1 sccm, 5.8mT, <b>10W, 50V, 7mins</b>
F1	SiCl <sub>4</sub> , 4.1 sccm, 5.8mT, <b>10W, 50V, 9mins</b>
F4	SiCl <sub>4</sub> , 4.1 sccm, 5.8mT, <b>12W, 80V, 5mins</b>
F5	SiCl <sub>4</sub> , 4.1 sccm, 5.8mT, <b>12W,80V,7mins</b>
B4	SiCl <sub>4</sub> , 4.1 sccm, 5.8mT, <b>14W, 90V, 5mins</b>
F2	SiCl <sub>4</sub> , 4.1 sccm, 5.8mT, <b>12W, 50V, 9mins</b>

**Table 4-1.** The selective etching conditions used in the damage study.

### 4.2.3. Results of Selective etching for GaAs /Al<sub>0.3</sub>Ga<sub>0.7</sub>As MQW materials

The photoluminescence (PL) from the GaAs/AlGaAs quantum well samples was measured before and after etching. PL measurements were carried out at a temperature of 5K and pumping laser power of 4mW on samples with a spot diameter of 70μm. Figure 4-3 shows the change in the normalised PL intensity from exposed area of sample F5 compared to the protected area of the same sample. The equation for normalised PL intensity <sup>9</sup>

$$\eta = \frac{(I_{QW} / I_{QW6})^{Exposed}}{(I_{QW} / I_{QW6})^{Unexposed}}$$

is given in chapter 3. This sample was etched using a selective etching process with a 12W RF power giving dc self bias of 80V and an etching time of 7 minutes. The etching depth measured by TallyStep is smaller than 20nm. Under this etching condition, PL intensity dropped 65% for QW1, and 25% for QW2. Figure 4-4 shows the change for sample F3, etched under same condition except for an etching power of 10W. As shown in the figure, PL intensity dropped 45% for the QW1, and 15% for QW2. It will be seen that if the PL from first quantum well QW1 in both etching processes is compared, less etching power produces less damage as might be expected.

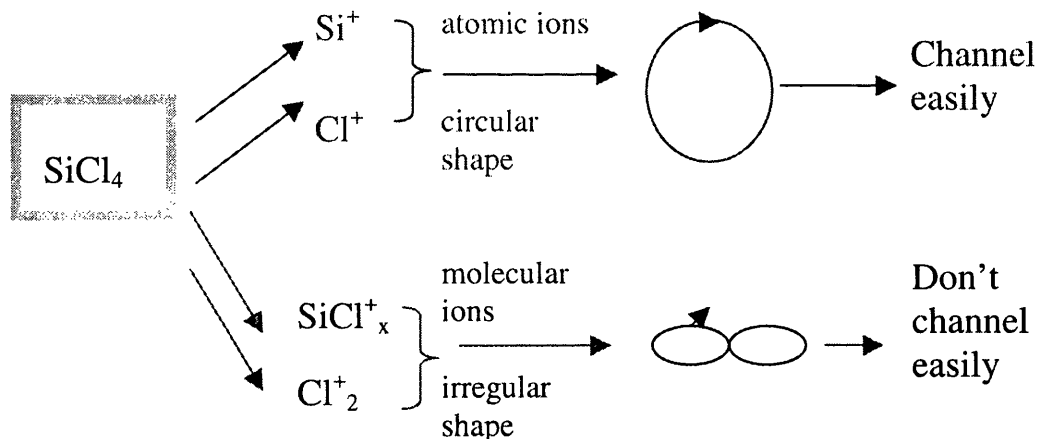
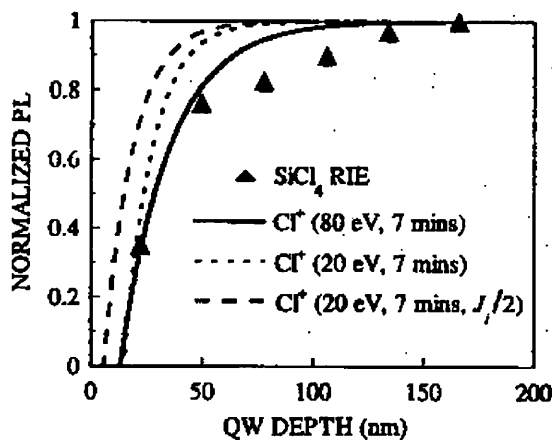
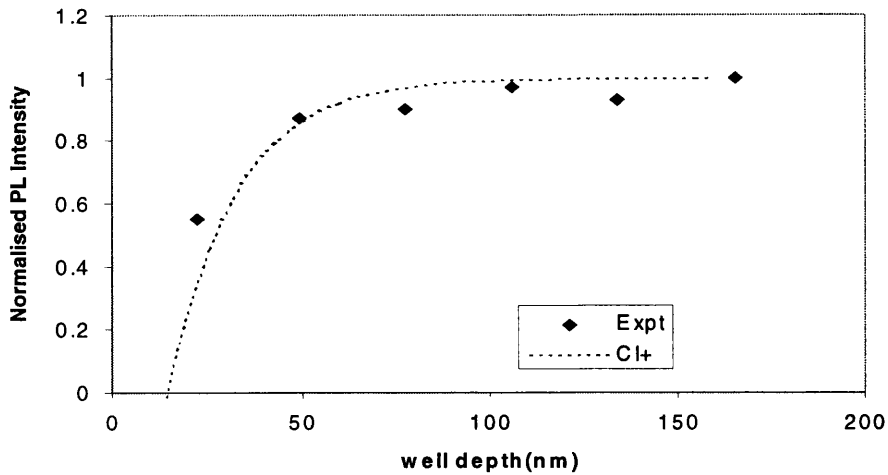


Figure 4-2. Diagram of SiCl<sub>4</sub> in the plasma.

This relatively simple etching process involved only one gas,  $\text{SiCl}_4$ , and the resulting discharge comprises atomic ions  $\text{Cl}^+$ ,  $\text{Si}^+$ , and molecular ions  $\text{SiCl}_x^+$ ,  $\text{Cl}_2^+$ . The atomic ions should channel easily due to their regular circular shape, and consequent smooth motion. But molecular ions have an irregular shape, and therefore their motion is possibly tumbling, so they may not channel easily, as shown in Figure 4-2. Earlier experiments using an ion implanter suggested that  $\text{Si}^+$  does not channel at very low energies, preferring instead to deposit.<sup>10</sup> Therefore in this case, only the  $\text{Cl}^+$  can channel deeply. The theoretical curve calculated from equation (5) for  $\text{Cl}^+$  channelling is also plotted in Figure 4-3. The parameters have been taken as ion flux  $J_i = 4 \times 10^{13}$  ions/cm<sup>2</sup>s,  $n_a = 3 \times 10^{18}$  cm<sup>-3</sup>, and  $\alpha = 10^{-3}$ . The channelling depth  $\lambda$  is calculated according to Eq(a1). Although it is believed that molecular ions  $\text{SiCl}_x$  or  $\text{Cl}_2^+$  do not channel, when  $\text{SiCl}_x^+$  or  $\text{Cl}_2^+$  impacts, however, some of them will be fragmented into atomic ions, and these secondary atomic ions may channel at a smaller energy and possibly with reduced flux. Therefore calculated curves for secondary  $\text{Cl}^+$  for fluxes  $J_i$  and  $J_i/2$  are also shown. The secondary  $\text{Cl}^+$  energy is chosen at 20eV, which is an estimated value by momentum and energy calculation. The calculations suggest that primary  $\text{Cl}^+$  ions contribute predominantly to deep damage in this  $\text{SiCl}_4$  RIE process.



**Figure 4-3.** Normalised PL Intensity from the GaAs/AlGaAs MQW material etched in low power  $\text{SiCl}_4$ , dc self-bias 80V, etch time 7mins. Theoretical PL calculated for  $\text{Cl}^+$  channelling is also given.



**Figure 4-4.** As in Figure 4-3 but with etching power of 10W. Dashed line shows the theoretical PL profile.

A summary of the related PL results is listed in Table 4-2. It shows that the normalised PL intensity of the first quantum well has reduced to different extent after etching in processes listed in Table 4-2. It is very clear to see in this table that the etching damage is increased when using higher etching power. This is because higher power leads to higher energy ions bombarding the sample surface (as shown in both). From the calculated channelling depths  $\lambda$  using the microscopic theory, also listed in this table, it is evident that the channelling depth increases with increasing etching power, therefore giving rise to more damage. Increasing etching time also result in increasing damage. This is because increased etching time leads to increased number of ions. As a result more ions have chance to channel (as shown in Table 4-2), although their channelling depth is independent of etching time.

Sample No	Etching condition	$\lambda$ (nm)	Etching depth	Phenomenon
B2	SiCl <sub>4</sub> , 4.1 sccm, 5.8mT, 10W, 50V, 5mins	17.8	< 20nm	20%
F3	SiCl <sub>4</sub> , 4.1 sccm, 5.8mT, 10W, 50V, 7mins	17.8	< 20nm	45%
F1	SiCl <sub>4</sub> , 4.1 sccm, 5.8mT, 10W, 50V, 9mins	17.8	< 20nm	64%
F5	SiCl <sub>4</sub> , 4.1 sccm, 5.8mT, 12W, 80V, 5mins	20.6	< 20nm	40%
B4	SiCl <sub>4</sub> , 4.1 sccm, 5.8mT, 14W, 90V, 5mins	22	< 20nm	54%
F2	SiCl <sub>4</sub> , 4.1 sccm, 5.8mT, 12W, 50V, 9mins	17.8	110nm	Etch didn't stop at QW1

**Table 4-2.** Summary of PL intensity reduces in first quantum after etching for GaAs/AlGaAs

Sample F2 in Table 4-2 has an etching depth of 110nm, which means the first several quantum wells have been etched away. The etching did not stop at the first AlGaAs barrier layer. The reason for this may be the chamber was not clean enough, and more residual gases existed. Impurities in the chamber can come from various sources and can change the dominant ions in the discharge. It has been reported that the chamber surface condition affects the etching processes, in particular the chlorine containing discharges are very sensitive<sup>11-13</sup>, because Cl loss can be significant and can affect the discharge chemistry. And it is also reported<sup>14</sup> that the Cl-based plasma is critically sensitive to H<sub>2</sub>O and O<sub>2</sub> contamination which can effect the etching rate from hours to days after the contamination has been introduced, depending on the pumping system. A very useful method used to solve these problems is to make the etching chamber as clean as possible by regular plasma cleaning in a hydrogen and a subsequent oxygen discharge after each etching run. Treatment of the etching chamber with H<sub>2</sub> plasma is likely to lead to formation of volatile species of hydrogenated chlorosilicons and HCl and hence lead to the cleaning of the chamber from deposits. To eliminate the effect of residual H<sub>2</sub>, the chamber is further cleaned in O<sub>2</sub> discharge. It is thought that the O<sub>2</sub> will react with any residual hydrogenated chlorosilicon species in the chamber and form volatile compounds of OH, thereby reducing the residual H<sub>2</sub> level in the chamber. Cleaning the chamber before each run using H<sub>2</sub> for 15 minutes and then O<sub>2</sub> for 15 minutes is effective in obtaining repeatable etching results.

### **4.3. Selective etching for $In_{0.53}Ga_{0.47}As/In_{0.52}Al_{0.48}As$ MQW materials**

#### **4.3.1. $In_{0.53}Ga_{0.47}As/In_{0.52}Al_{0.48}As$ QW structure for dry etch damage**

The detailed design of InGaAs/InAlAs multiple quantum well structures have been given in chapter 2. Figure 4-5 re-plots the material structure, which has been grown on (100) InP semi-insulating substrates by molecular beam epitaxy in the department's MBE group. Again good depth resolution while permitting only low inter-QW coupling was the main consideration in the designing of the structure. The 5nm InGaAs cap layers is to be removed in the etching processes, with the underlying Al-containing layer acting as an etch stop layer.

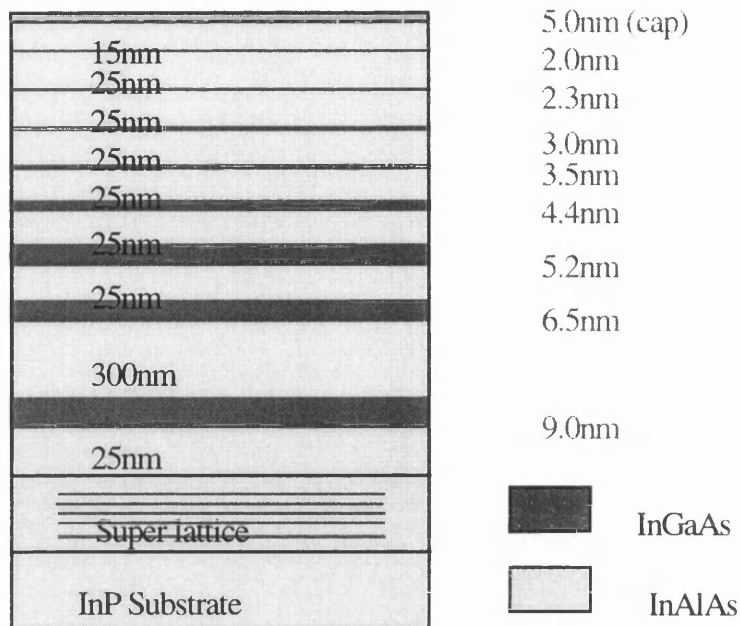


**Figure 4-5.**  $\text{In}_{0.53}\text{Ga}_{0.47}\text{As}/\text{In}_{0.52}\text{Al}_{0.48}\text{As}$  multiple quantum well structure

### 4.3.2. RIE etching for InGaAs/InAlAs multiple QWs

#### *RIE process systems*

The sample preparation is exactly the same as GaAs/AlGaAs quantum well materials. The InGaAs/InAlAs selective dry-etching was carried out in a  $\mu\text{P}$  system which is similar to the RIE 80 system, except that it has a load lock. The temperature of the sample table was kept around  $42^{\circ}\text{C}$ .

Selective reactive etching of InGaAs over InAlAs using a mixture of  $\text{SiCl}_4/\text{SiF}_4/\text{HBr}$  gases was developed by Murad<sup>5</sup> *et al.* Due to the existence of  $\text{SiF}_4$ , an etch stop layer of  $\text{AlF}_3$  is formed on the InAlAs layer. Using a  $\text{SiCl}_4/\text{SiF}_4/\text{HBr}$  flow rate ratio of 5/6/25 sccm, a dc self bias of  $< 70\text{ V}$ , and a pressure of 100mTorr, the selectivity for this material system was as high as 600:1. The etching can be stopped by a 5nm thick InAlAs layer for at least 60 minutes.

Using this process, the samples were again etched at fixed gas flow rate and etch pressure, while the RF power and etch times were varied as listed in Table 4-3. The etching processes have been slightly modified from Murad's, but they still gave very high selectivity, and satisfied the purpose of this work.

Sample No	etching condition
A3	SiCl <sub>4</sub> /SiF <sub>4</sub> /HBr, 6/2/20, 150mT, 5mins, 50W,46V
F4	SiCl <sub>4</sub> /SiF <sub>4</sub> /HBr, 6/2/20, 150mT, 5mins, 60W,80V
B3	SiCl <sub>4</sub> /SiF <sub>4</sub> /HBr, 6/2/20, 150mT, 5mins, 80W,141V
C3	SiCl <sub>4</sub> /SiF <sub>4</sub> /HBr, 6/2/20, 150mT, 5mins, 100W,204V
B2	SiCl <sub>4</sub> /SiF <sub>4</sub> /HBr, 6/2/20, 150mT, 5mins, 150W,240V
C4	SiCl <sub>4</sub> /SiF <sub>4</sub> /HBr, 6/2/20, 150mT, 80W,141V, 10mins
D4	SiCl <sub>4</sub> /SiF <sub>4</sub> /HBr, 6/2/20, 150mT, 80W,141V, 12.5mins

**Table 4-3.** The selective etching conditions used in In<sub>0.53</sub>Ga<sub>0.47</sub>As/In<sub>0.52</sub>Al<sub>0.48</sub>As MQW materials

### 4.3.3. Results of Selective etching for In<sub>0.53</sub>Ga<sub>0.47</sub>As/In<sub>0.52</sub>Al<sub>0.48</sub>As MQW materials

Figure 4-6 to Figure 4-8 show PL results for three InGaAs/InAlAs samples, sample B3, C4, and C3 using three different processes, respectively. Figure 4-6 presents the percentage change (e.g., 36% reduction for QW1) in normalised PL efficiency for sample B3, using the same data normalisation method as in Figure 4-2. This sample was etched using a mixture of SiCl<sub>4</sub>/SiF<sub>4</sub>/HBr gases at flow rates of 6/2/20sccm, RF power of 80W, dc self-bias of 140V, etching pressure of 150mTorr, and etching time of 5 minutes.

Sample C4, plotted in Figure 4-7, has been etched using the same etching conditions as sample B3 except for a longer etching time of 10 minutes. The normalised PL intensity is reduced by 67% for QW1. Because of the long etching time, damage manifested itself not only in shallow wells, but also in deeper wells such as QW5, even QW6.

Sample C3 was etched with an increased RF power of 100W and dc self-bias of 205V, see Figure 4-8. The normalised PL intensity is reduced by 83% for QW1. In Murad's <sup>5</sup> recipe, the dc self-bias was required to be smaller than 70V to achieve selective etching. The dc self bias used here was 205V, but etching still stopped at the first InAlAs barrier. The etch depth in all cases except B2 measured by Tallystep is less than 20nm. This means the etching stopped before the first QW (see wafer structure in Figure 4-). When the etching power was increased to 150W for sample B2, it was found that the etching didn't stop at the first InAlAs layer, but proceeded to the depth of 117nm in 5 minutes.

The theoretical calculation<sup>9</sup> for PL intensity reduction resulting from Cl<sup>+</sup>, F<sup>+</sup>, Br<sup>+</sup> channelling has been plotted for each etching condition, and presented together with experimental data in Figure 4-6, Figure 4-7, and Figure 4-8, respectively. The curves have been calculated assuming that the ion fluxes are in the Cl<sup>+</sup>:F<sup>+</sup>:Br<sup>+</sup> proportion of 6:2:20 with the net flux J<sub>i</sub> taken as 4× 10<sup>13</sup> ions/cm<sup>2</sup>s, n<sub>a</sub> = 3×10<sup>18</sup> cm<sup>-3</sup>, and α=10<sup>-3</sup> as before. As discussed previously, Si<sup>+</sup> at low energies and molecular ions do not channel. At the ion energies in above etching conditions, H<sup>+</sup> does not transfer sufficient energy per collision (<10eV) to create defects, the displacement threshold being about 15eV<sup>15</sup>. In above calculations the precise ratio of the ion fluxes Cl<sup>+</sup>:F<sup>+</sup>:Br<sup>+</sup> could not be known. The gas molecules will break into ions such as Cl<sup>+</sup>, (SiCl)<sup>+</sup>, (SiCl<sub>2</sub>)<sup>+</sup>, (SiCl<sub>3</sub>)<sup>+</sup>, (Cl<sub>2</sub>)<sup>+</sup>, etc. The ratio used in the calculation presumes: (i) that a single Cl<sup>+</sup> arises on average from a cracked SiCl<sub>4</sub> molecule, a single F<sup>+</sup> from a cracked SiF<sub>4</sub>, and a single Br<sup>+</sup> from a cracked HBr; and (ii) that the resulting ion abundance ratio reflects the gas ratio entering the chamber. This is a reasonable working hypothesis in the absence of more detailed information. Indeed, the measurements are explained well by this assumption.

With etching power of 80W and 100W, channelling lengths calculated by microscopic theory are 52nm and 45nm for F<sup>+</sup>, 36nm and 31nm for Cl<sup>+</sup>, 25nm and 21nm for Br<sup>+</sup>, respectively. Higher etching power lead to greater channelling depth. From experimental profile, the extent of damage also clearly worsens with increased ion energy while keeping other etching parameters unchanged. In Figure 4-9, a plot of normalised PL intensity vs. etching time of the first quantum well is shown. It indicates that longer etching time without changing dc self-bias results in more damage due to increased number of ions, as indicated in Eq.3-6. Summary of etching conditions and related PL phenomenon are listed in Table 4-4 and Table 4-5, respectively.

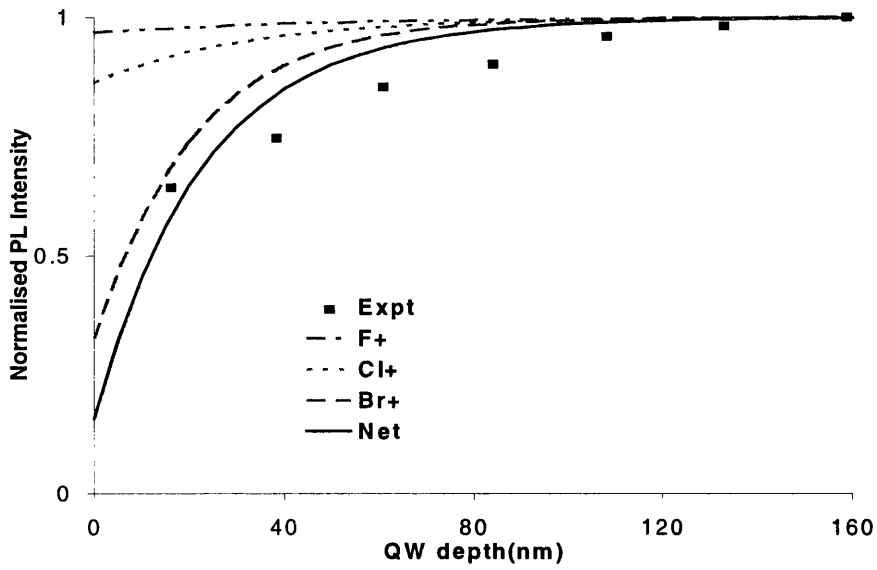


**Figure 4-6.** Normalised PL intensity from the InGaAs/InAlAs MQW material etched in SiCl<sub>4</sub>/SiF<sub>4</sub>/HBr (6:2:20) at 80W (dc self-bias 140V) for 5mins. The solid line shows the theoretical PL profile, while the dotted curve indicate the relative contributions of individual atomic ions.

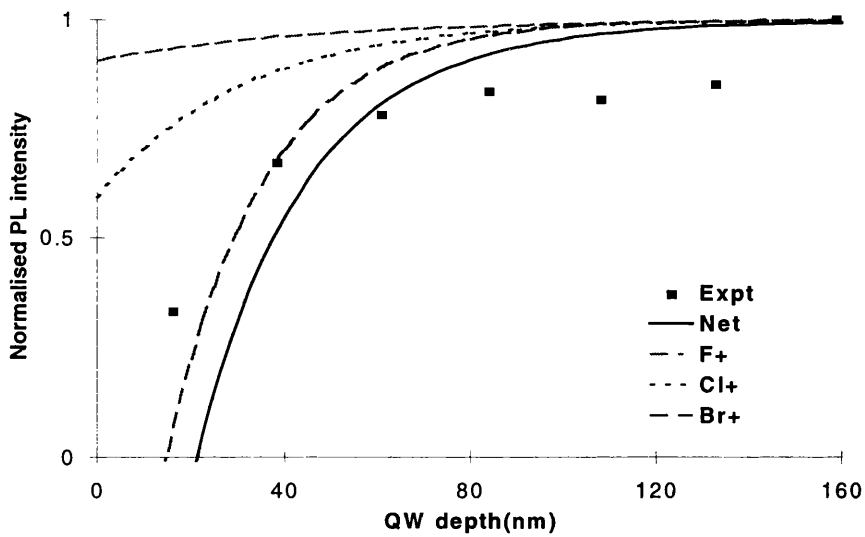


**Figure 4-7.** As Figure 4-6 but etched for 10 minutes.

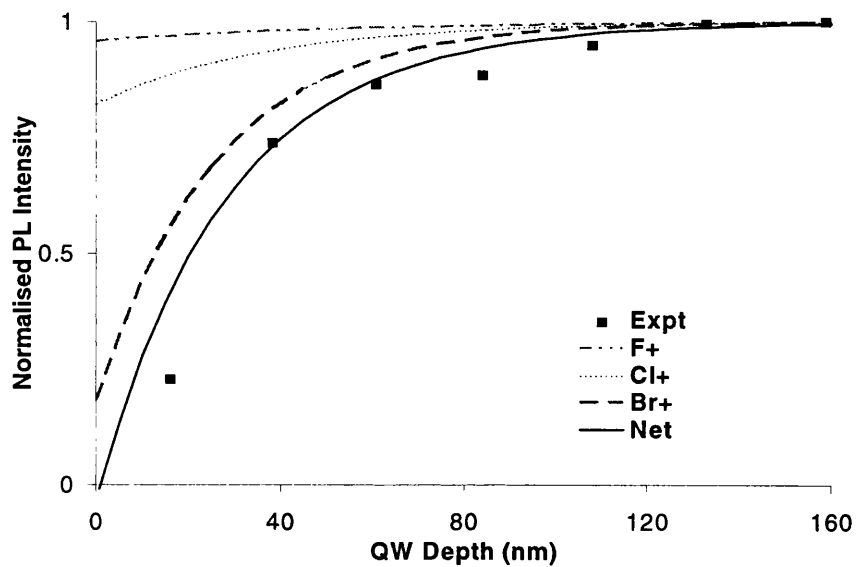


Figure 4-8. As Figure 4-6 but etched at 100W(dc self-bias 205V)

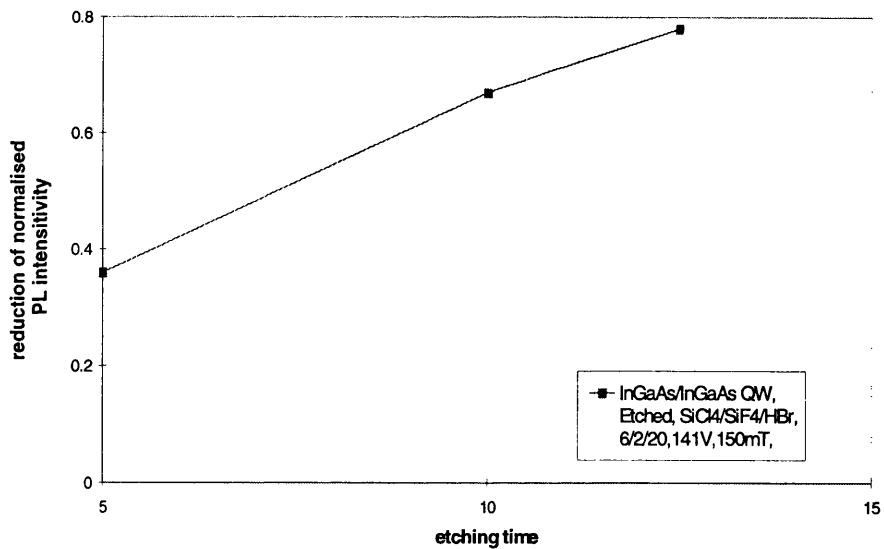


Figure 4-9. Reduction of the normalised PL from the first well as a function of the etching time.

Sample No	etching condition	$\lambda_c$ (nm)	etch depth(nm)	Phenomenon
A3	SiCl <sub>4</sub> /SiF <sub>4</sub> /HBr, 6/2/20, 150mT, 5mins, <b>50W</b> , 46V		< 20nm	damage free
F4	SiCl <sub>4</sub> /SiF <sub>4</sub> /HBr, 6/2/20, 150mT, 5mins, <b>60W</b> , 80V	36(Cl <sup>+</sup> ),51(F <sup>+</sup> ) 25(Br <sup>+</sup> )	<20nm	22% reduced for QW1
B3	SiCl <sub>4</sub> /SiF <sub>4</sub> /HBr, 6/2/20, 150mT, 5mins, <b>80W</b> , 141V	45(Cl <sup>+</sup> ),64(F <sup>+</sup> ) 31(Br <sup>+</sup> )	<20nm	36% reduced for QW1
C3	SiCl <sub>4</sub> /SiF <sub>4</sub> /HBr, 6/2/20, 150mT, 5mins, <b>100W</b> , 204V	52(Cl <sup>+</sup> ),74(F <sup>+</sup> ) 36(Br <sup>+</sup> )	<20nm	83 % reduced for QW1
B2	SiCl <sub>4</sub> /SiF <sub>4</sub> /HBr, 6/2/0, 150mT, 5mins, <b>150W</b> , 240V		117nm	etching didn't stop at first QW1

**Table 4-4.** Summary of PL intensity changes after using different etching power.

Sample No	etching condition	$\lambda_c$ (nm)	etch depth(nm)	Phenomenon
B3	SiCl <sub>4</sub> /SiF <sub>4</sub> /HBr, 6/2/0, 150mT, 80W,141V, 5mins	45(Cl <sup>+</sup> ), 64(F <sup>+</sup> ), 31(Br <sup>+</sup> )	< 20nm	36% reduced for QW1
C4	SiCl <sub>4</sub> /SiF <sub>4</sub> /HBr, 6/2/0, 150mT, 80W,141V, 10mins	45(Cl <sup>+</sup> ), 64(F <sup>+</sup> ), 31(Br <sup>+</sup> )	< 20nm	67% reduced for QW1
D4	SiCl <sub>4</sub> /SiF <sub>4</sub> /HBr, 6/2/0, 150mT, 80W,141V, 12.5mins	45(Cl <sup>+</sup> ), 64(F <sup>+</sup> ) 31(Br <sup>+</sup> )	< 20nm	78% reduced for QW1

**Table 4-5.** Summary of PL intensity changes after using different etching time.

#### 4.3.4. Effect of ambient oxygen on Al

It had been pointed out, by the growers of the MBE layers, that the inevitable oxidation of InAlAs after the etching and before the PL measurement might cause a change in the PL intensity. To verify the effects of ambient oxygen on Al in InAlAs, the InGaAs/InAlAs structure was etched using the following damage-free condition: a mixture gases of SiCl<sub>4</sub>/SiF<sub>4</sub>/HBr, flow ratio of 6/2/20sccm, pressure of 150mT, etching power of 50W, self dc bias of 46V and etching time of 5mins. The etching stopped at first InAlAs surface. Figure 4-10 shows no change in normalised PL before and after etching. Therefore any subsequent oxidation of the surface exposed to air does not affect the PL of the topmost quantum well.

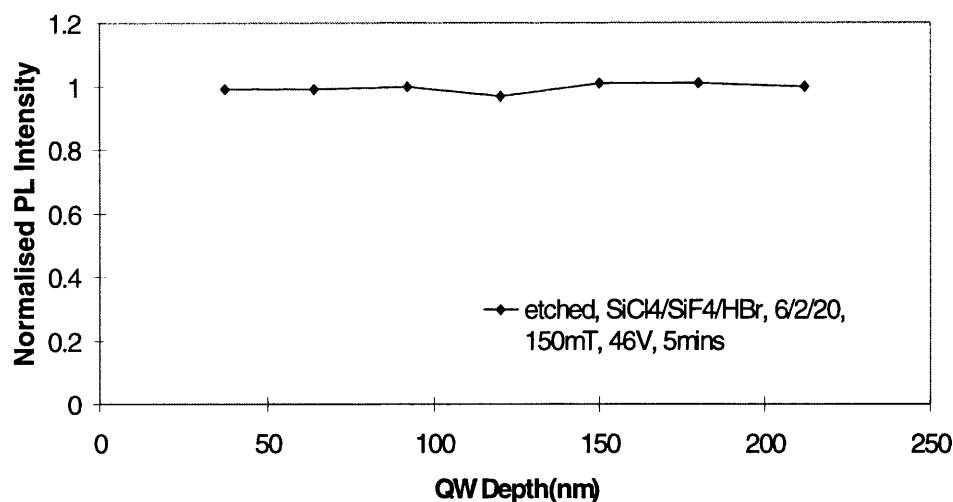


**Figure 4-10.** Lower power damage free etching process which shows no ambient effect on Al in the PL measurement.

#### **4.4. summary**

Dry-etching damage in III-V semiconductors under very low ion energy conditions has been studied in real etching environments. Due to the relatively low damage nature of these processes, a technique using selective etching has been used to accumulate damage in the etched material. Damage profiles have been measured using PL measurements on QW probe materials. By comparing photoluminescence spectra for damaged and undamaged areas, normalised damage distributions at various RIE selective etching conditions have been obtained. A microscopic theory has been used to model the distribution of the damage in such dry-etching processes, taking into consideration different ion masses, self bias voltages (RF power), etch times, and fluxes. It is significant that the experimental data is consistent with calculated damage effects for just atomic ions not molecular ions.

The results suggest therefore that atomic-ion channelling is responsible predominantly for dry-etching damage inflicted in low-energy multi-component gas discharges. Molecular ions do not channel because their extended structures do not permit it. Generation of atomic ions upon their impact is possible, but at energies far less than the incident energy. Thus it would appear, ideally, that low damage etch chemistries should not only have low ion energies but should use only molecular ions.

#### 4.5. References

- [1] S. K. Murad, M. Rahman, N. Johnson, S. Thoms, S. P. Beaumont, and C. D. W. Wilkinson, *J.Vac.Sci.Technol.* **B 14**, 3658(1996).
- [2] M. A. Foad, S. Thoms, and C. D. W. Wilkinson, *J.Vac.Sci.Technol.* **B 11**, 20(1993).
- [3] H. F. Wong, D. L. Green ,T. Y. Liu, D. G. Lishan, M. Bellis, E. L. Hu, P. M. Petroff, P. O. Holtz, and J. L. Merz, *J. Vac. Sci. Technol.* **B6**, 1906 (1988).
- [4] S. K. Murad, N. I. Cameron, S. P. Beaumont, and C. D .W. Wilkinson, *J. Vac. Sci. Technol.* **B 14**, 3668(1996).
- [5]. S. K. Murad, S. P. Beaumont, M. Holland and C. D .W. Wilkinson, *J. Vac. Sci. Technol.* **B 13**, 2344(1995).
- [6] S. K. Murad, C. D. W. Wilkinson, and S. P. Beaumont, *MNE* **23** , 357(1994).
- [7]. M. Rahman, *J. Appl. Phys* **82** 2215 (1997).
- [8] M. Rahman, (unpublished).
- [9]. L. G. Deng, M.Rahman, S. K. Murad, A. Boyd, and C.D.W.Wilkinson, *J. Vac. Sci. Technol.* **B 16**, 3334(1998).
- [10]. K. G. Orrmann-Rossiter, A. H.Al-Bayati, D. G. Armour, S. E. Donnelly and J. A. van den berg, *Nucl. Instr. Meth.* **B59/60**, 1991(1991)
- [11]. H. H. Sawin, B. E. Thomson, and A. D. Richardson in “Plasma Processing”. The Electrochemical Society Softbound proceedings Series, Penington, NJ, pp.434(1985). Editors, G. S. Mathad, G. C. Schwartz, and G. Smolinsky.
- [12]. K. D. Allen, H. H. Swain, and A. Yokozeki, *J. Electrochem. Soc.* **133**, 2331.
- [13]. A. D. Richards and H. H. Swin, *J. Appl. Phys.* **62**, 799, (1987).
- [14]. G. C. H. Zau, L. D. Baston, D. C. Gray, I. Tepermeister, H. H. Sawin, and M. T. Mocella, *J. Electrochem. Soc.* **137**, 3526(1990).
- [15]. S. M. Sze, “ Semiconductor devices Physics and Technology” John wiley& sons, 1985. P. 408

## Chapter 5

### Contribution of atomic and molecular ions to dry-etch damage

#### 5.1 Introduction

A reactive etch chemistry assists in achieving low damage etching as the enhanced etch rates shorten the exposure time to the bombarding flux. Low ion energies are essential too, to reduce the penetration range of the ions causing the damage<sup>2-7</sup>. As described in previous chapters, a small fraction of the incident flux is scattered at the surface and channel in low index directions. This small number of ions can create defects when they dechannel. The higher the incident energy the deeper the expected channelling distance.

However, this does not give the entire story.  $\text{SiCl}_4$  discharges created by electron cyclotron resonance (ECR) can lead to high levels of damage, despite the low ion energies<sup>1</sup>. This is associated with the relatively high  $\text{Cl}^+$  density in the ECR discharge, as determined by optical emission spectroscopy. In chapter 4, the etch-induced damage in GaAs/AlGaAs and InGaAs/InAlAs heterostructures due to the net bombardment in a  $\text{SiCl}_4$  discharge and in a discharge of  $\text{SiCl}_4/\text{SiF}_4/\text{HBr}$ , respectively, has been studied. The results clearly show that atomic ions, rather than molecular ions, have the dominant damaging effect. However in the practical etching processes, it is common to use mixture of gases which break down to form a range of atomic and molecular ionic species. As only the damage caused by all the species acting together can be measured after etching in an RIE machine, a way to measure the damage caused by each species was required.

A mass resolving low energy ion implanter at Salford University was used to carry out this study. The ion induced damage due to the separate effects of  $\text{Si}^+$ ,  $\text{Cl}^+$ ,  $(\text{SiCl})^+$ ,  $(\text{SiCl}_2)^+$  and  $(\text{Cl}^+)$  bombardment has been studied. The effects of ion exposure on the photoluminescence (PL) from multiple quantum well (QW) structure were probed by measuring the PL intensity from QWs at different depths. This profile was related to experimental parameters using the microscopic model of the damage distribution. The observed contribution to damage by these ions will be discussed in detail in this chapter.

## 5.2 Separate ions bombardment in mass resolved ion implanter

### *Sample preparation.*

The preparation of the sample was as described in Chapter 4. Each sample was covered on the photoresist-protected side by a piece of Aluminium film and fixed on a special holder. The fixed samples were able to move in any direction without falling down into the implanter chamber. The covered side was used as a reference area, and the other half side as the exposure area.

### *Mass resolved ion implanter*

An ion implantation system delivers a beam of ions of a particular type and energy to the surface. The major component parts are an ion source, a mass analyser, a drift tube, a beam scan system and a target station. The Salford machine has one additional component – a de-acceleration section to reduce the energy of the ions just before implantation.

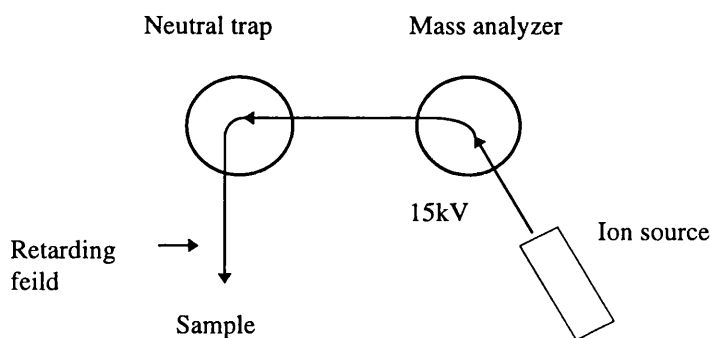


**Figure 5-1.** Schematic diagram of the Salford low energy ion implanter

A simplified diagram of this implanter is shown in Figure 5-1. In this machine ions are extracted at 15kV from ion sources (Applied Materials 9500 series ion sources) then mass analysed. The ions can be produced from a gas source (such as  $\text{BF}_3$ ), a solid source (such as a lump of As), or liquid source (such as  $\text{SiCl}_4$ ). The charged ions entering the analyser are deflected by the magnetic field through an angle that depends on their mass. Only ions of the desired mass can pass through a slit, which guards the entrance to the drift tube. To avoid high-energy neutral atoms (which

arise by the capture of an electron by an ion) bombarding the target, the beam is bent by a second magnet (near neutral trap). Finally a retarding field is applied to the ion beam to reduce the ion energy before it hits the target, enabling implantation from ultra-low energy of 10eV up to a high energy of 20keV. There are five stages of differential pumping with the capability of producing an ultra-high vacuum target environment ( $<10^{-9}$  mTorr). Very low pressure at the target ensures that no unwanted species is accidentally implanted by momentum transfer and that no new neutrals are formed between the neutral trap and the sample.

***Ion implantation processes***

The atomic ions  $\text{Si}^+$  and  $\text{Cl}^+$ , and the molecular ions  $(\text{SiCl})^+$ ,  $(\text{SiCl}_2)^+$  and  $(\text{Cl}_2)^+$  were implanted at various doses, and energies. Table 5-1 gives the ion bombardment conditions used in these experiments. TalyStep measurements confirmed the depth of any etching was  $<10\text{nm}$ . It was also confirmed that  $\text{Si}^+$  deposited on the sample surface, while  $\text{Cl}^+$  etched material.

ions	ion energy(eV)	$\tau$ (s)	dose(ions/cm <sup>2</sup> )
$\text{Si}^+$	300	12	1E(15)
$\text{Si}^+$	300	55	5E(15)
$\text{Si}^+$	300	75	1E(16)
$\text{Si}^+$	440	200	1E(16)
$\text{Cl}^+$	100	25	1E(15)
$\text{Cl}^+$	100	125	5E(15)
$\text{Cl}^+$	300	10	1E(15)
$\text{Cl}^+$	300	50	5E(15)
$\text{Cl}^+$	300	99	1E(16)
$\text{Cl}^+$	500	20	1E(15)
$\text{SiCl}^+$	300	50	5E(15)
$\text{SiCl}^+$	500	324	1E(16)
$\text{Cl}_2^+$	100		1E(15)
$\text{Cl}_2^+$	100		5E(15)
$\text{SiCl}_2^+$	300		1E(16)
$\text{SiCl}_2^+$	500		1E(16)

**Table 5-1.** A list of ion bombardment condition used in GaAs/AlGaAs multiple quantum well.

### 5.3 Results of separate ion bombardment for GaAs/AlGaAs multiple quantum well.

The damage profile in the GaAs/AlGaAs quantum well samples has been measured using PL in both the bombarded side and the aluminium foil protected side of samples. Again the PL measurements were carried out at a temperature of 5K and an Argon laser pump power of 4mW on samples.

Particular combinations of ion species, energy and dosage were selected for further study. Table 5-2 gives the measured beam current density  $J_i$ , and exposure time  $\tau$  for these samples.

ion	$E_0$ (eV)	$J_i \times 10^{13}$ (ions/cm <sup>2</sup> s)	$\tau$ (s)	Dose $\times 10^{15}$ (ions/cm <sup>2</sup> )	
Si <sup>+</sup>	440	5.3	200	10.6	Fig. 5-2
Cl <sup>+</sup>	300	10.3	10	1.1	Fig. 5-3
			50	5.2	
			99	10	
(SiCl) <sup>+</sup>	300	3.2	325	10.4	Fig.5-6
(SiCl <sub>2</sub> ) <sup>+</sup>	300	1.9	515	9.8	Fig. 5-7
(Cl <sub>2</sub> ) <sup>+</sup>	100	1.4	75	1.1	Fig. 5-8

**Table 5-2.** Bombardment condition used on the implanter

Figure 5-2 shows the normalised PL intensity resulting from Si<sup>+</sup> bombardment with a 440eV ion energy and an ion dose of  $1 \times 10^{16}$  ions/cm<sup>2</sup> s. The theoretical curve calculated from equation (3-5) for Si<sup>+</sup> channelling is plotted in the same figure assuming the same proportion of 0.1% ions channelling. At very low energies Si<sup>+</sup> is known to deposit on GaAs<sup>8</sup> as discussed earlier, because energy considerations make bonding favourable. But at this high energy of 440eV, the experimental data clearly shows evidence of damage. For the first quantum well, the PL intensity has dropped by 30%. Even if this is not very high damage when compared with Cl<sup>+</sup> ion bombardment of the same dose, but at a lower energy of 300eV, where the first quantum well has been totally destroyed, the sample was nevertheless damaged by this bombardment of Si<sup>+</sup> ions. Therefore at very lower energy Si<sup>+</sup> prefers deposition on sample surface, but at relatively high energies such as 440eV, some Si<sup>+</sup> ions will accidentally channel. For Si<sup>+</sup> the theoretical expression  $\eta_e(y)$  reproduces the trend of the experiment data<sup>9</sup>.

Figure 5-3 is the normalised PL intensity from samples exposed to 300eV Cl<sup>+</sup> for three different exposure times (see Table 5-2). Increased dose leads to accumulation of the damage, as expected. Here we chose the fifth quantum well as the reference for normalisation. The etch depth has been measured by Talystep to be less than 10nm.

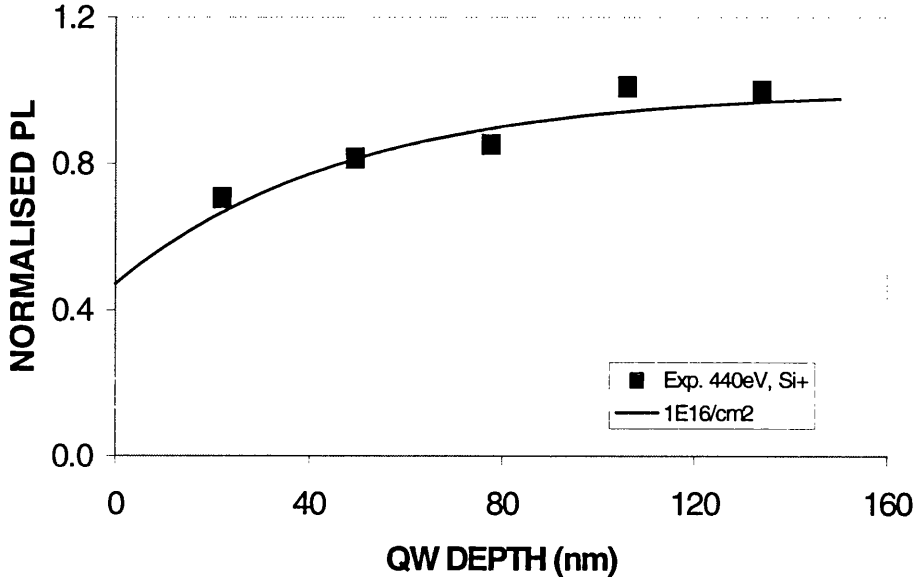
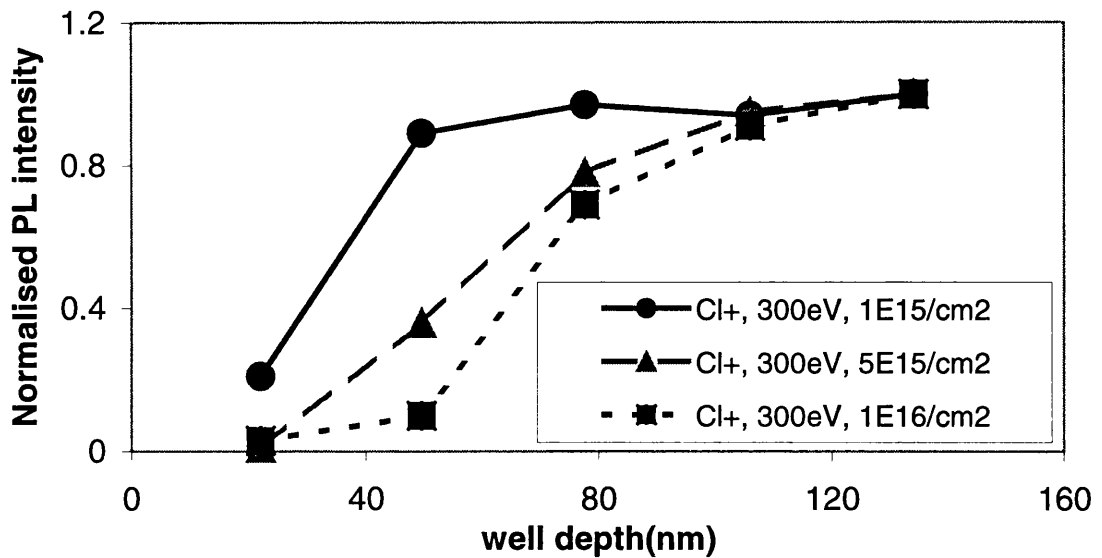


Figure 5-2. The normalised PL for Si<sup>+</sup> at 440eV. The line shows the theoretical value.

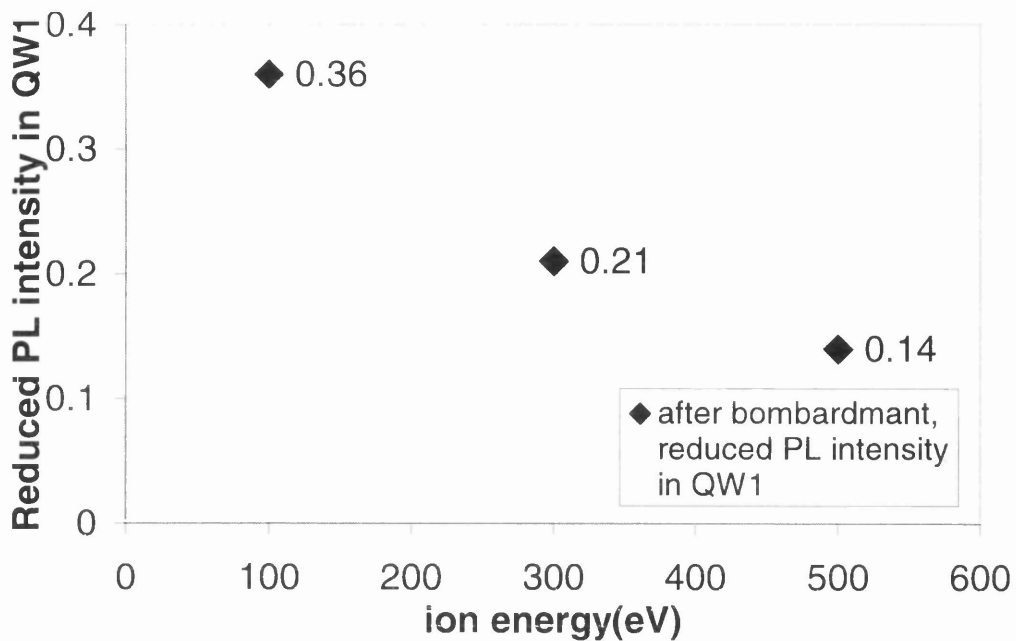


**Figure 5-3.** Experiment data from samples exposed to 300eV  $\text{Cl}^+$  for three different ion doses. “●” at  $10^{15}/\text{cm}^2$ , “▲” at  $5 \times 10^{15}/\text{cm}^2$  and “■” at  $10^{16}/\text{cm}^2$ . Here lines are a guide to the eye not theory.

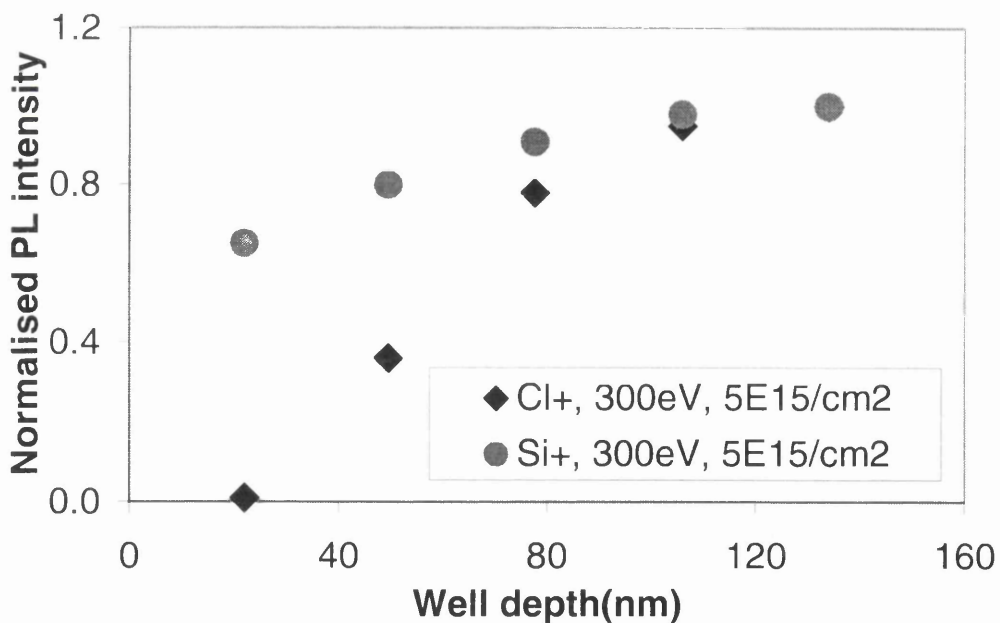
Figure 5-4 shows a normalised PL intensity from the first quantum well after  $1 \times 10^{15}/\text{cm}^2$  ions bombardment with ion energy of 100eV, 300eV and 500eV, respectively. As expected, increasing ion energy leads to more damage in the material. Figure 5-5 shows normalised PL intensity from both  $\text{Si}^+$  and  $\text{Cl}^+$  ions of  $5 \times 10^{15}$  ions/ $\text{cm}^2$  at an energy of 300eV. This figure results that  $\text{Cl}^+$  ions created more damage than  $\text{Si}^+$ .

Figure 5-6 and Figure 5-7 show the effect of exposure to the molecular ions  $(\text{SiCl})^+$  and  $(\text{SiCl}_2)^+$ , respectively, at an energy of 300 eV and ion dose of  $10^{16}$  ions/ $\text{cm}^2$ . Figure 5-8 shows the effect of exposure to molecular ions  $(\text{Cl}_2)^+$  at an energy of 100eV and an ion dose of  $10^{15}$  ions/ $\text{cm}^2$ . In all cases the etch depth was  $< 10\text{nm}$ .

We have argued already that molecular ions do not channel, but fragmentation upon impact may give lower energy atomic  $\text{Si}^+$  and  $\text{Cl}^+$  ions which may channel. As mentioned earlier, at very low energies  $\text{Si}^+$  has been observed to deposit, therefore can be assumed to cause no significant measurable damage. It is then appropriate to consider the effect of  $\text{Cl}^+$  ions only.



**Figure 5-4.** Reduced normalised PL intensity in first quantum well after  $1 \times 10^{15}/\text{cm}^2$   $\text{Cl}^+$  ions bombardment with ion energy of 100eV, 300eV and 500eV, respectively.



**Figure 5-5.** Experiment data for both  $\text{Si}^+$  and  $\text{Cl}^+$  ions at ion energy of 300eV, and ion doses of  $5 \times 10^{15}$ .

The calculations plotted in the figures are for  $\text{Cl}^+$  at two different energies, one at the incident energy of the molecular ions, the other at a proportion of the incident

molecular ion energy. The share of energy carried by the secondary  $\text{Cl}^+$  generated can be estimated from energy and momentum conservation conditions assuming elastic collision, with further reduction to account for loss of energy due to the actual inelastic collisions. Also, the generation of secondary  $\text{Cl}^+$  from di-chlorinate molecular ions  $(\text{SiCl}_2)^+$  and  $(\text{Cl}_2)^+$  is assumed at two different rates, one at the dose of the molecular ions the other at twice their dose.

From Figure 5-6, it is clear that the lower energy  $\text{Cl}^+$  fits the experimental data better, while Figure 5-7 and Figure 5-8 all show that the  $\text{Cl}^+$  flux of twice the total molecular ion dose fit the experiment data better. It therefore becomes evident that secondary atomic ions, rather than the original molecular ions, are the major factors for producing defects in the materials.

Table 5-1 gives a list of ion bombardment conditions, the results of most of which have been shown in above figures. It is clear shown that increasing ion dose while keeping ion energy constant results in more damage in materials. Increasing ion energy while keeping dose constant also results in more damage in materials.  $\text{Cl}^+$  ions cause more damage than  $\text{Si}^+$  if the samples have been bombarded under the same conditions, and atomic ions produce more damage than molecular ions if they have exactly the same ion bombardment conditions.

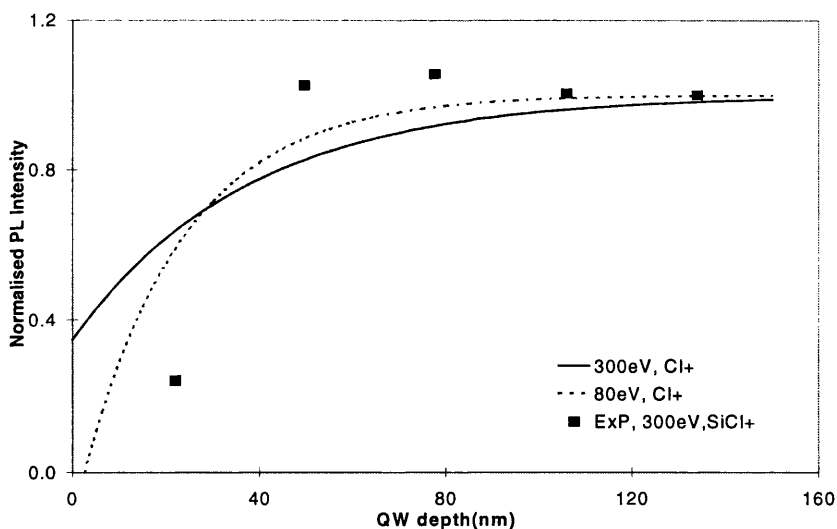


**Figure 5-6.** Experiment data and calculations for 300eV  $\text{SiCl}^+$ .

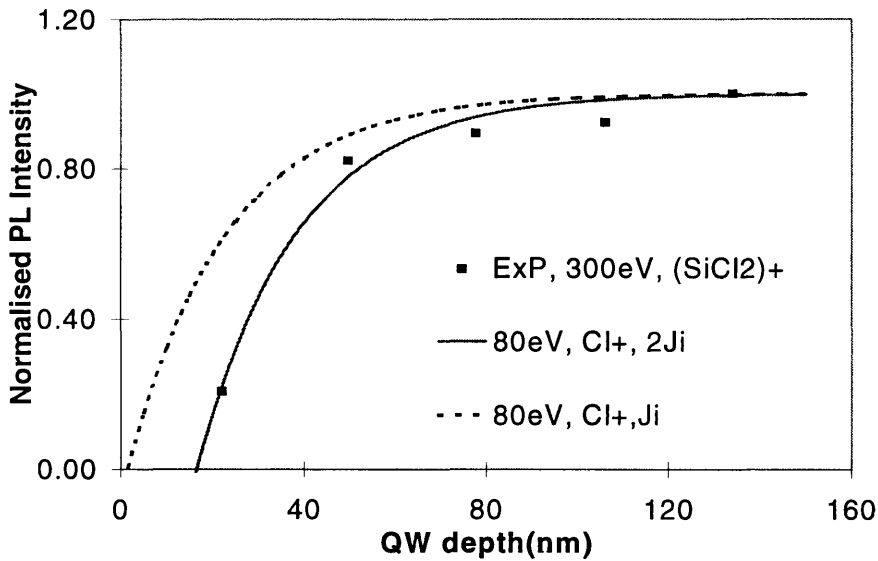


**Figure 5-7.** Experimental data and calculations (line) for 300eV, (SiCl<sub>2</sub>)<sup>+</sup>. Better agreement is found when two Cl<sup>+</sup> ions are assumed to be created from each fragmented (SiCl<sub>2</sub>)<sup>+</sup>.

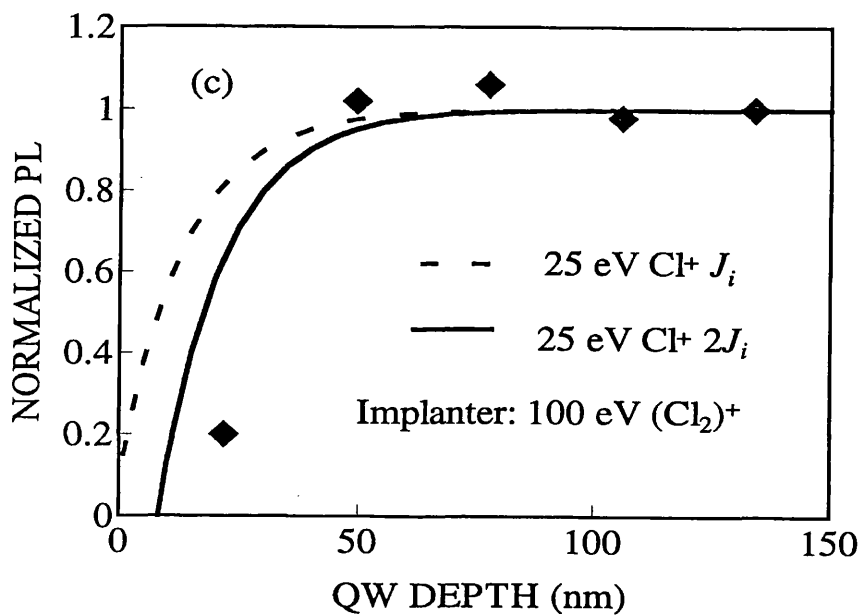


**Figure 5-8.** 100eV (Cl<sub>2</sub>)<sup>+</sup> bombardment with ion flux of  $1.5 \times 10^{13}$  ions/cm<sup>2</sup> and exposure times 350s.

#### 5.4 Propagation of ion damage in GaAs and InGaAs materials

An extensive characterisation of ion damage in materials of different bandgap would be helpful in understanding the nature of defect propagation during ion exposures.

GaAs- and InGaAs-based materials are very important for optoelectronic and electronic devices. Comparisons of plasma induced damage in GaAs and InP based materials have been carried out by different ways such as DLTS or Schottky barrier measurements<sup>10-12</sup>, etc., some understanding has been gained. But the inherent difference in defect propagation in both materials is still not yet clear.

For the different materials there are different etching processes. Therefore it is very hard to compare the extent of etching damage for different materials at ‘the same’ etching condition. For example, in low damage etching processes using RIE, GaAs based materials can be etched by SiCl<sup>+</sup> around etching power of 10W, but InGaAs based materials can only be etched using gas mixture of SiCl<sub>4</sub>/SiF<sub>4</sub>/HBr at an etching power of at least 60W. However using an ion implanter, it is possible to bombard different materials with the same ion species at the same energy.

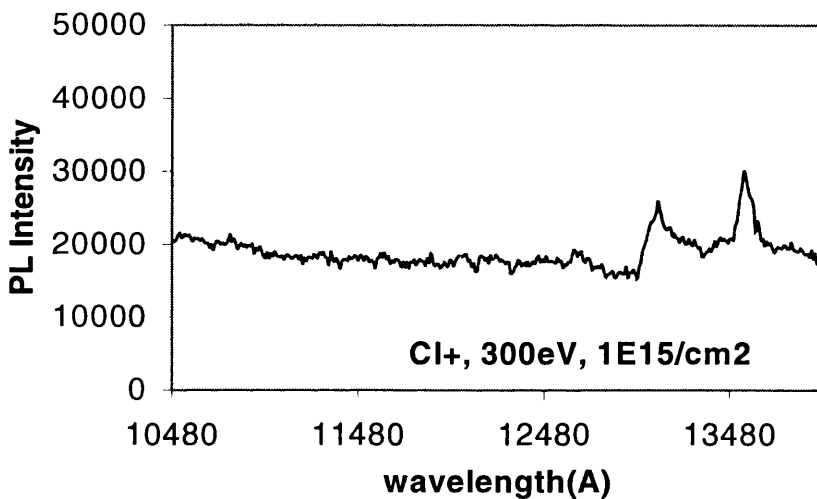


**Figure 5-9.** PL spectrum from InGaAs/InAlAs sample exposed to 300eV Cl<sup>+</sup> for 1 minutes, and ion dose was 10<sup>15</sup> ions/cm<sup>2</sup>.

ions	ion energy(eV)	τ(s)	dose(ions/cm <sup>2</sup> )	Phenomenon
Cl <sup>+</sup>	300	60	1E15	2 peaks
Cl <sup>+</sup>	300	180	5E15	1peak
Cl <sup>+</sup>	300	540	1E16	No

**Table 5-3.** A list of ions bombardment conditions and related PL Phenomenon.

The InGaAs/InAlAs samples were prepared in the same way as GaAs/AlGaAs samples. The damage profile of InGaAs/InAlAs quantum well samples were again

determined by PL measurements on both the bombarded and protected side of the sample. PL measurements were carried out at a temperature of 5K and using an Argon laser power density  $2.9 \times 10^3 \text{W/cm}^2$  on samples. To be comparable with GaAs samples, ion energy of 300eV was chosen to bombard InGaAs samples at various ion doses. Figure 5-9 shows a PL spectrum from an InGaAs/InAlAs sample exposed to 300eV  $\text{Cl}^+$  for 1 minute, and the ion dose was  $10^{15}$  ions/cm<sup>2</sup>. The first four quantum wells have been completely destroyed. Table 5-3 gives detailed ion bombardment conditions and corresponding PL phenomena of InGaAs/InAlAs multiple quantum well samples. The ion induced damage increases significantly with the increase ion dose.

Comparing GaAs and InGaAs based quantum well samples, it is found that using the same  $\text{Cl}^+$  bombardment conditions, ion induced defects penetrate much more deeply into InGaAs than into GaAs materials. Even though direct comparison cannot be made because their structures are slightly different. It has been observed that, when using a  $\text{Cl}^+$  ion dose of  $10^{15}$  ions/cm<sup>2</sup> at an ion energy of 300eV, in GaAs all six PL peaks remained and the first quantum well PL intensity was reduced by 79%, while the other wells were slightly reduced, but in InGaAs the quantum wells 1 to 5 have all been completely destroyed.

The microscopic theory of dechannelling has been used to calculate the channel depth for both materials. The channelling depth  $\lambda_c$  along  $\langle 011 \rangle$  is 52nm for GaAs material and 62nm for InGaAs material. Figure 5-10 shows the ions channeling depth against ion energy in both GaAs and InGaAs-based materials.

Figure 5-11(a) replots the channelling depth in GaAs and InP based materials for 10,000  $\text{Ar}^+$  ions incident along  $\langle 110 \rangle$  direction using the SCHLEICH model<sup>13</sup>. The calculations for a given energy, it is also clear shown that the channelling depth of argon ions in InP is also greater than GaAs, and the amount of atoms in InP displaced by incident ions is also greater than in GaAs as shown in Figure 5-11(b). These calculations according to both theories correlates with our experimental data that InGaAs is more sensitive to ion damage than GaAs.

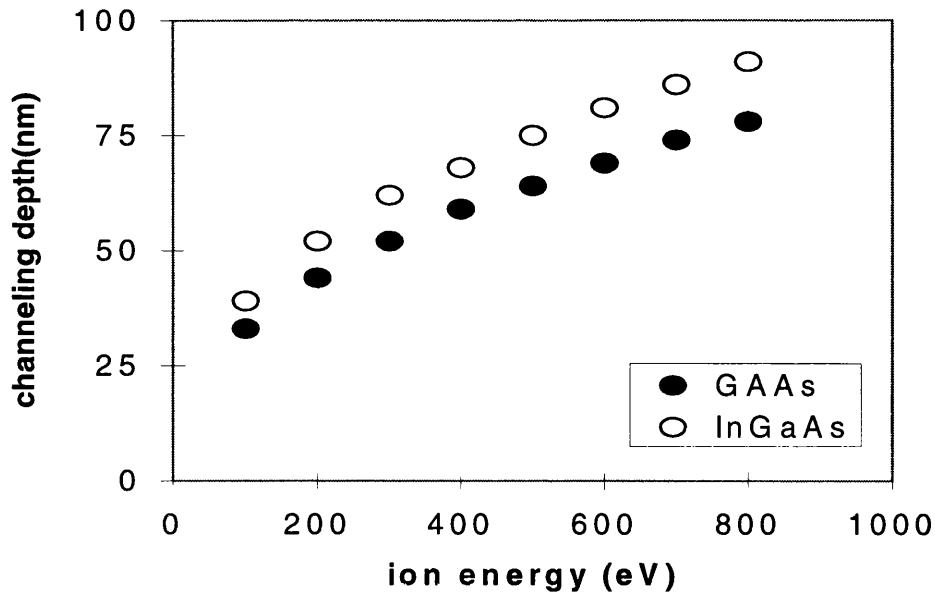


**Figure 5-10.** Theoretical calculation of ions channeling depth against ion energy in both GaAs and InGaAs-based materials.

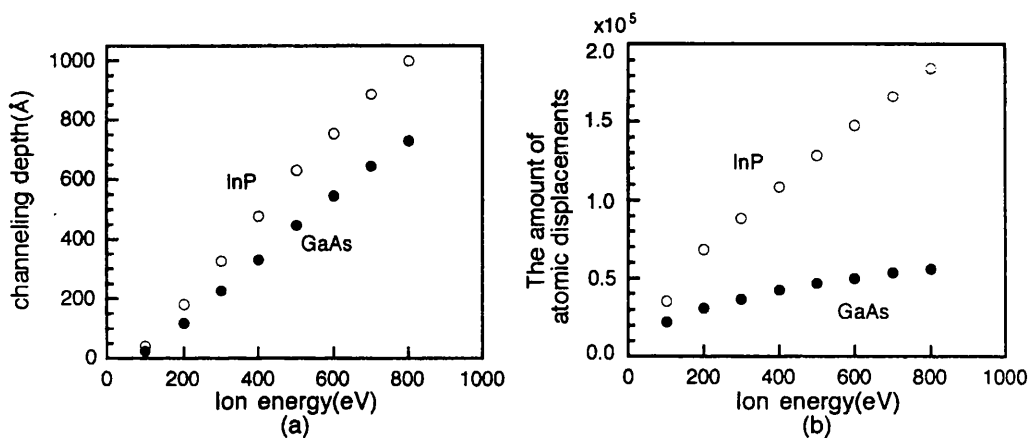


**Figure 5-11.** SCHLEICH calculations (a) channeling depth and (b) number of atoms displaced in GaAs (dots) and InP (circles) for 10,000 argon ion incident along  $\langle 011 \rangle$  direction at ion energies of 100-800 eV.

### 5.5 summary

We have used a low energy ion implanter to study ion induced damage in III-V semiconductors due to separate  $\text{Cl}^+$ ,  $\text{Si}^+$ ,  $(\text{Cl}_2)^+$ ,  $(\text{SiCl})^+$ , and  $(\text{SiCl}_2)^+$  ion bombardment. Damage profiles have been measured using PL measurements on QW

probe materials. By comparing photoluminescence spectra from damaged and undamaged areas, normalised damage distributions at various ion bombardment conditions have been obtained. A microscopic theory has been used to model the distribution of the damage in such ion bombardment processes, taking into consideration different ion masses, ion energy, exposed time, and ion dose. The experimental data fits well with the theoretical calculation. It is established that

- (1) Increasing the amount of ions, the damage increases significantly,
- (2) Increasing ion energy will also increase damage in materials,
- (3)  $\text{Cl}^+$  ions make more damage in material than  $\text{Si}^+$ .
- (4) InGaAs based materials are more vulnerable to  $\text{Cl}^+$  ion damage than GaAs based materials because their greater channelling depth, and
- (5) Atomic ions play the major role in producing damage rather than molecular ions. Although damage have been observed in materials bombarded by molecular ions of  $\text{SiCl}^+$ ,  $\text{SiCl}_2^+$ , and  $\text{Cl}_2^+$ , the measured PL data were consistent with theoretically calculated damage effects due to the secondary atomic ions rather than that of original molecular ions.

Secondary atomic ions can be expected to have the ion energies far less than the incident molecular ion energy. This explains why Electron Cyclotron Resonance – RIE using  $\text{SiCl}_4$  gives more damage than low power RIE: The strongly ionized conditions in ECR lead to a greater channelled  $\text{Cl}^+$  flux. Thus for low damage etching, reactive chemistries should be used that not only have low ion energies but also have a low atomic to molecular ion fraction in the discharge.

Thus, for low damage etching, one should choose discharge conditions that provide low energy molecular ions of a reactive species and as few atomic ions as possible.

## 5.6 References

- [1]. S. K. Murad, M. Rahman, N. Johnson, S. Thoms, S. P. Beaumont, and C. D. W. Wilkinson, *J.Vac.Sci.Technol.* **B 14**, 3658-3662 (1996).
- [2]. R.Germann, A. Forchel, M.Bresch, and H.P. Meier, *J.Vac.Sci.Technol.* **B 7**, 1475 (1989).
- [3]. N. G. Stoffel, *J. Vac. Sci. Technol.* **B 10**, 651-658 (1992).
- [4]. N.G. Stoffel, S. A. Schwartz, M. A. A. Pudensi, K. Kash, L. T. Florez, J. P. Harbison, and B. J. Wilkens, *Appl. Phys. Lett.* **60**, 1603 (1992).
- [5]. Ching-Hui Chen, Debora L. Green, and E. L. Hu, *J.Vac.Sci.Technol.* **B 13**, 2355-2359 (1995).
- [6]. D.L. Green, E. L. Hu, and N. G. Stoffel, *J. Vac. Sci. Technol.* **B 12**, 3311 (1994).
- [7]. M. Rahman, *J. Appl. Phys* **82** 2215 (1997).
- [8]. K. G. Orrmann-Rossiter, A. H. Bayati, D. G. Armour, S. E. Donnelly and J. A. van den berg, *Nucl. Instr. Meth.* B59/60, 1991(1991).
- [9]. M.Rahman, L. G. Deng, A. Boyd, , C.D.W.Wilkinson, J. A. van den Berg and D. G. Armour, *Electrochem. Soc. Proc.* 98-12, 213(1998).
- [10]. H. Iber, S.Mo, E. Peiner, Gvollrath, A. Schlachetzki, and F. Fiedler, *Semiconductor Sci. and Technol.* **12**, 755 (1997).
- [11]. R. S. Williams, *Solid State Commun.* **41**, 153, (1982).
- [12]. D. G. Yu, Ching-Hui Chen, A. L. Holmes, Evelyn L. Hu, and s. p. DenBaars, *Microelectron. Eng* **35**,95 (1995).
- [13]. Ching-Hui Chen, Ph. D Thesis, University of California at Santa Barbara, (unpublished).

## Chapter 6

### Enhanced damage in low damage RIE processes caused by light

#### 6.1 Introduction

With ion energies up to 500eV range, the depth of the damage exceeds the expected implantation depth of ions. It is now clear that some ions accidentally channel<sup>1-4</sup> along  $\langle 110 \rangle$  crystallographic directions. The damage depth or the mean channelling length can be calculated by solving a Fokker-Planck equation<sup>2, 5</sup>. Whether channelling is sufficient to explain the observed damage depth, or an additional mechanism also plays a role, however, remains a mute point.

In a very interesting experiment, Chen *et al*<sup>6</sup> observed the damage in a series of GaAs/GaAlAs quantum wells at different depths caused by etching in Argon, with and without red light being projected on the sample during etching. They found that the depth of the damage was increased if the irradiation was present. This result was interesting scientifically and worrying technologically as there is always ambient light present in the etching chamber. However Chen's experiment was carried out in Argon, which is an inherently damaging gas. It is therefore a question if the effect is observed under etching conditions likely to cause little damage. This situation is investigated in this chapter.

Again specially designed GaAs/Al<sub>0.35</sub>Ga<sub>0.65</sub>As and In<sub>0.53</sub>Ga<sub>0.47</sub>As/In<sub>0.52</sub>Al<sub>0.48</sub>As multiple quantum well (MQW) layers have been dry etched in reactive ion etching environments with or without laser illumination during the etching. The technique of selective etching<sup>7, 8</sup> has again been employed as a way to damage the material for long times without changing the etch depth. The damage profile has been evaluated by measuring photoluminescence (PL) intensity from the quantum wells.

## 6.2 Illumination experiments with both GaAs and InGaAs based multiple quantum well materials.

The multiple quantum well (MQW) structure of both GaAs/AlGaAs and InGaAs/InAlAs materials have been given in chapter 2. The GaAs and InGaAs cap layers, both 5nm thick were removed in the etching process, with the underlying AlGaAs and InAlAs layers acting as the etch stop<sup>7, 8</sup>. The widest QW deeply embedded in both materials served as a reference for normalisation of the luminescence intensity.

### Experimental set up

Figure 6-1 shows the schematic diagram of the experiment set up. The laser source used in these experiments was a HeNe laser with a wavelength of 632.8nm, and an output power of 0.2-10mW, which provided above-band-gap illumination. The laser was mounted vertically on the etching chamber. Therefore, the red light was able to directly illuminate the sample during the etching through the window of etching chamber. A partial reflecting mirror was used to help adjusting the light spot position on the sample. To compare the extent of damage with and without illumination, two samples (A and B) were always etched at the same time. Sample A was far away from the light but sample B was directly illuminated by the laser light.

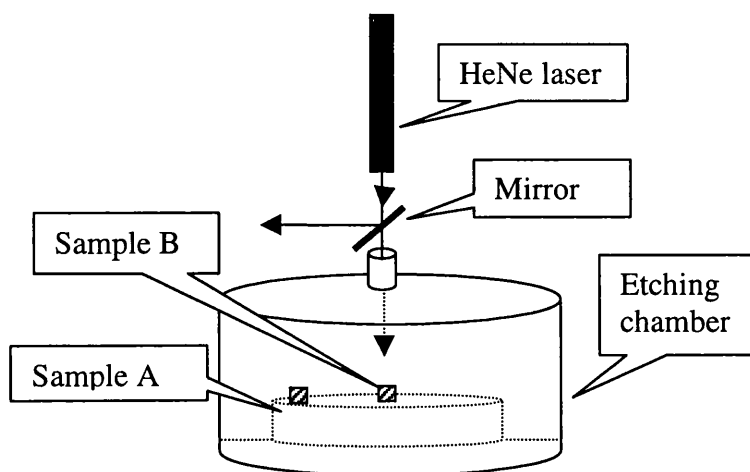


**Figure 6-1.** Schematic diagram of the experiment set up for the studies of illumination enhanced ion damage.

### ***Sample preparations***

The wafers were cleaved as  $3 \times 4 \text{ mm}^2$  pieces, and marked. The illuminated sample was protected by a photoresist mask covering the entire surface except a  $1 \text{ mm}^2$  circular area, which was left open to exposure to ions. A  $3 \times 2 \text{ mm}^2$  reference area on the non-illuminated sample was also protected from ion exposure by a photoresist mask. The photoresist mask was removed after etching. The etching depth was then measured using Talystep to make sure the etching stops at the first AlGaAs layer. The unetched area can also be used as a reference to compare the difference between before and after etching.

### ***RIE etching processes for both GaAs/AlGaAs and InGaAs/InAlAs materials***

GaAs/AlGaAs samples have been etched in a reactive ion etching (RIE) environment in a 13.56 MHz RIE system (Plasma Technology RIE80) which was described in detail in chapter 2.

A selective  $\text{SiCl}_4$  RIE process originally designed<sup>7</sup> for gate recessing in GaAs MESFETs was used, with a rf power of 6W (dc self-bias 60 V), a flow rate of 4.1 sccm, and a pressure of 5.3 mTorr. When the rf power is less than 15 W, the process gives a selectivity of greater than 10000:1 between GaAs and AlGaAs, ensuring that the QWs remain intact during exposure to the ions. The sample table temperature was maintained at around 40°C.

The HeNe laser power density on the sample during etching was about  $1000 \text{ mW/cm}^2$ . The incident laser beams were normal to the substrate surface. The etching was carried out with varying etching periods, while the gas flow rate, RF powers and etching pressure were kept constant.

The InGaAs/InAlAs selective dry etching was carried out in another RIE80 which has a load lock. A gas mixture of  $\text{SiCl}_4/\text{SiF}_4/\text{HBr}$  was used, which gives a selectivity higher than 600:1 between InGaAs and InAlAs<sup>8</sup>. The samples were etched at RF power of 65 W, dc self bias 115 V, at a flow rate of 6/2/20 sccm ( $\text{SiCl}_4/\text{SiF}_4/\text{HBr}$ ), and an etching pressure 150 mTorr, while the etch periods were varied. The temperature of the table was around 42°C.

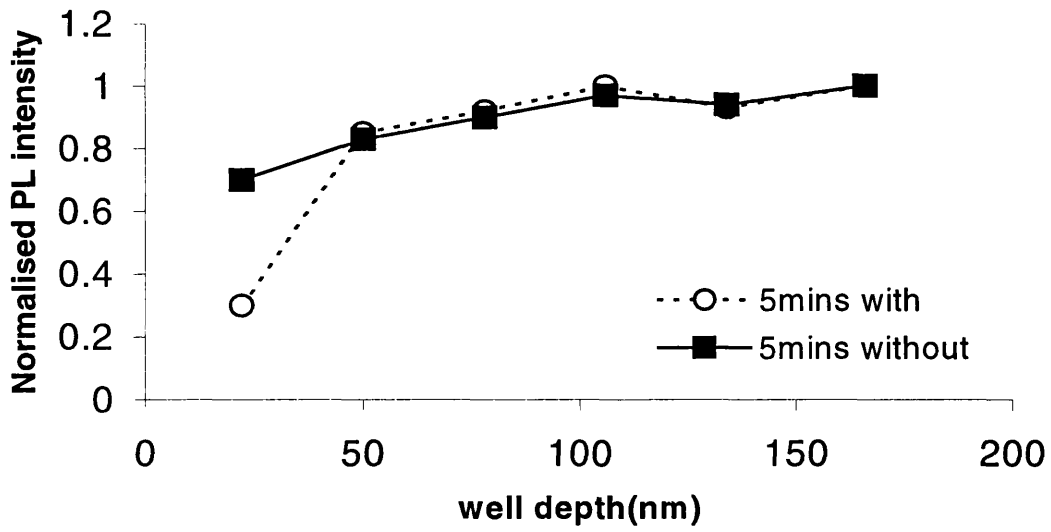
### **6.3 Illumination induced additional damage in both GaAs/AlGaAs and InGaAs/InAlAs MQW materials**

#### **6.3.1 Results of damage assessment in illuminated GaAs/AlGaAs MQW samples**

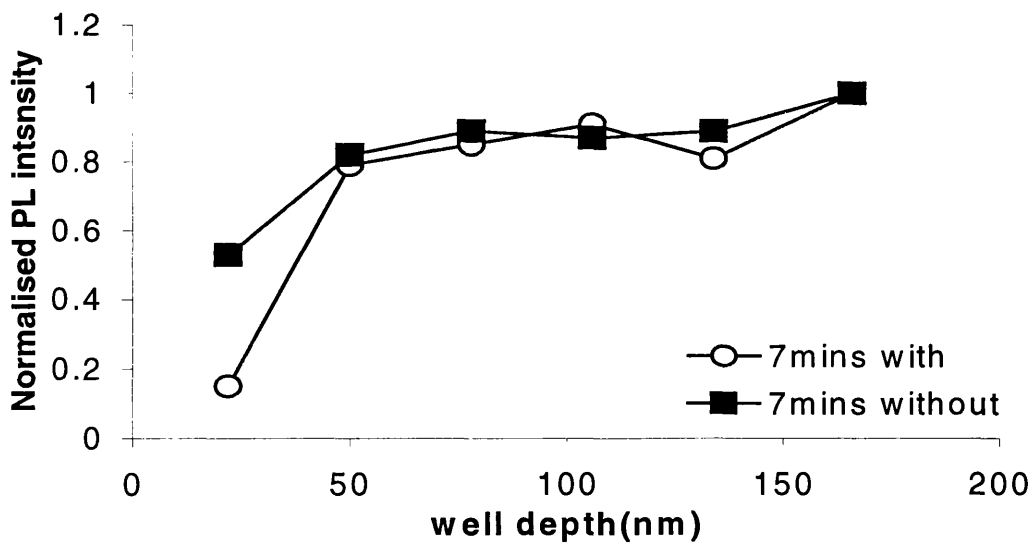
As in previous experiments, PL measurements were carried out at a temperature of about 5 K on samples with and without ion exposure and illumination. Again the 514.5nm line of an Argon laser was employed to excite the luminescence from the QWs. Detection was carried out using a photomultiplier tube for GaAs. In both exposed and protected reference areas, the PL intensity from the deepest quantum well was chosen as the reference for the normalisation of the PL intensity.

The normalised PL intensity indicates the relative change in the photoluminescence in the ion-bombarded regions with respect to the reference area for every quantum well. Figure 6-2 shows a comparison between the normalised PL intensity from etched GaAs samples with and without illumination by the HeNe laser at 10mW power. These samples have been etched in the SiCl<sub>4</sub> RIE environment under conditions mentioned above, for periods from 5 minutes to 9 minutes. When light is applied during etching, an additional effect is observed. The damage, as witnessed by the fall in PL intensity, increases with the time of exposure. Whenever the HeNe illumination was present during etching, the damage was increased significantly, particularly for the shallow quantum wells. For the sample without laser illumination, the PL intensity from the first quantum well dropped to 70%, 53% and 40 % of its as-grown value for etching times of 5 min., 7 min. and 9 min., respectively. However, for the other sample etched simultaneously with laser illumination, PL intensity from the first quantum well dropped to 28%, 15% and 2% of its as-grown value for the same etching times of 5 min., 7 min. and 9 min., respectively.

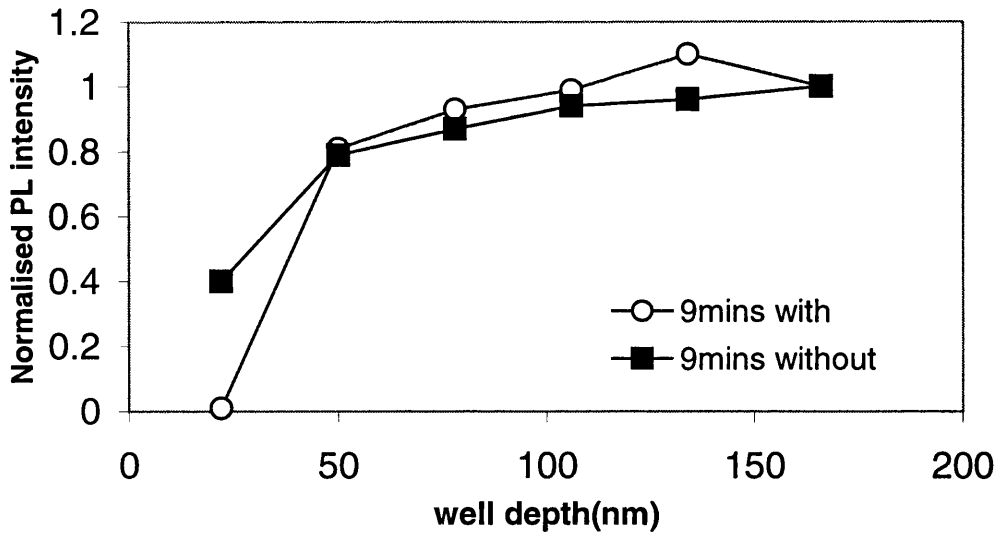
When the etching was done with no laser illumination and light was applied subsequently for a period as long as the etching time, there was no change in the observed damage, as shown in Figure 6-3. So illumination induces additional damage only during the etching process.



(A)



(B)



(C)

**Figure 6-2.** PL from GaAs etched in  $\text{SiCl}_4$  for 5, 7 and 9 minutes, with (○) and without (■) simultaneous laser illumination. (A) for 5 minutes etching, (B) for 7 minutes etching, (C) for 9 minutes etching.

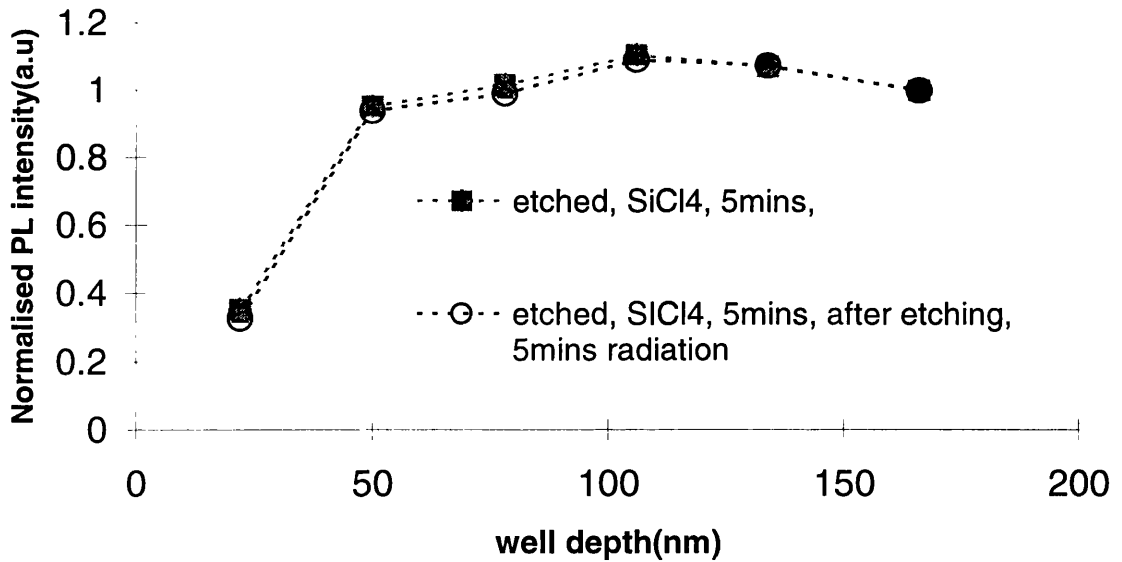
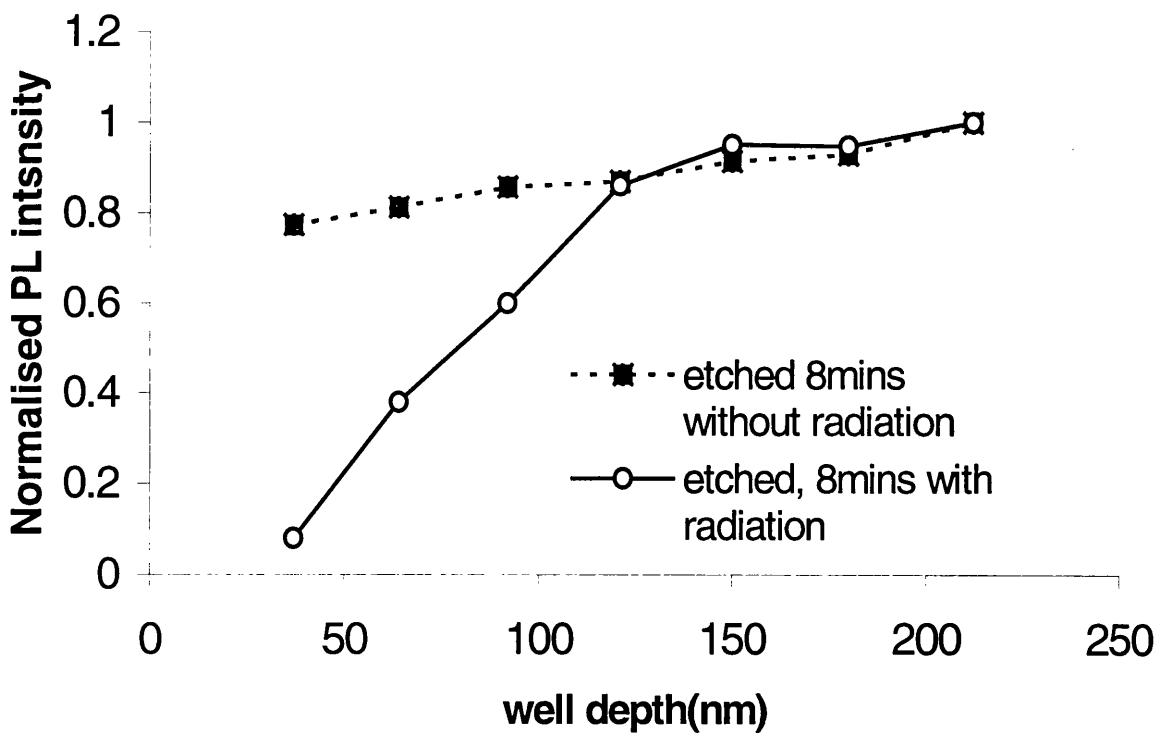


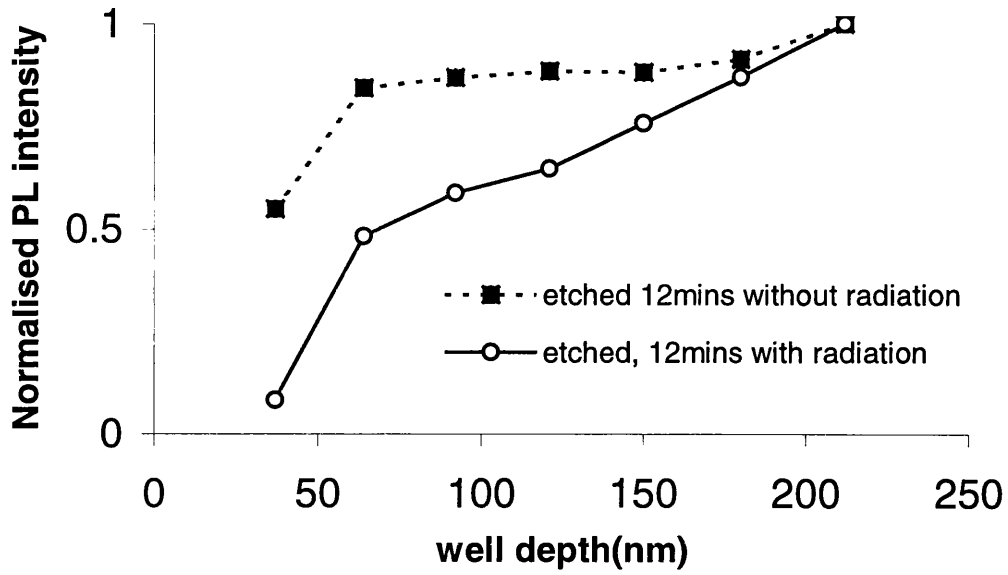
**Figure 6-3.** PL from GaAs etched in  $\text{SiCl}_4$  for 5 minutes, (◊) no laser illumination, (○) 5 minutes illumination subsequent to etching.

### 6.3.2 Results of damage assessment in illuminated InGaAs/InAlAs MQW samples

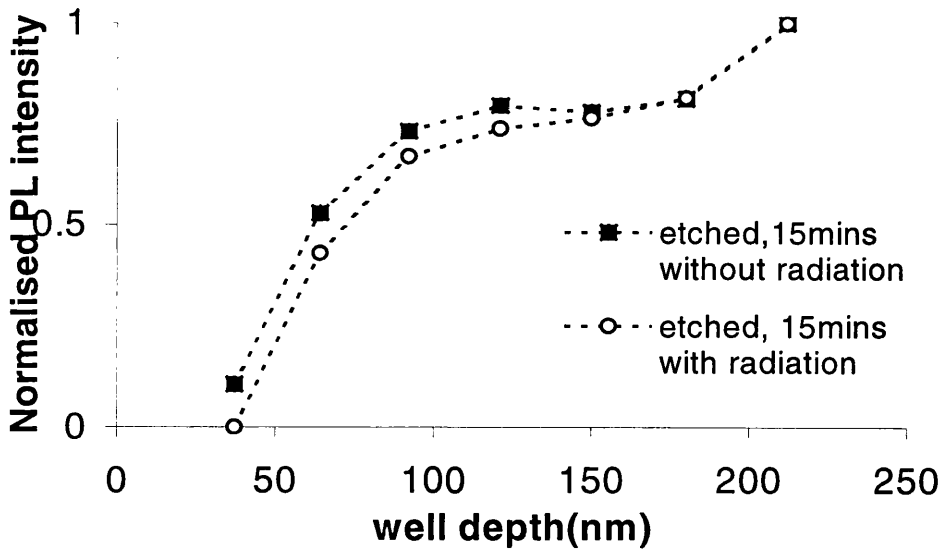
The same experiment was repeated for InGaAs/InAlAs for periods between 8 min. and 15 min. under the etching conditions mentioned in section 6.2. The comparison between normalised PL intensity from etched InGaAs samples with and without illumination is shown in Figure 6-4. The laser power during etching was also 10mW. Additional reductions in PL intensities similar to that in GaAs/AlGaAs samples were observed. Notably, in the 15-minute etching, while the PL intensity from the first quantum well was reduced to 10% without laser illumination, it was completely extinguished with laser illumination.



(A)



(B)



(C)

Figure 6-4. PL from InGaAs etched in  $\text{SiCl}_4/\text{SiF}_4/\text{HBr}$  for 8, 12 and 15 minutes, with (O) and without (■) simultaneous laser illumination. (A) etched for 8 minutes, (B) etched for 12 minutes, (C) etched for 15 minutes.

#### 6.4 The mechanism of illumination contribution to additional damage

The microscopic mechanism for the above phenomenon must explain why light and ion bombardment are required simultaneously to observe the enhanced defect density, light alone or sub-bandgap light<sup>6</sup> being insufficient. Recall that for ion bombardment alone, most of the ion flux is stopped at the semiconductor surface. However, a small fraction is scattered by the surface disordered layers into low index <110> along which channeling can occur. These ions travel a certain characteristic distance  $\lambda_c$  after which they dechannel and create defects.

Several contributions to the enhancement of damage may be identified when light is shone on the sample during bombardment, in part related to the strong electron-phonon coupling in III-V lattices. Incident light is absorbed in the material through the creation of electrons and holes. These can recombine at defects, liberating phonons because of the electron-lattice coupling<sup>9,10</sup>. These excess phonons have two immediate effects on the bombarding ions.

Firstly, the effective temperature  $T_{di}^*$  of the disordered surface layer may be raised, with a consequent change in the scattered distribution. This may cause a small increase in the number of ions scattered into <110> channels. We estimate that such a temperature rise is negligible at the power density used in above experiment. The spot size of the laser beam used is around 1mm. Lax's theoretical calculations<sup>12</sup> of temperature rise induced by Gaussian laser beam absorbed in the solid indicate that the maximum temperature rise at beam center on the material surface is

$$\frac{P}{2\sqrt{\pi} \times K \times w} \times N$$

where P is the incident laser power, K is the thermal conductivity of solid, w is the beam radius and N is a reduction factor which depends on the absorption coefficient of the material itself and approaches unity as  $w \rightarrow \infty$ . The laser power is 10 mW and  $K=0.455\text{Watt/cmdeg}$  for GaAs, therefore the temperature rise is around  $0.06^\circ\text{C}$  at the MQW surface, which is not expected to be high enough to produce a change in the MQW damage profile.

Secondly, the phonons liberated by electron-hole recombination at defects would increase the vibration amplitude of the nuclei lining the  $\langle 110 \rangle$  channels. Any significant increase in vibration amplitude of a nucleus along the path of a channelling ion would result in immediate de-channelling. As such vibrations are a cause of de-channelling, they could affect the defect distribution. The effect may be modelled by an effective channel temperature  $T_{ch}^*$ . Due to enhanced de-channelling rates, more damage is created nearer the material surface, less deep, as compared to the zero illumination case. Such an effect is partly visible in the experimental data of Figure 6-2 although less evident in Figure 6-4. However, the effect is not sufficiently strong to explain entirely the experimental results.

In principle, the channeling ion itself can be a recombination centre at which an electron-hole pair could annihilate. Such annihilation would cause de-channelling. However, the ion motion would cause the electron-hole bound state to be destroyed in a time shorter than the recombination time. Thus, it is not expected this to be a significant source of de-channelling.

The most likely contribution, however, is a type of radiation enhanced diffusion. The process was analysed qualitatively by Chen *et al*<sup>6</sup>. Electron-hole recombination at a defect imparts almost sufficient energy, via electron-phonon coupling, to cause the defect to move. The extra factor that does cause the defect to move arises from the bombarding ions generating an excess flux of phonons. The net effect leads to defect diffusion. Although light from the glow discharge is present on the sample, this appears to be too weak to cause the above effect, as the experimental curves obtained without illumination are adequately modelled by channeling alone.

The absorption length in GaAs<sup>11</sup> for laser light of wavelength 632.8 nm is ~230 nm so the generated electron-hole concentration is approximately uniform over the damaged depth, and an effective enhanced defect diffusion coefficient results. The combined effect of channeling and diffusion can be calculated by the theory, which was given detailed description in chapter 3. The theory introduces two parameters,  $D$ , the defect diffusion coefficient and  $F$ , the defect flux at the surface resulting from defect creation by ion bombardment. Equations (A2) were integrated using a commercial mathematics package, with etch rate  $v = 0$ .<sup>2</sup>

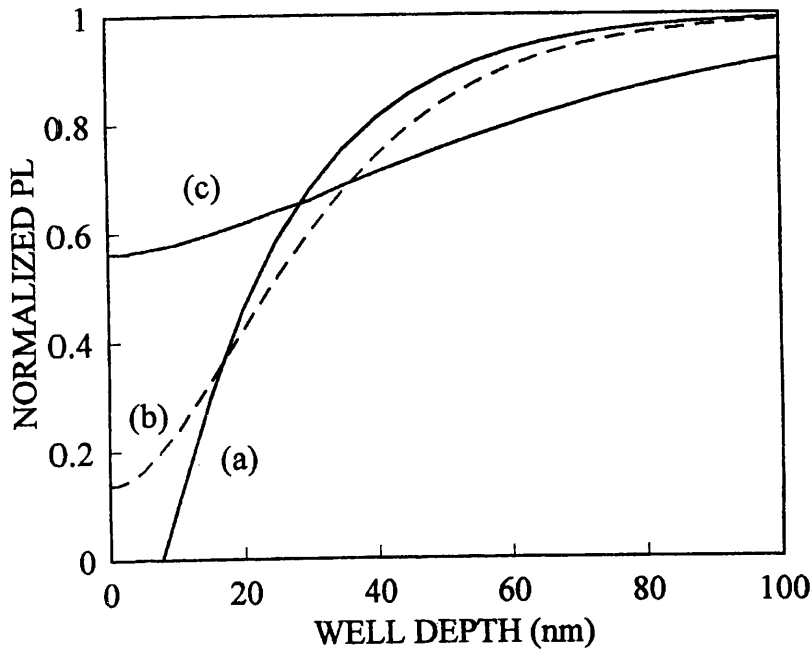


**Figure 6-5.** Effect of diffusion on 60 eV  $\text{Cl}^+$  in GaAs at 300 K with  $F = 0$ : (a)  $D = 10^{-15} \text{ cm}^2/\text{s}$  (b)  $D = 10^{-14} \text{ cm}^2/\text{s}$  (c)  $D = 10^{-13} \text{ cm}^2/\text{s}$ .

Figure 6-5 shows the effect on PL of enhanced diffusion rates. For  $D < 10^{-15} \text{ cm}^2/\text{s}$  there is no appreciable impact on the damage distribution. For increased  $D$  the damage near the surface *decreases*, contrary to experiment.

The above trend is appreciable considering diffusion always results in particle movement from high density regions to low density regions. As the channelling-related defect profile decreases in depth, as indicated by all experiments, it is not surprising that the diffusion of the channelling-related defects alone only serve to flatten the PL profile. The disagreement between theory and experiment suggests other sources of defects. In fact, accidental ion channelling is not the only source of defects near the surface. Within the implant depth of the ions (a few nanometers), defects exist in a much higher concentration than the channelled proportion. These defects created at the surface being etched, independent of the channelling process and usually stationary can also diffuse into the material with the assistance of the illumination. This diffusion can significantly increase the defect density at the depth of the first QW, which is closest to the surface

defect 'pool'. This explains the experimental observation that the first QW PL signal suffers the most decrease with illumination, as shown in Figure 6-2 and Figure 6-4.

## **6.5 Summary**

In summary, we have studied enhanced damage in GaAs/GaAlAs and InGaAs/InAlAs quantum well structures due to additional illumination in low-power RIE environments. Significant additional damage has been observed when illumination was present. The enhancement of damage has contributions both from the influence on the channeling process and from radiation enhanced diffusion as a result of illumination during etching. Comparison between experiment and theory shows that the radiation enhanced diffusion must have caused the inward movement of the high surface defect concentration, resulting in significant reduction in the PL signal from the shallowest QW. Light from the glow discharge is *usually* too weak to cause this effect. Nevertheless adequate shielding from ambient lighting is obviously required during dry etching to minimise any potential diffusion effects.

## **6.6 References**

- [1]. E. L. Hu, C. H. Chen, and D. L. Green, *J. Vac. Sci. Technol. B* **14**, 3632 (1996)
- [2]. M. Rahman, *J. Appl. Phys.* **82**, 2215 (1997).
- [3]. N. G. Stoffel, *J. Vac. Sci. Technol. B* **10**, 651 (1992).
- [4]. L. G. Deng, M. Rahman, S. K. Murad, A. Boyd, and C. D. W. Wilkinson, *J. Vac. Sci. Technol. B* **16**, 3334 (1998).
- [5]. M. Rahman, (unpublished).
- [6]. C. H. Chen, D. L. Green, and E. L. Hu, *Appl. Phys. Lett.* **69**, 58 (1996); C. H. Chen, D. G. Yu, and E. L. Hu, *J. Vac. Sci. Technol. B* **14**, 3684 (1996).
- [7]. S. K. Murad, C. D. W. Wilkinson, and S. P. Beaumont, *Eng.* **23**, 357. (1995).
- [8]. S. K. Murad, S. P. Beaumont, M. Holland, and C. D. W. Wilkinson, *J. Vac. Sci. Technol. B* **13**, 2344 (1995).
- [9]. D. Stievenard and J. C. Bourgoin, *Phys. Rev. B* **33**, 8410 (1986);
- [10]. R. Car, P. J. Kelly, A. Oshiyama, and S. T. Pantelides, *Phys. Rev. Lett.* **52**, 1814 (1984).
- [11]. D. E. Aspnes and A. A. Studna, *Phys. Rev. B* **27**, 985 (1983).
- [12]. M. Lax, *J. Appl. Phys.* **48**, 3919 (1977).

## Chapter 7

### Simultaneous optical and electrical characterisation of dry-etch damage

#### 7.1 Introduction

The characterisation techniques developed over recent years for the study of etch-induced damage, in the main, use either optical or electrical techniques<sup>1-9</sup>. While much information about ion-induced damage has been obtained by conducting such electrical and optical experiments separately, the relationship between optical and electrical manifestations of these damages has still not been explored in detail. For instance, no information is available on the relative extent of degradation in the material's optical and electrical properties when etched under the same conditions. In other words, is the electrical or the optical characterisation more sensitive to ion induced damage? Yet this information is important for the fabrication of devices involving both electrical and optical functions, such as semiconductor lasers and optoelectronic integrated circuits.

In order to answer the above questions, it is necessary to find an approach that is able to explore both characterisations at the same time. In particular, special structures are needed that can be used for measuring both electrical and optical characterisations.

In this chapter, an attempt has been made to combine the optical characterisation methods used earlier in this investigation with electrical characterisation methods. A GaAs-based structure has been specially designed to allow sensitive optical and electrical characterisation. As in earlier experiments, selective etching processes have been employed to damage materials without change to the material structure. The extent of the damage is evaluated electrically by both resistance and Hall measurements, which enables electrical parameters such as material resistivity, carrier concentration and carrier mobility to be obtained, and optically by measuring PL intensity from the quantum wells.

## ***7.2 Design of modulation doped structure for both electrical and optical experimental measurement.***

### **7.2.1 Design consideration**

In order to measure both electrical and optical properties of the sample simultaneously, several problems have to be considered at the design stage of the material.

The material has to be doped in some manner to allow useful electrical measurements to be carried out. But doping usually results in deviations in both optical and electrical parameters from those of the undoped material. For example, both the carrier mobility and the luminescence efficiency drop with increased doping level. It is therefore important to choose a suitable doping method and level to minimise these adverse effects, so that changes caused by the ion damage will not be drowned by the effects of doping, and so that the data be comparable with earlier optical results.

Based on above considerations, it seemed that modulation doping could be useful. Modulation doping separates the carriers from the dopants (the donors or the acceptors). The carriers would be concentrated in an undoped lower bandgap layer, which has high carrier mobility and can be used as the PL emitting layer (the quantum well) at the same time. This forms the main scheme used in the design of the material in this part of the project.

#### ***Modulation doping***

In *modulation doping*, the doping is present in one region but the carriers subsequently migrate to another<sup>10</sup>; in other words, at equilibrium charge transfer occurs across a heterojunction to equalise the chemical potential (i.e., the Fermi level<sup>11</sup>) on both sides. Thus, if doping the wide-bandgap side of a GaAs/AlGaAs heterojunction is doped with donors, electrons are transferred into the GaAs layer until equilibrium is reached. The transfer of electrons fills the electron states and so raises the Fermi energy on the GaAs side; the electrostatic potential of the interface region is raised because of the numerous ionized donors in the AlGaAs side. This is illustrated for a heterojunction between n-AlGaAs and undoped GaAs in Figure 7-1. The material is neutral everywhere and the bands are flat if the electrons sit on their donors in the n-AlGaAs (Figure 7-1 (a)). The electrons travel around after being released and some cross into the GaAs. There they

lose energy and become trapped because they cannot climb the barrier presented by  $\Delta E_c$ . This motion separates the negatively charged electrons from their positively charged donors, which sets up an electrostatic potential  $\phi(z)$  that tends to drive the electrons back into the AlGaAs.

The total energy for electrons is the sum of two terms<sup>10</sup>. Their kinetic energy is given by the band structure. This does not vary with position inside each material but changes at the heterojunction, the main effect being the discontinuity  $\Delta E_c$ . The second term is the potential energy due to the electrostatic potential,  $-e\phi(z)$  for electrons. This must be added to the kinetic energy to give the total energy at the bottom of the conduction band  $E_c(z)$ , shown in Figure 7-1(b). This discontinuity has a major effect because it prevents the electric field from returning the electrons to their donors; the field can squeeze the electrons against the interface, where they are trapped in a roughly triangular potential well. This well is typically about 10nm wide at the energy of the electrons, and the energy levels for motion along  $z$  are quantified in a similar way to those in a square well. Often only the low-level is occupied. All electrons then occupy the same state for motion in  $z$ , but remain free in the other two dimensions  $x$  and  $y$ . This is the *two-dimensional electrons gas* or 2DEG. It is used in the majority of electronics heterostructure devices, occupying much the same position as the quantum well for optical devices.

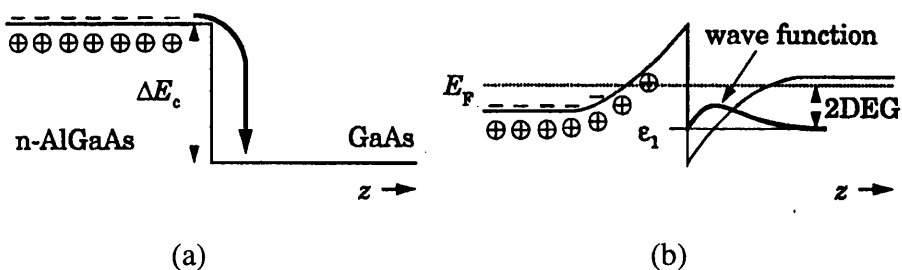


**Figure 7-1.** Conduction band around a heterojunction between n-AlGaAs and undoped GaAs, showing how electrons are separated from their donors to form a two-dimensional electron gas.

Thus modulation doping has achieved two benefits: it has separated electrons from their donors to reduce scattering by ionized impurities, and confined the electrons to two dimensions.

### 7.2.2 Structure

The conventional modulation doped material structure has to be modified for the purpose of this project. For optical as well as electrical measurements to be carried out on the same structure, the triangular well appearing automatically at the heterojunction has to be replaced by a square well. The square well has better quantum confinement, therefore a better-defined PL peak.

The basic requirement of the study is that the observed changes in optical and electrical properties are of the same layer. Therefore the quantum well should also serve as the conduction channel in the electrical measurement. This requires that the free carriers should concentrate in the quantum well. It is therefore necessary to make sure that the bottom of the quantum well is the only potential in the structure lower than the Fermi level.

A basic structure would therefore have at least the following layers: a GaAs cap layer, a n-doped AlGaAs barrier layer, an undoped GaAs quantum well layer, and an un-doped AlGaAs barrier layer.

The layer thickness and the doping level were optimised by simulation using a modelling program developed by Snider<sup>12</sup>, which solves the self – consistently 1D Poisson and Schrödinger equations. This program calculates the energy of the conduction band  $E_c(z)$  was calculated by input a layer structure file to the modelling program, the carrier concentration as a function of vertical position in the structure.

The calculated structure sheet resistance and carrier sheet concentrations in each layer are shown in Table 7-1. The calculation is for room temperature.

\*\*\*\*\*

Structure Sheet Resistance = 2.824E+03 Ohms/square

layer sheet concentrations  
surface ohmic

Thickness (Å)	Material	ns (cm <sup>-2</sup> )	ps (cm <sup>-2</sup> )
150	gaas	9.054E+05	9.374E-01
300	algaas x=.350	4.723E+09	2.725E-09
50	algaas x=.350	1.804E+10	0.000E-01
20	gaas	4.096E+10	0.000E-01
500	algaas x=.350	2.564E+10	5.930E-14
5000	gaas	1.963E+11	4.086E-07
substrate		slope=0	

Temperature = 300.0K

Schrodinger solution from 2.500E+02 to 6.400E+02

**Table 7-1.** Status of layer structure as shown in Figure 7-3.

The sheet concentrations of electron (ns) and hole (ps) are shown in each layer. Note the layer thickness are in Å (=0.1nm).

The band diagram of above modulation doped structure is shown in Figure7-2.

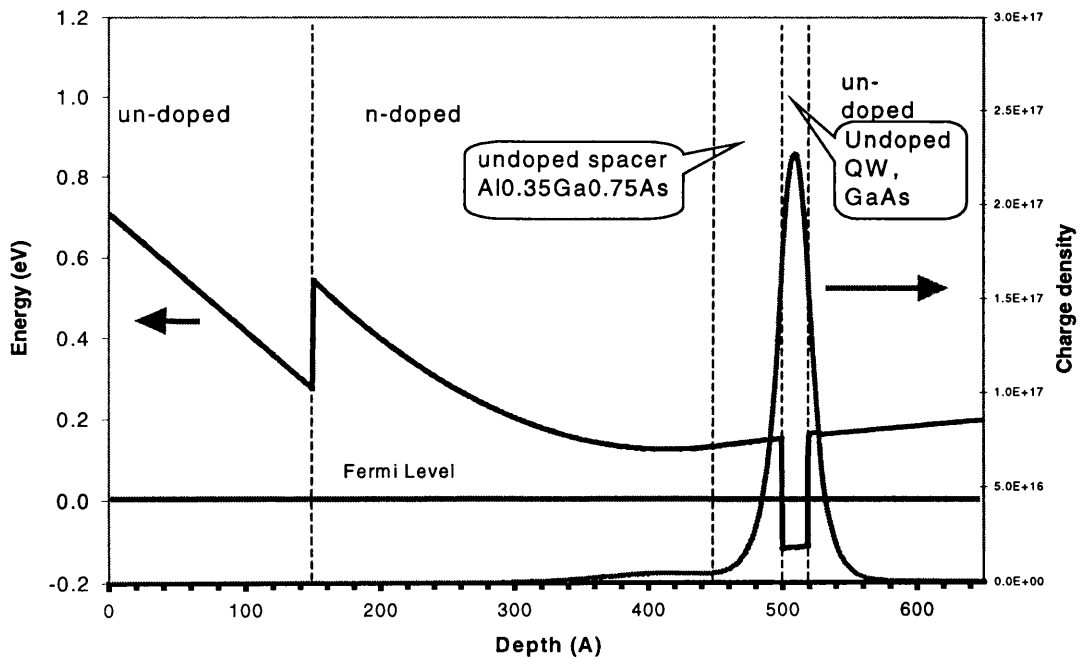


**Figure 7-2.** Band diagram of modulation doped structure as shown in Figure 7-3.

The 2nm thick GaAs quantum well (QW) is as a channel for carriers. The thickness of the quantum well was 2nm. The first QW in the earlier PL experiment material also had this thickness so allowing the PL to be compared. The carrier sheet concentration in the 2nm QW channel is  $\sim 4.1E+10 \text{ cm}^{-2}$ (see table 7-1), much higher than that in the doped layer which is  $\sim 4.7E+9 \text{ cm}^{-2}$ . This is because the conduction band level in the quantum well is  $\sim 0.1 \text{ eV}$  lower than the Fermi level (0 eV), concentrating the carriers in the undoped quantum well.

In a QW of finite depth, the wavefunction of the electrons extends outside the QW into the barrier. So to avoid scattering from ionised impurities, the barrier layer next to the QW should also be undoped. Therefore a 5nm undoped AlGaAs layer has been inserted between the doped AlGaAs layer and the GaAs QW as a spacer layer to separate the ionized donor atoms further from the electrons in the channel. Increasing this spacer layer diminishes the Coulomb interaction between the ionised donors and electrons, resulting in an increased mobility<sup>13, 14</sup>. However this spacer thickness cannot be increased too much: since the electric field is constant in the spacer layer, the electrostatic potential builds up there, although it does not correspond to transferred charges. The consequence is that increasing the spacer layer width tends to decrease the channel electron density. The spacer layer was chosen as 5nm after a number of simulations.

The layer structure is shown in Figure 7-3

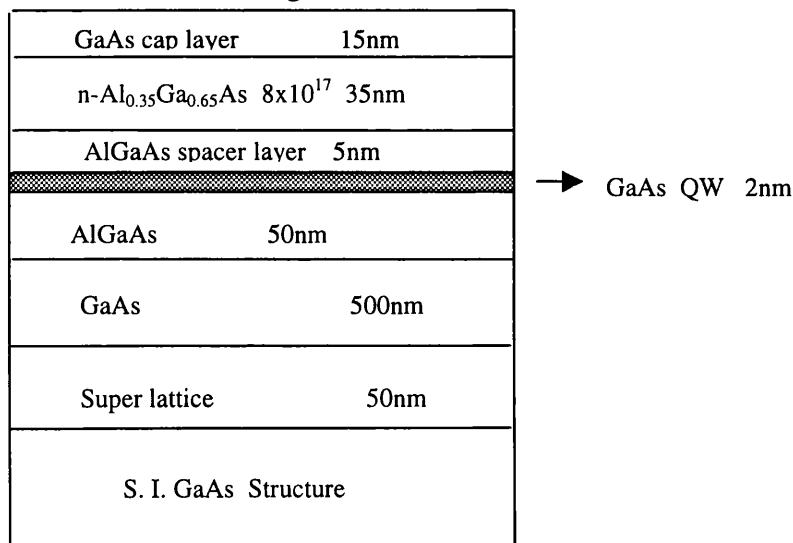


**Figure 7-3.** Modulation doping structure for both electrical and optical measurement.

The 15nm GaAs cap layer on the surface prevents oxidation of the AlGaAs underneath and serves as the contact layer on which ohmic contact is to be made. When selective etching is used to accumulate damage in the material, this layer is removed but etch stops at the GaAs/AlGaAs interface.

The structure shown in Figure7-3 was again grown in the MBE group in the Department and used throughout the following experiments.

### ***7.3 Electrical and optical experiments for investigating characteristics of the material change during dry etching***

#### **7.3.1 Sample preparation**

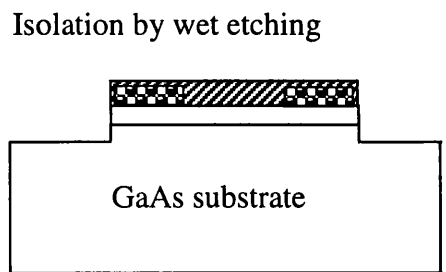
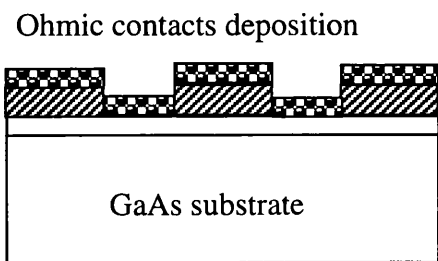
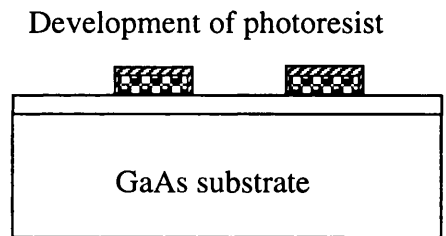
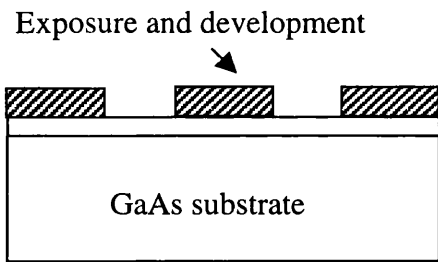
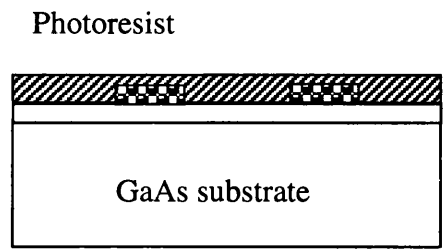
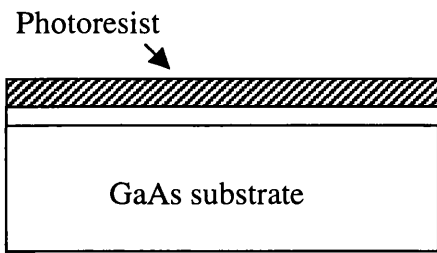
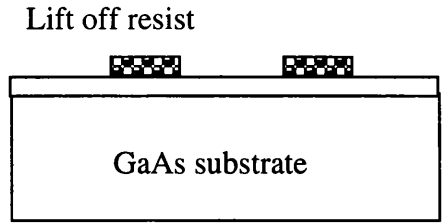
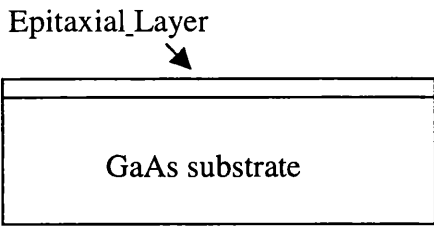
The preparation of sample for electrical and optical measurements is more complicated than for the samples used for earlier optical measurement only. Several process steps are needed to make a device for the electrical measurement. Here the fabrication process for Hall measurement patterns is described. (see Figure7-4)

#### ***Cleaning:***

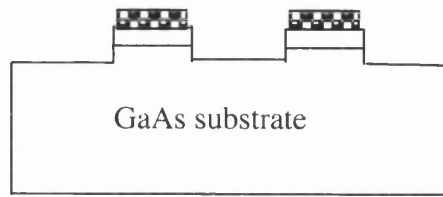
This step is same as that described in section 2.4. a) Wafer blown with N<sub>2</sub>, b) Wafer submersed for 5 minutes first in acetone and then IPA. The wafers are placed in a beaker that itself is put into a bath driven by ultrasound. c). Rinse with abundant RO water and dry with N<sub>2</sub>.

#### ***Photolithography:***

- 1). Photoresist S1818 was spin coated at 4000rpm (revolutions per minute) for 30 seconds to give a film thickness of 1.8 μm.
- 2). The sample was baked in an oven at 90° for 30 minutes.
- 3). The sample was exposed with a ultraviolet (UV) light source for 12 seconds (S1818) with a mask (No. GU0103) made by electron beam lithography. The pattern, as shown in Figure7-5 (A) is designed for the ohmic layer in a Hall Bar.



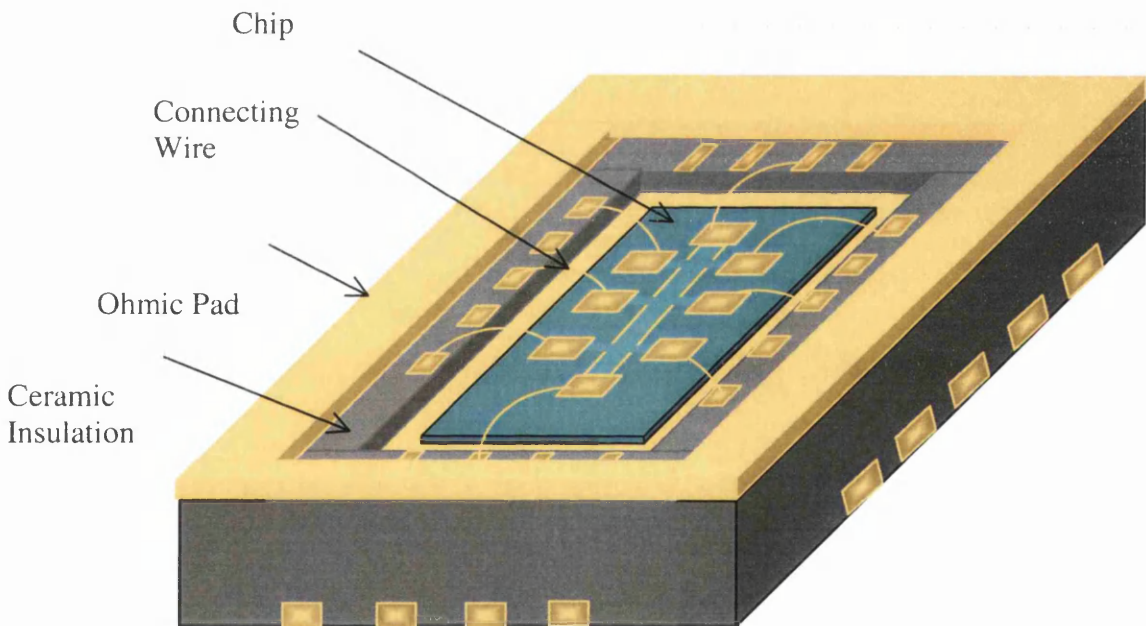
Lift off resist



GaAs substrate

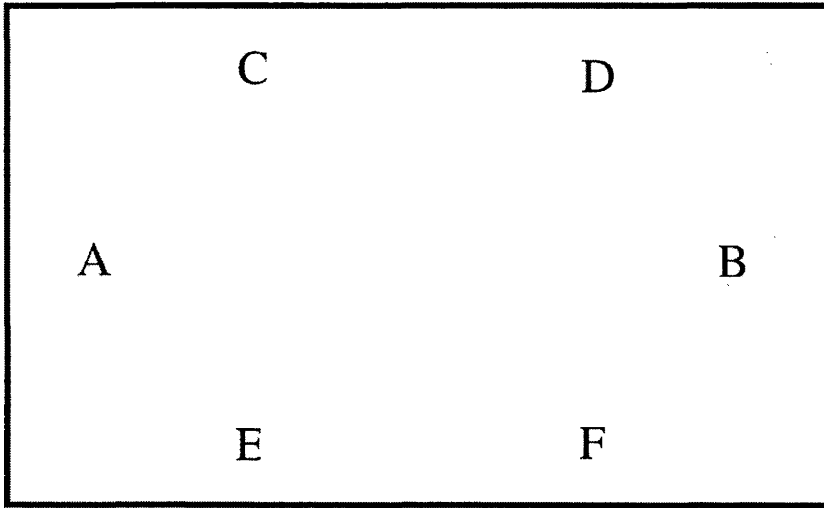
(J)

Completed device for Hall measurement

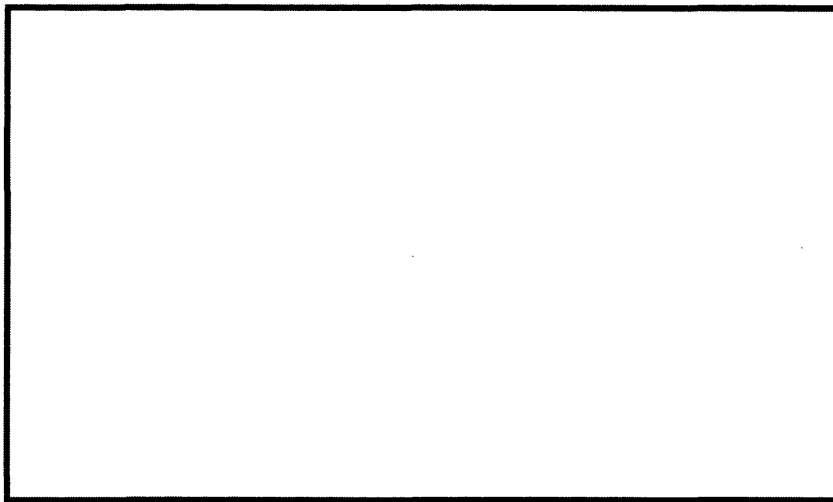


(K)

**Figure 7-4.** Stages of fabrication of the samples used for Hall measurement.



(A)



(B)

**Figure 7-5.** (A) Pattern for the ohmic layer, (B) Pattern for the isolation layer. (developed by E. Skuras).

4). The sample was immersed in chlorobenzene for 20 minutes. Chlorobenzene reduces the solubility of the surface layer of the photoresist, resulting in an undercut profile when the photoresist is developed. This helps in achieving successful lift-off of the metal contact layer.

5). The pattern was developed in Shipley Microposit Developer for 75 seconds, the developer washing away the exposed photoresist solubility.

### ***Ohmic contact metallization***

1). In order to remove the oxides, which grow on a GaAs surface exposed to air, the wafer was submerged in a de-oxidizing solution for 60 seconds. The solution consisted of a mixture of 100ml of reverse osmosis (RO) water and 1ml of concentrated hydrochloric acid (HCl).

2). After the acid dip the sample was rapidly loaded into the evaporator.

The evaporator was a Plassys MEB450 with two chambers. The transfer chamber-permitted both the loading of the holder, and when under a vacuum of less than  $10^{-4}$  bar, the transfer of the holder to the evaporation chamber. When the evaporation chamber was pumped down to less than  $2 \times 10^{-6}$  bar, deposition of the appropriate metal could begin.

3). Each metal was evaporated separately in the following order during a process requiring about one hour.

The software recipe which initiates this sequence is 'Ohmic 7', which deposits the following layers:

- (a). Nickel: 8nm.
- (b). Germanium: 120nm.
- (c). Gold: 130nm.
- (d). Nickel: 80nm.
- (e). Gold: 250nm.

4). After venting and unloading, the sample was transferred to a beaker of acetone for lift-off.

### ***Lift off***

The lift-off has been described in section 2.4. For this particular case, the sample should be put in *warm* acetone for at least 1 hour.

### ***Annealing***

The metal layers have to be heated so that they form an ohmic contact.

To achieve this, alloying and annealing are required in order to allow contact with the 2DEG sited below in the channel layer. The metal undergoing rapid thermal annealing (RTA) is able to diffuse the metal into the epitaxially grown layers of the material to make good contact, as shown in Figure 7-6.

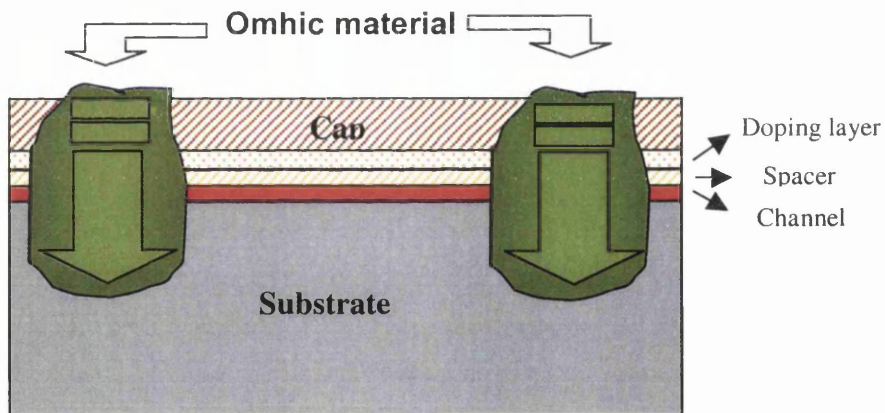


**Figure7-6.** The diffusion of the ohmic metal into the epitaxially grown layers of the wafer during the annealing process. Note that the channel layer has been accessed.

The principle for forming ohmic contacts is that Ge diffuses into lattice sites vacated by Ga which out-diffuses into the contact metallic layer. The Ni also plays an active role in the formation of low resistivity ohmic contacts<sup>16</sup>. A low temperature annealing process has been developed for the fabrication of low resistivity ohmic contacts to very thin n<sup>+</sup> GaAs epilayers by W. Patrick<sup>17</sup>.

In above-mentioned samples, the following annealing processes were used to make the ohmic contact:

Annealing temperature: from 350° to 400°.

Annealing time: from 20secs to 3minutes.

In RTA (Rapidly Thermal Annealing), normally the increase time is 35secs, and reduction time is less 2minutes.

### ***Isolation***

The final step in the fabrication of a hall bar is electrical isolation. This step is necessary to ensure that the electric current flows only in the conduction channel between the two ohmic contact pads, and to separate the patterns on the same sample from each other. This is carried out in the following steps:

(1). Patterning photoresist on the sample to cover the ohmic contact pads and the conduction channel as shown in Figure7-5 (B).

(2). Isolation by wet etching. The recipe for this wet etching is:

$\text{NH}_3$  (1ml) +  $\text{H}_2\text{O}_2$  (1ml) + RO Water (100ml)

The etch-rate is 60nm/mins.

### ***Scribing, Mounting and Bonding***

When a Hall pattern has been made, has to be scribed, mounted and bonded.

(1). Scribing and cleaving cut out the selected 'device' chip, which contained three Hall bars.

(2). The chosen chip was then thoroughly rinsed with a flow of acetone in the cleanroom. This was vitally important, as scribing dust could lodge between the ohmic pads and the wire bonds. This may degrade both the physical stability and the electrical properties of the bonds.

(3). The cleaned chip was glued into a chip carrier with up to 18 insulated gold bonding pads.

(4). The bonding was carried out after glue had completely dried. The first bond was made on the gold pad, second was on the relevant ohmic pad on the chip.

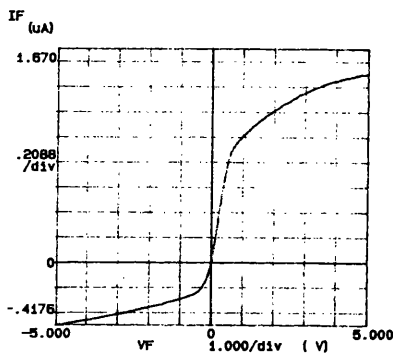
The device was now ready for Hall measurement as shown in Figure7-4 (K).

### ***PL measurement***

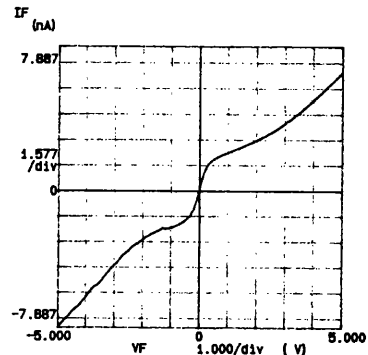
The samples for the PL measurements were prepared as detailed in section 4.2.2.

### 7.3.2 The problems in the sample preparing processes

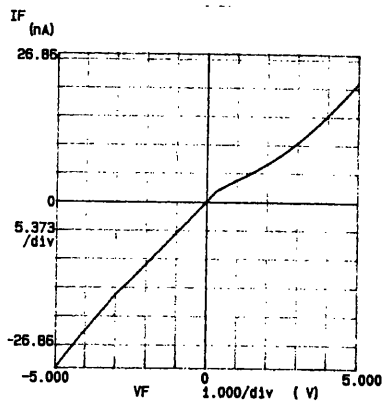
For this particular wafer structure, due to its very thin channel layer and undoped cap layer, it is very difficult to get a good ohmic contact. The quality of ohmic contact is very sensitive to annealing temperature and time. Figure 7-7 shows I-V curves at different annealing temperature and time. The best annealing condition seems to be around 380°C for 40sec. With a lower temperature and a shorter time as shown in Figure 7-7(a), or higher temperature with longer time as shown in Figure 7-7(c), it is not possible to make a good contact. Even at the temperature of 380°C and with an annealing time around 40sec, the ohmic contacts are not always good. Making a reasonable ohmic contact for the 2DEG structure is a problem yet to be solved, particularly for this special structure which has thinner channel layer compared with a standard 2DEG structure. It posed a big problem for the later stages of the experiments.



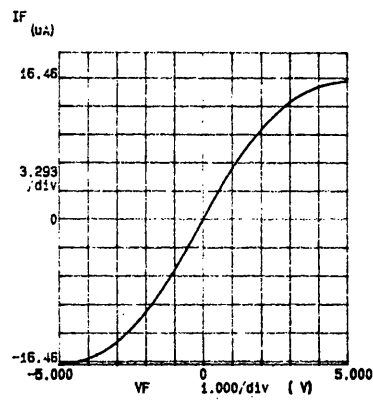
(a)



(b)



(c)



(d)

**Figure 7-7.** I-V curves after annealing; (a) 355°C, 20sec; (b) 370°C, 40sec; (c) 400°C, 60sec; (d) 380°C, 40sec.

### 7.3.3 Hall effect

If one places a semiconductor carrying a current  $I$  in a transverse magnetic field  $B$ , an electric  $E_H$  will be induced in the direction normal to both  $I$  and  $B$ . This phenomenon, known as the Hall effect, is frequently employed to distinguish an n-type from a p-type sample and to determine the carrier concentration. It can also be used to calculate the carrier mobility if the conductivity is measured separately.

In n-type semiconductors the Hall theory predicts the hall coefficient  $R_H$  as<sup>18</sup>

$$R_H = -\frac{r}{qn} \quad \text{Eq. 7-1}$$

This equation shows that knowledge of the Hall coefficient leads to the determination of the carrier concentration  $n$  per unit area or volume,  $q$  is electron charge and  $r$  is assumed to be unity

The Hall voltage  $V_H$  is related to Hall coefficient through the equation<sup>18</sup>

$$R_H = \frac{wV_H}{BI} \quad \text{Eq. 7-2}$$

where  $w$  is the active layer thickness,  $I$  is the current, and  $B$  is the magnetic field. Here the active layer thickness is not the total layer thickness, but the equivalent thickness of the QW channel layer after taking into account the distribution of the electron wavefunction.

The conductance of the sample is

$$\sigma = q\mu_B n \quad \text{Eq. 7-3}$$

which can be rewritten as

$$\mu_n = \frac{\sigma}{qn} = \sigma R_H \quad \text{or} \quad R_H = \mu_H \rho \quad \text{Eq. 7-4}$$

Where  $\rho$  is the sheet resistivity.

Thus, the mobility can be determined using both the Hall and conductance measurements if the conduction is due primarily to one type of carriers.

In practice, a patterned semiconductor bar (the Hall bar) shown in figure 7-8 is employed, where the conductivity is obtained by measuring  $V$  across the outer pairs of contacts (C-D), while the Hall voltage  $V_H$  is measured as shown for a constant current  $I$ .

Thus, carrier concentration and mobility of the sample are determined together accurately.

Therefore by knowing  $R_H$  and  $\rho$ , the carrier mobility in the layer, the sheet carrier concentration and the sheet resistance can be obtained.

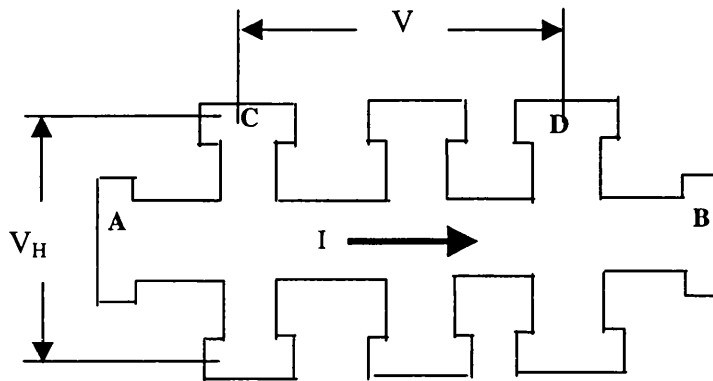


**Figure 7-8.** A semiconductor Hall sample with current flowing through the horizontal bar.

***Carrier Concentration and Mobility of Unetched Modulation Doped Material***

A Hall bar sample made on the modulation doped material has been measured. The Hall experimental setup used in the department is computer-controlled, with the ability to carry out the measurement in the temperature range from 4K to room temperature. The only parameter to be input is the current value. The measured parameters are automatically printed out.

The sample was unetched. I-V characterisation gives the resistance values between different contact points as  $R_{AB}=174K\Omega$  and  $R_{CD}=74K\Omega$ . The measured carrier sheet concentration is  $7.22 \times 10^{10} \text{cm}^{-2}$  and carrier mobility is  $7.17 \times 10^3 \text{cm}^2/\text{Vs}$  at room temperature. The carrier concentration value agrees reasonably with the calculated value of  $4.08 \times 10^{10} \text{cm}^{-2}$  (Table 7-1) considering the limited doping accuracy in the growth. The mobility value is also consistent with reported room temperature values<sup>19</sup> in n-GaAs/GaAlAs.

### 7.3.4 RIE etching for modulation doped 2DEG material of GaAs/AlGaAs

#### *RIE process systems*

The reactive ion etching of the modulation doped GaAs /AlGaAs material was carried out using the Plasma Technology RIE 80 as before.

Again the purpose of this work is to study etching damages in real etching environments, in which material removal takes place. Again the structure of the etched samples should not be changed by the etching in order for the PL and Hall measurements to be meaningful. In other words, it is necessary to accumulate damage in samples without changing the structure. As before, selective etching technique is used to serve this purpose.

The detailed selective etching processes of GaAs/AlGaAs have been given in previously chapters. In this study, the etching was carried out using a mixture of SiCl<sub>4</sub>/SiF<sub>4</sub> for varied times, while the 1.2/8.4sccm of gas flow rate, 10W of etching power (self bias ~ 20V), and 145mTorr of etching pressure were kept constant. The temperature of the cathode (sample table) was maintained at around 40<sup>0</sup>C. Table7-2 specifies etching conditions used in this work. Each time two samples numbered as B\*1 and B\*2 were etched as a group. One of the samples (B\*1) was with Hall patterns and the other (B\*2) was only half covered with photoresist. This was to ensure that both the Hall experiment (B\*1) and the PL (B\*2) samples were etched under exactly the same conditions.

Sample No	Etching condition
B41 and B42	SiCl <sub>4</sub> /SiF <sub>4</sub> , 1.2/8.4 sccm, 145mT, 10W, 20V, <b>1.5mins</b>
B51 and B52	SiCl <sub>4</sub> /SiF <sub>4</sub> , 1.2/8.4 sccm, 145mT, 10W, 20V, <b>3mins</b>
B31 and B32	SiCl <sub>4</sub> /SiF <sub>4</sub> , 1.2/8.4 sccm, 145mT, 10W, 20V, <b>5mins</b>

**Table 7-2.** The details of etching conditions for modulation doped materials.

### 7.3.5 Results of selective etching for modulation doped GaAs/AlGaAs.

#### *Optical Assessment Results*

Figure 7-9 presents the percentage change of normalised PL efficiency in the GaAs channel for above three samples (B32, B42, and B52). After 1.5 minutes of etching, the PL from the GaAs channel reduced by 15%, but for the 5 minutes of etching, the PL from the GaAs channel reduced by 76%. As expected, longer etching time results in more damage, hence more PL reduction in the GaAs channel layer. These results are consistent with earlier PL experimental results.

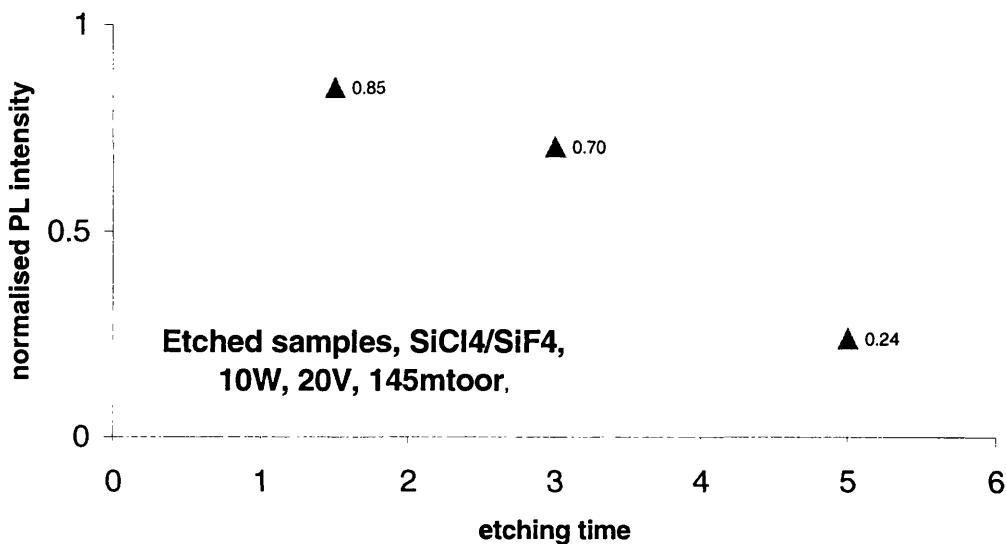


**Figure 7-9.** Normalised PL intensity from modulation doped GaAs/AlGaAs material etched in SiCl<sub>4</sub>/SiF<sub>4</sub> (1.2/8.4) at 10W (dc self-bias 20V) for varies times.

#### *Electrical Assessment Results*

Before the etching, the resistance values of the samples with Hall patterns had been measured. The resistance between contacts A and B (i.e., along the Hall bar) was 240K $\Omega$  for sample B41, 156K $\Omega$  for sample B51, and 174K $\Omega$  for sample B31, respectively. The resistance values of above samples should be roughly the same if good ohmic contacts had been consistently obtained. However, as mentioned earlier, there were slightly different annealing processes used for different sample, which result in difference in resistance between those samples.

Table 7-3 shows that, after etching in conditions shown in Table 7-2, the resistance values were increased significantly. Comparing with original values, the resistances had been increased by 46, 51, and 57 times, respectively.

Because the resistance after etching was unexpected by high, it was very difficult to continue to carry out Hall measurement because the Hall experiment relies on the accurate measurement of voltage on the lateral electrodes. With an internal resistance over  $10\text{M}\Omega$ , this is not possible on the set-up used.

A Hall sample has been wet etched to remove the GaAs cap layer using a very slow etchant ( $\text{NH}_4:\text{H}_2\text{O}_2:\text{H}_2\text{O}$  1:8:400, etch rate $\sim$ 1nm/s) and the resistance before and after etching has been measured. The pre-etching and the post-etching resistance values are practically the same. Therefore it can be confirmed that the increased resistance is related to ion bombardment. However the modest (76%) reduction in normalised PL intensity for the 5-minute etching, and the sharp resistance increase (by a factor of 46) even for a 1.5 minute etching, need to be explained.

Sample No	B31	B42	B51
$R_0$ ( before etching)	240K $\Omega$	156K $\Omega$	174K $\Omega$
R (after etching)	13.3M $\Omega$	11.1M $\Omega$	15.87M $\Omega$
$R/R_0$	46	51	57

**Table 7-3.** The resistances change after dry etching which etching processes shown in Table 7-2.

### 7.3.6 Discussion and Summary of Results

#### *Photoluminescence efficiency and damage concentration*

The photoluminescence (PL) observed in this project originates from the inter-band recombination of the photo-generated carriers. Apart from this radiative recombination, there are other recombination processes in the semiconductor which do not result in the emission of photons. These non-radiative recombinations serve to reduce the excess carrier concentration in the semiconductor, leading to reduced PL efficiency.

It is believed that one of the main mechanisms of dry etch damage is for the ions to form traps in the semiconductor. The luminescence process in the semiconductor can be described by the following rate equation<sup>20</sup>:

$$\frac{dn}{dt} = G - \sigma_t v_n n N_t (1 - f_t) + A N_t f_t - Bnp \quad \text{Eq.7-5}$$

The equation indicates that the change rate of the electron concentration  $n$  is determined by following factors.

- 1) Generation of excess carriers by optical pumping. The rate is denoted by  $G$ .
- 2) The capture of electrons by traps. The rate is denoted by the second term on the right hand side, where  $N_t$  is the concentration of traps,  $f_t$  is the probability of a trap having an electron,  $\sigma_t$  is the cross-section of the trap and  $v_n$  is the velocity of the electron.
- 3) The release of electrons from traps. The rate is denoted by the third term on the right hand side, where  $A$  is a constant.
- 4) The radiative recombination resulting in the emission of a photon. The rate is denoted by the fourth term on the right hand side, where  $B$  is the spontaneous recombination rate and  $p$  is the concentration of the holes.

The probability  $f_t$  itself is a solution of the rate equation

$$\frac{df_t}{dt} = \sigma_t v_n n (1 - f_t) - \sigma_r v_p p f_t - A f_t \quad \text{Eq.7-6}$$

Where the second term on the right hand side stands for the non-radiative recombination through the capture of a hole. At steady state, derivatives in both equations are set to zero and the following equation can be obtained:

$$G = Bnp + \sigma_r v_p N_t f_t p \quad \text{Eq.7-7}$$

This is simply a statement that the total generation rate equals the total recombination rate. The luminescence efficiency, defined as the ratio of radiative recombination to total recombination can then be written as

$$\eta = \frac{Bnp}{G} = \left( 1 + \frac{\sigma_r v_p N_t f_t}{Bn} \right)^{-1} \quad \text{Eq.7-8}$$

From this equation it is clear that luminescence efficiency is affected by the concentration of traps in the semiconductor to the first order.

For Equations 7-5 to 7-8, symmetrical equations which look at the situation from a hole concentration point of view can be written. When these equations are examined closely, it can be found that, in a doped semiconductor, the change in the minority carrier concentration would have more profound effect in reducing the luminescence efficiency. The traps must have been occupied mainly by the majority carriers before excessive carrier pairs are generated by pumping. Further capture of the excessive majority carrier would have little effect to its general concentration when pumping rate is low. However the capture of minority carrier by the traps through nonradiative recombination will result in a more effective change in the radiative recombination efficiency. For n-doped samples this is evident in Eq.7-7, while for p-doped sample it can be made evident by its counterpart containing the capture of minority electrons.

### ***Resistivity and damage concentration***

The resistivity of an n-doped semiconductor is determined by the carrier concentration  $n$  and carrier mobility  $\mu_n$  through Eq.7-4, which can be re-written as

$$\rho = \frac{1}{en\mu_n}$$

where  $e$  is the electron charge. There are two ways through which increased damage concentration can contribute to the increase of resistivity, i.e., through the reduction of carrier concentration and through the reduction of carrier mobility.

The reduction of mobility is mainly by increased scattering of the carrier movement. Suppose the channelled ions eventually exist as neutral impurities in the semiconductor, the limited mobility by neutral impurity scattering is given by the following formula <sup>21</sup>

$$\mu_n = \frac{1.44}{N} \frac{10^{22} \text{ cm}^{-3}}{\epsilon} \frac{m}{m_0} \quad \text{Eq.7-9}$$

Where  $N$  is the concentration of the impurities,  $m$  and  $m_0$  are the effective and free electron mass, respectively, and  $\epsilon$  is the permittivity of the semiconductor.

With  $\epsilon \approx 13$  and  $m/m_0 \approx 0.067$  in GaAs/AlGaAs, the unetched mobility of  $7.17 \times 10^3 \text{ cm}^2/\text{sV}$  corresponds to an impurity concentration  $N$  value of  $7.2 \times 10^{18} \text{ cm}^{-3}$ . Under an ion flux <sup>8</sup>

of approximately  $4 \times 10^{13} \text{cm}^{-2} \text{s}^{-1}$ , the increase in the neutral density is about  $2 \times 10^{18} \text{cm}^{-3}$  assuming an etching time of 100 seconds, a mean damage depth of about 20nm and a  $10^{-3}$  channeling proportion. If the decrease of mobility alone is responsible for the increase in resistivity, the resistivity would only have increase by about 28%.

The fact that an increase in the resistance by a factor of about 50 after etching is observed therefore points to a large decrease of another term, i.e., the electron concentration  $n$ , in the denominator of  $\rho$ . The electron concentration  $n_0$  in the quantum well before etching is about  $2 \times 10^{17} \text{cm}^{-3}$  according to the design calculations presented earlier in this chapter. The creation of traps  $N_t$  by the de-channelling ions would result in the reduction of the electron concentration. As described above, the reduction in the carrier concentration through capture of electrons by the traps is described by Eq.7-6. The difference here is that there is no creation of excess carriers, therefore  $G=0$ , and there is no recombination process involved because of lack of holes. All that remain are the entrapment and release of electrons at the traps. At steady state, the following is obtained from Eq.7-6 or 7-7,

$$\sigma_t \nu_n n (1 - f_t) = A f_t \quad \text{Eq.7-10}$$

which simply means that the electron trapping rate is equal to its releasing rate. The electron concentration can then be written as:

$$n = \frac{A f_t}{\sigma_t \nu_n (1 - f_t)} \quad \text{Eq.7-11}$$

where  $f_t$  again is the probability of a trap occupied by an electron.

It is clear that, with the embedded ion concentration at about  $2 \times 10^{18} \text{cm}^{-3}$  and with a large portion of these forming traps, the situation of  $N_t \gg n_0$  ( $n_0 = 2 \times 10^{17} \text{cm}^{-3}$  is the initial electron concentration) exists. In such a case most of the electrons will be trapped because of the deep nature of the trap level. Therefore

$$f_t \approx \frac{n_0}{N_t}$$

and the electron concentration can be approximated by

$$n \approx \frac{A n_0}{\sigma_t \nu_n N_t} \quad \text{Eq.7-12}$$

The exact value of  $n$  is determined by the escape coefficient  $A$ , which is a result of thermal ionisation, and the cross section of the trap  $\sigma_t$ . It is difficult to quantify these parameters. But even for a trap level only 100meV below the conduction band edge, the ionisation probability is only about 2% at room temperature, so it is possible that the reduction of  $n$  is enough to increase the resistivity significantly to the measured level. Any residual conductivity measured from the experimental samples is a result of thermal ionisation of the trapped electrons, which arise from the small tail of electron energy distribution above the conduction band edge.

It remains difficult to quantitatively link the PL variation with the resistivity variation using above simple theory because of the many unknown parameters. It can be understood from earlier analysis in the chapter that the reduction of photoluminescence efficiency is mainly due to the non-radiative capture of the excessive *minority* carriers at the trap sites created by channelling ions, in competition of radiative combination. This change of luminescence efficiency is related to the non-radiative combination cross section  $\sigma_r$ , and the velocity of the minority carrier (in this case hole velocity  $v_p$ ). Due to the large effective mass of holes,  $v_p$  is usually much smaller the  $v_n$ , which seems to explain the relative insensitivity of PL to damage in the n-doped samples used.

On the other hand, the change in electric properties, such as the conductivity, is mainly due to the influence on the *majority* carriers, such as reduction in their mobility by increased scattering, and more predominantly, by the reduction in their concentration by trapping.

## **7.4 Summary**

The investigation described in this chapter is intended to establish links between the changes in optical and electrical properties of dry-etched III-V semiconductor material. This is carried out with a specifically designed modulation doped QW structure. The structure allows dry etch damage to be assessed by both photoluminescence and electrical measurements. The structure, grown by the MBE group in Glasgow University, has a surprisingly high measured electron mobility of  $7.17 \times 10^3$  cm<sup>2</sup>/Vs.

The initial experimental results presented above indicate that the resistivity of the material is far more sensitive to the etching than the PL efficiency is. This phenomenon

seems to be explained by theoretical analysis based on capturing of carriers by ion damage related traps. The significant increase of resistivity can be explained by the depletion of majority carriers by capturing, while the luminescence reduction by capture of excessive minority carriers.

Due to the dramatic increase in sample resistivity, it was impossible to carry out Hall measurements on etched samples. If by optimising the wafer design and the quality of the ohmic contact, the initial resistance value can be reduced, it should still be possible to do the Hall experiments on etched samples, even if the resistance increase by the same factor observed here.

It should be pointed out that, as a novel attempt to link the change in material optical and electrical properties after dry etching, both the method and results presented here are preliminary and can be further improved. Possible ways of improvement is detailed in the future works section in Chapter 8.

## **7.5 References**

- [1]. S. K. Murad, M. Rahman, N. Johnson, S. Thoms, S. P. Beaumont, and C. D. W. Wilkinson, *J.Vac.Sci.Technol.* **B 14**, 3658-3662 (1996).
- [2] N. I. Camerson, S. P. Beaumont, C. D. W. Wilkinson, N. P. Johnson, A. H. Kean, and C. R. Stanley, *J.Vac.Sci.Technol.***B 8(6)**, 1990, P1966-1969.
- [3]. N. P. Johnson, M. A. foad, S. Murad, M. C. Holland, and C. D. W. Wilkinson, *Mater. Res. Soc. Symp. proc.* **325**, 443, (1994).
- [4]. M. A. Foad, S. Thoms, and C. D. W. Wilkinson, *J. Vac. Sci. Technol.* **B 11(1)**, 1993, P. 20-25.
- [5]. M.Watt, C.Sotomayor-Torres, R.Cheung, C.D.W.Wilkinson, H.E.G.Arnott, and S.P.Beaumont, *J.Mod. Opt.* **35**, 1988, P365.
- [6]. P. D. Wang, M. A. Foad, C. M. Sotomayor - Torres, S. Thoms, M. Watt, R. Cheung, C. D. W. Wilkinson, and S. P. Beaumont, *J.Appl. Phys.* **71(8)**, 1992, P.15.
- [7]. H. F. Wong, D. L. Green ,T. Y. Liu, D. G. Lishan, M. Bellis, E. L. Hu, P. M. Petroff, P. O. Holtz, and J. L. Merz, *J.Vac.Sci.Technol.* **B 6**, 1906-1909 (1988).
- [8]. M. Rahman, *J. Appl. Phys* **82** 2215 (1997). [9]. Ching-Hui Chen, Debora L. Green, and E. L. Hu, *J.Vac.Sci.Technol.* **B 13**, 2355- 2359 (1995).
- [10]. John H. Davies, “ The physics of low dimensional semiconductors”, Cambridge University Press, 1998. P.93.
- [11]. S. M. Sze, “ Semiconductor devices Physics and Technology” John wiley& sons, 1985. P. 16.
- [12]. Commercial program developed by G.Snider
- [13]. L.C. Witkowski, T. J. Drimmond, C. M. Stanchak and H. Moekoc, *Appl. Phys. Lett.* **37**, 1033(1980).
- [14]. H. L. Stormer, A. Pinczuk, A. C. Gossard, and W. Wiegmann, *Appl. Phys. Lett.* **38**, 69 (1981).
- [15]. C. Weisbuch, B. Vinter, “Quantum semiconductor structures”. Academic Press, (1991). p32.
- [16]. N. Braslau, “Thin Solid Film” **104**, 391 (1983).

- [17]. W. Patrick, W. S. Mackie, S. P. Beaumont, and C. D. W. Wilkinson, *Appl. Phys. Lett.* **48**, 986 (1986).
- [18]. Edward S. Yang, “Microelectronic Devices”. McGraw-Hill Book Company, 1988, P39.
- [19]. Sadao Adachi, “Properties of Aluminium Gallium Arsenide”. Academic Press, 1991.
- [20]. K. Seeger, “Semiconductor Physics”, Springer-Verlag Berlin Heidelberg New York, 1982. P403.
- [21]. K. Seeger, “Semiconductor Physics”, Springer-Verlag Berlin Heidelberg New York, 1982. P155.
- [22]. M. Rahman, *J. Appl. Phys* **82** 2215 (1997).

## Chapter 8

### Conclusions and further work

#### 8.1 Conclusions

As set out in chapter 1, the aim of this project is to investigate dry-etching damage in III-V semiconductors under very low ion energy conditions in real etching environments. This investigation has been carried out by studying the changes in both optical and electrical properties of GaAs/GaAlAs and InGaAs/InAlAs materials.

Firstly, the optical manifestation of dry etching damage in these materials has been studied using photoluminescence (PL) measurements on quantum well (QW) probe materials. Due to the relatively low damage nature of the etching processes studied, a technique using selective etching has been used to accumulate damage in the etched materials. By comparing photoluminescence spectra for damaged and undamaged areas, normalised damage depth distributions for various RIE selective etching conditions have been obtained. A microscopic theory has been used to model the distribution of the damage in such dry-etching processes, taking into consideration different ion masses, self bias voltages (RF power), etch times, and fluxes.

It is significant that the experimental data is consistent with calculated damage effects by channeling atomic ions alone, rather than molecular ions. The results therefore suggest that atomic-ion channeling is responsible predominantly for dry-etching damage inflicted in low-energy multi-component gas discharges. Molecular ions do not channel because their extended structures do not permit it. Generation of atomic ions upon their impact is possible, but at energies far less than the incident energy. The results indicates that, ideally, low damage etch chemistries should not only have low ion energies but should use only molecular ions.

To further investigate the damage effects of individual ion species, a low energy ion implanter has been used to study ion induced damage in III-V semiconductors due to separate  $\text{Cl}^+$ ,  $\text{Si}^+$ ,  $(\text{Cl}_2)^+$ ,  $(\text{SiCl})^+$ , and  $(\text{SiCl}_2)^+$  ion bombardment. Damage profiles have again been measured using PL measurements on same QW probe materials. By comparing photoluminescence spectra obtained under comparable ion energy,

exposed time, and ion dose as found in previous etching conditions, it is established that

- (1) Increasing the amount of ions, the damage increases significantly,
- (2) Increasing ion energy will also increase damage in materials,
- (3)  $\text{Cl}^+$  ions cause more damage in materials than  $\text{Si}^+$ .
- (4) InGaAs based materials are more vulnerable to  $\text{Cl}^+$  ion damage than GaAs based materials because their greater channelling depth, and
- (5) Atomic ions play the major role in producing damage rather than molecular ions. Although damage have been observed in materials bombarded by molecular ions of  $\text{SiCl}^+$ ,  $\text{SiCl}_2^+$ , and  $\text{Cl}_2^+$ , the measured PL data were consistent with theoretically calculated damage effects due to the secondary atomic ions rather than that of original molecular ions.

For secondary atomic ions, the ion energies would be far less than the incident molecular ion energy. Thus for low damage etching, reactive chemistries should be used that not only have low ion energies but also comprise a low atomic to molecular ion fraction in the discharge.

Above investigations highlighted the importance of ion channeling as the main mechanism for low energy ions to penetrate the etched substrate. However there have been suggestions that defect diffusion contributes to the final damage profile.

Experiments have been carried out using radical ion beam exposure at fixed dose, but varying exposure time. Under normal conditions this failed to show conclusive evidence of diffusion taking place. However, in the presence of additional above-bandgap (632.8nm) photon illumination, significant additional damage has been observed in low-power RIE environments. It is believed that the enhancement of damage has contributions both from the influence on the channeling process and from radiation enhanced diffusion as a result of illumination during etching. Comparison between experiment and theory shows that the radiation enhanced diffusion must have caused the inward movement of the high surface defect concentration, resulting in significant reduction in the PL signal from the shallowest QW. Light from the glow discharge is *usually* too weak to cause this effect. Nevertheless adequate shielding from ambient lighting is obviously required during dry etching to minimise any potential diffusion effects.

Having carried out extensive optical assessment of dry etching damage distribution, the investigation has been further advanced to establish links between the changes in optical and electrical properties of dry-etched III-V semiconductor materials.

Modulation doped QW structures have been designed to combine optical and electrical measurements on the same materials. The extent of damage have been evaluated electrically by both resistance and Hall measurements, which enable electrical parameters such as material resistivity, carrier concentration and carrier mobility to be obtained, and optically by measuring PL intensity from the quantum wells.

The experimental results indicate that the resistivity of the material is far more sensitive to the etching than the PL efficiency is. This phenomenon seems to be explained by theoretical analysis based on capturing of carriers by ion damage related traps. The significant increase of resistivity can be explained by the depletion of majority carriers (electrons) by capturing, while the luminescence reduction by capture of excessive minority carriers (holes).

## **8.2 Future Work**

The methods used in this work can obviously extended to other material systems such as InGaAsP/InP, and other dry etching processes. Lower damage etch processes can be developed using information obtained from these investigations.

The majority of further work would be in the combined electrical and optical assessment area. More information is needed to support and refine the preliminary results and theoretical explanation provided in chapter 7.

Immediate improvement on the experiment can be achieved by increasing the width of QW so that carriers are more bound inside the QW. Doping levels should be optimised so that better electrical measurements can be carried out. Simulations of material property should be carried out to predict possible influence by changing material structure (e.g., the removal of cap layer) and other parameters after etching.

Present results show very high post etching resistivity. More useful data can be obtained by damaging the material less severely, so that modest increase in resistivity can be measured, and a relationship can be established between resistivity and the amount of damage.

New samples would need to be designed to have, for example, p-type modulation doping to provide complementary evidence about the relative sensitivity of PL and

resistivity to damage. According to the theory employed in chapter 7, the relative sensitivity of PL and resistivity in p-type material may be very different from that in the n-type material because of the different carrier velocity and capture cross-section. The combined information gained in both n- and p-type materials should give more insight into the mechanisms of material degradation.

The scheme can also be extended to place the QW at different depths, so that a comparison between depth profiles of resistivity and PL efficiency can be made.

Improvement in the ohmic contact needs to be addressed, so that accurate measurement of mobility can be carried out by Hall measurement. The quality of ohmic contact should be verified by TLM before accurate electrical measurement is carried out.

Finally, same experiment should also be carried out on InGaAs/InAlAs materials, which already have a wealth of optical data available as a result of this project.

## Publications

1. L. G. Deng, M. Rahman, S. K. Murad, A. Boyd, and C.D.W.Wilkinson, "Can dry etching systems be designed for low damage ab initio". J. Vac. Sci. Technol. **B 16**, 3334(1998).
2. L. G. Deng, M. Rahman, J. A. van den Berg, and C.D.W.Wilkinson, "Contribution of atomic and molecular ions to dry-etch damage". Appl. Phys. Lett., 75(2), 211(1999).
3. M. Rahman, L. G. Deng, A. Boyd, A. Ribayrol, C.D.W.Wilkinson, J. A. van den Berg and D. G. Armour, "Design considerations for low damage precess plasmas". Micro Nano Eng. 46,299 (1999).
4. M. Rahman, L. G. Deng, A. Boyd, , C.D.W.Wilkinson, J. A. van den Berg and D. G. Armour, "Criteria for low damage III-V dry etching" Electrochem. Soc. Proc. 98-12, 213(1998).
5. M. Rahman, L. G. Deng, A. Boyd, , C.D.W.Wilkinson, J. A. van den Berg and D. G. Armour, Secondary atomic channelling from molecular ion impacts at semiconductor surfaces; "Energetic Molecules and Cluster Interactions with Solid Surfaces Conference in Salford, May, 1999.
6. L. G. Deng, M. Rahman, and C.D.W.Wilkinson " Enhanced damage in low damage RIE processes caused by light" Appl. Phys. Lett. 76(20), 2871(2000).
7. M. Rahman, L. G. Deng, A. Boyd, J. A. van den Berg, C.D.W.Wilkinson " Studies of damage in low-power reactive-ion etching of III-V semiconductors" submitted to J. Appl. Phys.

